NORTHWESTERN UNIVERSITY

Characterization of HKDC1 and Involvement in NAFLD Development

A DISSERTATION

SUBMITTED TO THE GRADUATE SCHOOL
IN PARTIAL FULFILLMENT OF THE REQUIREMENTS

for the degree

DOCTOR OF PHILOSOPHY

Field of the Driskill Graduate Program in Life Sciences

By

Carolina Marie Pusec

EVANSTON, ILLINOIS

December 2018

ABSTRACT

The literature has established glucokinase (GCK) to be the principal hexokinase (HK) in the liver, operating as a glucose sensor to regulate glucose metabolism and lipid homeostasis. We have recently proposed Hexokinase Domain Containing-1 (HKDC1) to be a novel 5th HK with expression in the liver. Here, we reveal HKDC1 to have low glucose-phosphorylating ability and demonstrate its association with the mitochondria in hepatocytes. As we have shown previously that genetic deletion of *HKDC1* leads to altered hepatic triglyceride levels, we also explored the influence of overexpression of HKDC1 in hepatocytes on cellular metabolism observing reduced glycolytic capacity and maximal mitochondrial respiration with concurrent reductions in glucose oxidation and mitochondrial membrane potential, suggesting a defect in mitochondrial function. However, acute *in vivo* overexpression of HKDC1 was not enough to alter energy storage in the liver, but led to mild improvement in glucose tolerance. We next investigated the conditions necessary to induce HKDC1 expression, observing HKDC1 expression to be elevated in human patients whose livers were at more advanced stages of NAFLD and similarly found high liver expression in mice on diets causing high levels of liver inflammation and fibrosis. Overall, our data suggests HKDC1 expression in hepatocytes results in defective mitochondrial function and altered hepatocellular metabolism and speculate that its expression in liver may play a role in the development of NAFLD. Future studies will explore how defective mitochondrial function from HKDC1 expression may contribute to the reprogramming of hepatocellular metabolism seen in NAFLD.

List of Abbreviations

2HPG	2 Hour Plasma Glucose
CDA-HFD	High fat, methionine-restricted and choline deficient
G6P	Glucose-6-Phosphate
GCK	Glucokinase
GKRP	Glucokinase Regulatory Protein
GLUT	Glucose Transporter
GSK3β	Glucose Synthase Kinase 3 Beta
GWAS	Genome Wide Association Study
HAPO	Hyperglycemia and Pregnancy Outcomes
HCC	Hepatocellular Carcinoma
HF+HF	High Fat High Fructose
HF+HG	High Fat High Glucose
HK	Hexokinase
HK1	Hexokinase 1
HK2	Hexokinase 2
HK3	Hexokinase 3
HKDC1	Hexokinase Domain Containing 1
IR	Insulin Resistance
LF	Low Fat
MCD	Methionine and Choline-deficient
MSD	Methionine and Choline-supplemented

MSDHFD	Methionine- restricted and Choline-supplemented High Fat Diet
mtDNA	Mitochondrial DNA
NAFLD	Non-alcoholic Fatty Liver Disease
NASH	Non-alcoholic Steatohepatitis
PFK2/FBPase2	Phosphofructokinase-2/ Fructose bisphosphatase-2
PKB	Protein Kinase B
PTPC	Permeability Transition Pore Complex
UPR	Unfolded Protein Response
VDAC	Voltage Dependent Anion Channel

DEDICATION

"Life is not easy for any of us. But what of that? We must have perseverance and above all confidence in ourselves."
-Marie Curie

When I was a young girl, my mother showed me a documentary on the life of Marie Curie and her accomplishments. At the time, I could not fully comprehend the magnitude and significance of her life's work, but I was able to recognize the strength of her tenacity in pursuit of her ambitions. The distractions of the world were not enough to drown her inner confidence nor curiosity for scientific discovery, and I was determined to follow in her footsteps.

My doctoral career was met with a plethora of struggles and challenges that I have had to face and overcome, but it would have never been possible if it were not for the special people in my life. The honesty and rationality of my brother Nick taught me to be stronger at times of hopelessness and conflict. The humorous conversations and comfort from my father Steve reminded me to never lose sight of the bigger picture, and to accept and enjoy the difficulties of the path I chose. The loving nature and encouragement from my mother Luz inspired me to become a better person - forgiving and accepting others as they are and to never give up on my dreams.

Alongside my family were friends and mentors that kept me focused and excited for my journey in the sciences. I learned how to face my failures and transform them into stepping stones; that success itself almost never comes in the timeline you anticipate. My best friend Adam taught me this, and he continues to help me see how my true potential can surpass far beyond the limitations I set for myself. Finally, to my Ph.D advisor and friend Dr. Brian Layden – I dedicate

this dissertation to you. You have selflessly supported me time and time again and have helped me mature as a scientist, thinker, and teacher. I am truly blessed to have had you as a role model and I thank you for the faith you continue to have in me.

Table of Contents

List of Figures and Tables

Chapter 1

INTRODUCTION

DISCOVERY AND SIGNIFICANCE OF HKDC1

Prediction of a Possible 5th Hexokinase, HKDC1

Identification of the hexokinase-like gene, HKDC1, was reported approximately 10 years ago by *Irwin et al.* where its conservation was observed among all the mammalian genomes analyzed (1). Given that all the searches conducted only identified the four well-established hexokinase isoforms to have enzymatic activity, it was initially hypothesized that HKDC1 did not possess hexokinase activity. However, their sequence analysis predicted the HKDC1 gene to have an intact open reading frame of 917 amino acids and found the sequence possessed the amino acids necessary for glucose and ATP binding. The residues for glucose binding were in both the N- and C-terminal domains while ATP binding site was found exclusively in the C-terminal domain. Additionally, the HKDC1 gene lays tandem to the Hexokinase 1 (HK1) gene in a head-to-tail arrangement, which strongly suggests that it was a product of a gene duplication event. Furthermore, HKDC1 has 71% sequence homology with HK1, further supporting its potential to carry out the hexokinase function HK (2).

Hexokinase Domain Containing-1 (HKDC1) Associates with Gestational Glucose Metabolism

Maternal glucose metabolism undergoes unique metabolic adaptations in order to meet the energy demands of both the mother and developing fetus (3). Pregnant mothers with pre-existing gestational diabetes put themselves and their offspring at an increased risk of attaining a metabolic disorder, such as obesity and type II diabetes, later in their life (4,5). Given these consequential effects and the differences observed between gestational and non-gravid glucose

metabolism, a genome wide association study (GWAS) was conducted to examine the pregnancy-specific genetic variation that associates with glycemic traits. The GWAS was performed utilizing the Hyperglycemia and Adverse Pregnancy Outcomes (HAPO) cohort, an international study that collected data regarding maternal metabolism and fetal development from over 25,000 pregnant women from diverse backgrounds. In this study, it was found that variants near the *Hexokinase Domain Containing 1* (*HKDC1)* gene were found to associate with the glycemic trait, 2 hour plasma glucose (2HPG), that was measured in pregnant women during an oral glucose tolerance test (6).

In a follow-up study, our lab and collaborators found multiple variants that were proximal to HKDC1 (in regulatory elements) that alter regulatory element activity. These variants were coordinated across four enhancer elements where each variant that contained alleles associated with reduced HKDC1 expression also correlated with higher plasma glucose in gestational mothers. Furthermore, we examined how altering HKDC1 levels affects overall cellular hexokinase activity in various cell lines via overexpression and knockout studies. siRNA-mediated knockdown in HepG2 cells reduced HKDC1 mRNA by 35-60% and correspondingly reduced activity by 25%, whereas, overexpression of HKDC1 mRNA in HepG2 cells and INS-1 cells resulted in a 40-50% increase in hexokinase activity (7). Altogether, these studies provided the first evidence of HKDC1 to be associated with glycemic traits and that it contributes hexokinase activity. This has stimulated interest in its characterization and elucidating its role in maternal glucose metabolism and beyond.

INITIAL CHARACTERIZATION OF HKDC1

HKDC1 Tissue Expression and Mouse Model

HKDC1 has been found to be widely expressed and predominantly in the brain, small intestine, colon, kidney, lung, and with lower expression in the liver in humans (6) and recently shown to have similar expression patterns in mice (2). Given HKDC1's wide and differential expression amongst various tissues, similarly seen between humans and mice, these data suggested that mouse models will be useful to understand its role *in vivo.*

Therefore, we generated the first mouse models, the HKDC1 global knockout mice. We have reported that genetic global ablation of HKDC1 in mice is embryonic lethal, given no births were produced from crossing our heterozygous deletion mice ($HKDC1^{+/-}$ x $HKDC1^{+/-}$) after countless generations (2). Moreover, we observed that partial loss of *Hkdc1* expression impairs glucose clearance (in aged and pregnant mice), and reduces tissue-specific glucose disposal and hepatic triglycerides levels (2). These data suggest that *Hkdc1* may play an important role in glucose homeostasis and hepatic lipid accumulation, and this may be through a role in the liver. From this initial study, multiple substantial questions remain to be answered about HKDC1's function and influence on metabolism.

OVERVIEW OF HEXOKINASES

Hexokinase Function

Hexokinases function to transfer a phosphate moiety from ATP (or equivalent energy sources) to the sixth hydroxyl position of glucose to yield the product glucose-6-phosphate (G6P) as glucose enters the cell through facilitative glucose transporters (GLUTs) (8,9). This reaction represents the first rate-limiting step of glycolysis, where its phosphorylation restrains glucose from exiting the cell and allows G6P to continue through glycolysis, or enter other catabolic and anabolic pathways such as glycogen synthesis, pentose phosphate, hexosamine pathways, or cellular respiration (8,10).

Four mammalian HK isozymes have been well characterized and are identified as HK1, hexokinase 2 (HK2), hexokinase 3 (HK3) and hexokinase 4 [HK4, or more commonly known as glucokinase (GCK)]. All HK isozymes function to phosphorylate glucose (and less commonly equivalent sugar substrates); however, each contain distinctive properties that differentiates their role in mediating cellular metabolism. These properties include their structure, activity/kinetics, tissue expression, regulatory/catalytic capabilities, and sub-cellular localization (8,10). The following sections will highlight these differences.

Evolution and Structure of HK Isoforms

Non-vertebrate animals are reported to utilize only 50 kDa-sized hexokinases, whereas, most vertebrates and all mammalian hexokinases examined use both 50 kDa and 100 kDa hexokinases (1,10). HKI1-3 are approximately 100 kDa, containing two 50 kDa domains and subject to

product inhibition, while GCK is 50 kDa with a single domain and is not inhibited by its product. Extensive amino acid sequence analysis on the HK isozymes was performed (1) and indicated high sequence homology between HK1-3 and strongly suggested that each HK domain descended from an ancestor that contained a single hexokinase domain gene that underwent duplication and fusion (1,10). Each of the 100kDa HKs have high sequence similarity between the N- and C- terminal domains and each other, however, HK2 is the only HK that retained catalytic activity in both domains (11–13), leaving HK1 and HK3 to have catalytic activity only in the C-terminal domain. Because GCK is not product inhibited, some reports proposed that the 100kDa hexokinases descended from a different HK isoform that is not inhibited by G6P. Furthermore, it is predicted that the duplicated domain from the original gene evolved to become a regulatory domain. In support of this, studies have demonstrated that mutations in the regulatory domain that correspond to the catalytic half does not alter activity (14–16).

Tissue Expression and Glucose Affinity

HK isoforms share the common function of phosphorylating glucose and initiating glucose metabolism in the cell (14). Each tissue, however, has a distinct isoform dominantly expressed, but also, the possibility of other isoforms coexisting at varying levels. Importantly, this selectivity highlights the possible distinguishing roles that each isozyme plays in the regulation of each cell type where, additionally, the physiological state of the organism are also found to affect expression levels (8,17). HK1 has been reported to direct G6P primarily towards catabolism to generate ATP. HK1 has very high affinity for glucose with a very low Km at (0.04mM) (10). Additionally, this isozyme is ubiquitously expressed in nearly all tissues with highest expression in the brain, testis, kidney, and thymus (18). HK2, on the other hand, is

expressed in insulin-sensitive tissues such as adipose tissue, cardiac muscle, and skeletal muscle (19). The HK2 gene is regulated by many factors, some of which include the hormones insulin, glucagon, and catecholamines (20), but additionally are also influenced by hypoxic conditions (21,22). HK2 also has a high affinity for glucose with a Km of 0.13 (10) and is also regulated post-translationally. Additionally, it plays very important roles in development and in cancer cells (23). The HK3 isozyme is highly expressed in tissues such as kidney and lung, (24) and also has a low Km of about 0.02 for glucose (10). Glucokinase is a much more specialized hexokinase with dominant expression only in the pancreas and liver. It's affinity for glucose is much higher with a Km of approximately 4.5 and functions as the 'glucose sensor' of the cell (10).

Hepatic Glucose Metabolism

Glucose enters hepatocytes through the facilitative glucose transporter (glucose transporter-2; GLUT2) that allows bidirectional flow of glucose into and out of the cell. Unlike other peripheral tissues, liver glucose uptake is independent of insulin levels and is regulated primarily by circulating glucose concentration (25). Within the hepatocyte, GCK phosphorylates glucose to yield its product glucose-6-phosphate (G6P), and unlike the other HK isoforms, GCK is not inhibited by its product and has only a single active site (26). Studies *in vitro* have suggested that glucokinase is regulated transcriptionally by the hormones insulin and glucagon where insulin is found to upregulate GCK mRNA and activity while glucagon diminishes both (27). When glucose concentration is low in the cell, glucokinase regulatory protein (GKRP) acts as a competitive inhibitor of glucose binding to GCK and inhibits its function. The complex is then shuttled into the nucleus until intracellular glucose concentration increases and allows GCK to

return into the cytosol to perform its function (26). Furthermore, allosteric regulators have also been observed to modulate GCK activity such as fructose-1-phosphate (which activates GCK) and fructose-6-phosphate (which suppresses GCK activity) (28).

The hepatic G6P product can be directed into various metabolic pathways such as the pentose phosphate pathway (PPP), hexosamine pathway, glycolysis, and glycogen synthesis. In the postprandial state, insulin is released by the pancreas and hepatic glucose is predominately oxidized into carbon dioxide and generates an abundance of ATP. These pathways include glycolysis (which occurs in the cytosol), followed by the tricarboxylic acid (TCA) cycle (which occurs in the mitochondria), and then lastly through the electron transport chain (ETC), (which occurs in the inner mitochondrial membrane and is the site of oxidative phosphorylation) where most of the ATP is generated. The glycolysis pathway produces pyruvate from glucose, without the aid of oxygen, and additionally produces a small amount of ATP and NADH. Pyruvate may then be converted into lactate or enter the mitochondria and be subsequently converted into acetyl-coA by the enzyme pyruvate dehydrogenase (PDH). Acetyl-CoA may then enter the TCA cycle to build essential intermediates necessary for lipogenesis, nucleotide metabolism, and the ETC. In the fasting state, glucagon becomes the predominant hormone that is secreted by the pancreas and the liver produces glucose to be subsequently released into circulation to maintain healthy glucose levels. Glucose production is driven by the breakdown of glycogen (glycogenolysis) and by the synthesis of glucose (gluconeogenesis) (29,30).

HK Subcellular Localization

HK isozymes are not only differentially regulated and have distinct tissue expression profiles, but they also differ in their subcellular localization. Since HKs are glycolytic enzymes and glycolysis occurs in the cytoplasm, their localization was originally believed to be exclusively in the cytosol. However, since then, it has been shown that type I isozyme was found in particulate fractions that were primarily associated with the mitochondria (31–33). Interestingly, type II isozyme has also been found to be mitochondrial but a substantial amount was also observed in the cytosol (34–36). The N-terminal sequence forms an alpha helical secondary structure that is thought to interact with parts of the mitochondrial membrane via electrostatic and hydrophobic interactions. The N-terminal sequence is necessary for binding to the mitochondria since loss of binding to the mitochondria could be achieved by a peptide that corresponded to the N-terminal sequence, while not altering its activity (34,37–41). Specifically, voltage dependent anion channel (VDAC), an outer mitochondrial membrane protein, was found to interact with hexokinase where the interaction of isozyme I with a reconstituted VDAC1 required the N-terminal sequence domain (8,40,42,43). The other two isoforms, HK3 and GCK do not contain the mitochondrial N-terminal binding sequence and correspondingly, do not bind directly to the mitochondria.

Besides binding directly to the mitochondria, evidence suggests that the binding of HK isozymes can still associate with the mitochondria through additional protein-binding complexes. For example, it has been demonstrated that GCK association with liver mitochondria is comprised of a protein complex with BAD, protein kinase A and protein phosphatase 1 (PP1) catalytic units, and WAVE-1 (44). Additionally, GCK has been found to localize to the nucleus, where it is sequestered in an inactive state bound to glucokinase regulatory protein (GKRP)

under low glucose conditions. Furthermore, this effect is substantiated upon the addition of glucagon, mimicking the conditions that characterize a fasted physiological state. Upon higher extracellular glucose concentrations, mirroring the absorptive state, or low concentrations of fructose, GCK translocates back into the cytosol where it has been demonstrated to bind to 6-phosphofructo 2-kinase/fructose 2,6 bisphosphatase-2 (PFK2/FBPase2) and have increased capacity for glucose phosphorylation (45,46).

Effects of HK-VDAC Binding

Three VDAC isoforms exist in mammalian cells and are highly expressed on the outer mitochondrial membrane. VDACs are approximately 30 kDa in size and function to transport metabolites between the mitochondrial matrix and the cytosol (40,42,43,47,48). Studies have not confirmed that HK binding to the mitochondria requires VDAC, however, there is evidence suggesting HK localization to the mitochondria is enhanced via its interaction with VDAC, where the presence of their N-terminal sequence is required (47,49,50). Additional reports have observed that HK binding to VDAC occurs in mitochondrial sites where the inner mitochondrial membrane interacts with the outer mitochondrial membrane (51). VDAC binds with the inner mitochondrial membrane protein, adenine nucleotide translocase (ANT) to form the mitochondrial permeability transition pore complex (PTPC). Metabolites, such as the ATP, that are generated in the mitochondrial matrix, are transported through the PTPC to the cytosol. Furthermore, it has been shown that mitochondrial-bound hexokinase obtains preferential usage of mitochondrial-derived ATP for its function in phosphorylating glucose (8,52).

Localization of HKs to the mitochondria is dynamic, however, and has been reported to be influenced by many protein kinases (53). For instance, activation of protein kinase B (PKB), has been demonstrated to enhance HK binding to VDAC, while activation of glycogen synthase 3 beta (GSK3β) dislodges HK from VDAC. Consequently, the localization changes of HKs correspondingly alter the cell's metabolism and ultimately its fate. As an example, localization of HK2 to the mitochondria served to promote neuronal survival (54) whereas its localization to the cytosol was not sufficient to protect from cell death. Similarly, HK2 binding to the mitochondria in isolated hepatocytes prevented Bax-induced mitochondrial dysfunction and cell death, whereas localization in the cytosol promoted apoptosis (34). Overall, localization of the HK isoforms to the mitochondria, and in particular association with VDAC, have proven very important for downstream metabolism that may ultimately determine the fate of the cell.

Mitochondria and Mitochondrial Dynamics

Mitochondria play a vital role in cellular metabolism as it is a site for many metabolic processes such as the TCA cycle, β-oxidation of fatty acids, and oxidative phosphorylation (55,56) Crucial for maintaining normal function, mitochondrial health is regulated by many dynamic events that define its morphology which includes fusion (joining of mitochondria) and fission (division of the mitochondria). The dynamic regulation of these different events is necessary for normal physiology and its dysregulation is observed in diseased states (57,58).

Mitochondrial fusion is known to play a role in the regulation of mitochondrial DNA (mtDNA) levels which, in part, affects oxidative phosphorylation activity. Fusion occurs in a two-step process. First, the outer mitochondrial membrane proteins mitofusin1 (MFN1) and mitofusin2

(MFN2) mediate outer-membrane fusion and is then followed by inner-mitochondrial fusion regulated by optic atrophy 1 (Opa1). The genetic ablation of mitochondrial fusion genes causes increased fission events which results in the inhibition of essential content exchange between mitochondria and causes a significant decrease in mtDNA, membrane potential, and respiratory chain function (59–62)

On the other hand, mitochondrial fission is mediated by dynamin-related protein 1 (DRP1), a GTPase, that gets recruited by fission1 (FIS) to constrict the outer mitochondrial membrane for scission in a GTP-dependent manner. Fission events have also been involved with other mitochondrial events such as transport, mitophagy and apoptosis. There are two commonly discussed phosphorylation sites of DRP1 that correlate with different downstream events. Phosphorylation by protein kinase A (PKA) on the serine 637 site has been observed to inhibit DRP1 activity whereas the phosphorylation at the serine 616 site by mitogen-activated protein kinase (ERK) has been observed to promote mitochondrial fission. Overall mitochondrial fission is necessary for mitochondrial division, and for distributing mitochondria throughout the cell (63).

Global and Liver-Specific Rodent Models of HKs and Effects on Glucose Homeostasis

In vivo characterization of HKs, through both knockout and overexpression HK models, have advanced our understanding of the unique contributions each isozyme provides in terms of whole body glucose metabolism. For instance, global knockout of HK2 was observed to be important for development as the mice were embryonic lethal 7.5 days post-fertilization (64). Glucokinase global knockout mice were found to be either neonatally (65) or perinatally lethal (66). Specific

to the liver, one group found that GCK liver-specific knockout impaired glucose tolerance, hepatic glycogen stores, and reduced gene expression in genes important for *de novo lipogenesis* (DNL) but did not alter insulin secretion (67). Another utilized liver-specific heterozygous knockdown of GCK as a potential model of diabetes in mice and reported that after 6 weeks of age, mice had significantly higher glucose levels and impaired glucose tolerance (68). Overexpression models targeted to the liver have also been created with GCK where one group revealed adenoviral overexpression of hepatic GCK caused a 38% decrease in blood glucose with a corresponding 190% increase in circulating triglycerides and 310% increase in free fatty acids (69). Another study evaluated the effects of long term overexpression of hepatic GCK in mice and found after about one year, there were significantly increased rates of hepatic lipogenesis and circulating lipids which resulted in insulin resistance (4). Moreover, studies have demonstrated that hepatic GCK overexpression promotes hepatic fat accumulation in rodents and is positively correlated with fatty liver disease in humans (70,71).

HKs in the Liver

In the liver, GCK contributes a substantial amount of HK activity measured in hepatocytes where its product, G6P, enters the various anabolic and catabolic pathways such as lipid synthesis and glucose oxidation, respectively (27,72). However, in altered hepatic metabolic states, such as those seen in hepatocellular carcinoma, diabetes, and fatty liver diseases, GCK expression and function are considerably altered (70,73–76). In liver cancer, one of many reported changes that promotes the Warburg effect is an isozyme switch that occurs from GCK to HK2 (70,76). The Warburg effect, characterized by Otto Warburg, identified that unlike normal physiologic tissues, cancer tissues depend less on the mitochondria for ATP and obtain over 50% of their ATP via

glycolysis through conversion of pyruvate to lactate in the presence of oxygen. Bustamente and Pedersen et al. found that the hexokinase 2 isozyme is required for facilitating the highly glycolytic activity required in liver cancer cells. Moreover, they found that the Warburg effect was highly dependent on HK2 binding to the outer mitochondrial membrane as it greatly increased glycolytic flux given its direct coupling with the mitochondrial ATP synthesized on the inner membrane (77). A recent study also suggested that HKDC1 may be involved in hepatocellular carcinoma (HCC). HKDC1 expression was observed to be upregulated in HCC tissues when compared to normal adjacent tissue. Additionally, it was found that silencing of HKDC1 in HCC cells inhibited cell proliferation and migration and repressed expression of β-catenin and c-Myc (78). Besides liver cancer, however, the role of other HK isozymes in normal physiological states and in liver pathologies have not been extensively studied.

NON-ALCOHOLIC FATTY LIVER DISEASE (NAFLD)

NAFLD Disease and Significance

Non-alcoholic fatty liver disease (NAFLD) is a global health concern affecting over 1 billion people worldwide. In the United States alone, one-third of American adults are believed to have NAFLD and with the rising obesity and diabetes rates, it is projected to continue on the rise (79). NAFLD is characterized by having an accumulation of liver fat that is not due to excessive alcohol consumption nor through hepatitis. NAFLD can take the form of a simple fatty liver (benign fat accumulation) that does not lead to cirrhosis and also a more progressive form, nonalcoholic steatohepatitis (NASH), which can progress to cirrhosis, hepatocellular carcinoma, or liver failure (80). Additionally, about 20% of patients with prolonged simple steatosis will

develop into more severe forms of NAFLD (81). NASH is characterized by hepatocyte ballooning degeneration, lobular inflammation, and fibrosis, all in addition to the accumulation of steatosis. It is projected that within the next 20 years, NAFLD will become the major cause of liver-related morbidity and mortality, which greatly amplifies the need for understanding its progression (82).

The hallmark feature of NAFLD is the accumulation of hepatic free fatty acids and triglycerides that in part, may be contributing to the development of insulin resistance and obesity. The hepatic lipid accumulation is a product of increased dietary fat intake, esterification of free fatty acids, or due to hepatic de novo lipogenesis (DNL) (83). The components leading to the pathogenesis of NAFLD, however, are complex and defined in the literature by a few different theories. The most classic is the two-hit model of NAFLD development. This suggests that the "first hit" is characterized by the hepatic accumulation of lipids due to a high fat diet and sedentary lifestyle, and causing insulin resistance. The "second hit" is marked by the appearance of hepatic inflammation and associated fibrogenesis through the mechanisms of oxidative stress, lipid peroxidation, and mitochondrial dysfunction (84). Other models have challenged the two-hit model suggesting its development is much more complex where multiple hits play a role in the reprogramming of hepatocellular metabolism seen in NAFLD (85).

Multiple Hits Model of NAFLD

Insulin resistance (IR) is one of the multiple hits responsible for the development of NAFLD (86,87). There are many accumulating factors that may promote IR due to one's environment, dietary intake and content, and genetics. IR causes increased hepatic DNL and impairs inhibition

of adipose tissue lipolysis, resulting in an increased influx of fatty acids into the liver (88). Moreover, IR leads to dysfunction in adipose tissue that causes altered production and secretion of inflammatory cytokines and adipokines such as IL-6, TNFα, and IL1β (89).

Another hit is the accumulation of fat leading to hepatic lipotoxicity, where mitochondrial dysfunction, oxidative stress, ROS production, and endoplasmic reticulum (ER) stress can all be detrimental consequences in the liver (90). Fat accumulation takes the form of triglycerides, synthesized by the esterification of fatty acids and glycerol. Fatty acids may enter the liver either through direct absorption from the intestines, lipolysis from adipose tissues, or via hepatic DNL. Newly synthesized hepatic triglycerides can either be stored or secreted, each having distinct rates of turnover. Accumulation of fat may be due to impairment of TG secretion via VLDL, impairment of β-oxidation (commonly seen in insulin-resistant states) or increased rate of lipogenesis due to increased activation of hepatic DNL transcription factors and enzymes such as SREBP1c and ChREBP (91). Additionally, an excess of intake of nutrients causes ER stress, leading to activation of unfolded protein response (UPR), that can ultimately lead to eventual apoptosis of the cell (92).

Lastly, oxidative stress is another hit contributing to the progression of NAFLD. A decrease in mitochondrial DNA (mtDNA), morphological changes of the mitochondrial, and alterations in mitochondrial potential and respiration may all contribute to mitochondrial dysfunction causing oxidative stress. This stress is caused by an over production of ROS, which activates inflammasomes to secrete Il-1β, as well as, activates caspases signaling the cell for apoptosis (93).

POTENTIAL ROLE OF HKDC1 IN NAFLD PROGRESSION

Potential Link Between HKDC1 and Mitochondrial Dysfunction

A recent report indicated a possible role of HKDC1 in response to ER Stress and mitochondrial dysfunction. *Evstafieva et al.* observed induction of HKDC1 mRNA expression in HCT116 cells after incubation with mitochondrial dysfunction inhibitors myxothiazol (an electron transport chain (ETC) complex III inhibitor) and Piericidin A (an ETC complex I inhibitor). Additionally, induction of ER stress with incubation of tunicamycin and brefeldin A, both inducers of UPR, increased HKDC1 dramatically (94).

Overall, the precise mechanisms describing the progression from simple steatosis to steatohepatitis and beyond remains unclear. Given that HKs are the first enzyme to initiate glucose metabolism, and that the only HK isozyme that has been explored in the context of NAFLD has been GCK, we aim to explore how the novel hexokinase, HKDC1, contributes to the hepatocellular pathophysiology of fatty liver diseases.

Chapter 2

Characterization of HKDC1

ABSTRACT

Recent publications from our group have suggested Hexokinase Domain Containing-1 (HKDC1) to be a novel 5th hexokinase (HK). This was demonstrated in cancer cell lines that overexpressed and silenced HKDC1 where there was an increased and decreased cellular hexokinase activity, respectively. However, due to potential compensation by other endogenous HK isoforms, we developed a more precise method of measuring HKDC1's hexokinase activity. We first purified recombinant human HKDC1 alongside with GCK and HK1 and found we could not determine the Km of HKDC1 due to its low level of activity. Next, using MI54-CHO cells, a cell-line with low basal HK activity, we found stable overexpression of HKDC1 to contribute a modest amount of activity when compared to empty-vector, but less so than HK2 and GCK at all glucose concentrations measured. Altogether, we found HKDC1 to have low glucose-phosphorylating ability.

We then demonstrated HKDC1 subcellular localization to the mitochondria via the ubiquitous outer mitochondrial membrane protein voltage dependent ion channel (VDAC) in hepatocytes. After observing its localization to the mitochondria, we hypothesized that overexpression of HKDC1 would alter downstream metabolism. Surprisingly, we found that its overexpression results in a reduced glycolytic capacity and maximal mitochondrial respiration with reductions in both glucose oxidation and mitochondrial membrane potential. Together, this suggests a defect in mitochondrial function.

Lastly, to assess the effects of overexpression of hepatic HKDC1 on glucose homeostasis *in vivo*, we injected mice with adenovirus containing human HKDC1 and confirmed liver-specific overexpression. Anticipating that hepatic overexpression would influence liver energy storage, we found that it was not sufficient to alter hepatic energy storage, but did lead to a mild improvement in glucose tolerance. Overall, our data shows a more in depth characterization of HKDC1 and a possible link with mitochondrial dysfunction.

INTRODUCTION

About a decade ago, the hexokinase-like gene, HKDC1, was identified by *Irwin et al.* through extensive phylogenetic analyses. They hypothesized that HKDC1 would have hexokinase (HK) function since the gene possesses an intact open reading frame of 917 amino acids, conservation among all the mammalian genomes they analyzed, high amino acid sequence homology with hexokinase 1 (HK1), and contains the amino acids necessary for glucose and ATP binding (1).

HK isoforms differ greatly in their affinity for glucose (Km) and their catalytic efficiency. HK1, hexokinase 2 (HK2), and hexokinase 3 (HK3) all have high affinity for glucose, whereas glucokinase's (GCK) affinity is much lower and is described as the glucose sensor HK in tissues such as the pancreas and the liver (8). Previously, our group reported the first characterization of HKDC1's HK function using cancer cell lines. Overexpression of HKDC1 significantly increased the overall cellular HK activity, whereas its knockdown had diminished activity (7). Our studies, here, further examine its HK function *in vitro* and in cells that contain low basal HK activity to bypass any potential HK isozyme compensation (MI54-CHO cells).

In addition to their kinetic differences, HK isoforms are further distinguished by their subcellular localization. HK1 is primarily associated with the mitochondria, whereas HK2 is dynamic between the cytosol and the mitochondria. They both require their intact N-terminal sequence in order to associate with the mitochondria, whereas HK3 and GCK lack this sequence and consequently do not associate with the mitochondria (31–34,36–41). Specifically, HK1 and HK2 have been reported to bind to the outer mitochondrial membrane protein voltage dependent anion

channel (VDAC). In conjunction with other mitochondrial membrane proteins, VDAC forms the mitochondrial permeability transition pore, which is known to regulate metabolites and ions between the cytosol and mitochondria (8,40,42,43,47,49,50). Studies show that binding of HK to VDAC promotes changes in downstream metabolism that may ultimately affect the fate of the cell (8,40,42,43,47,52,95). The present studies investigate HKDC1's mitochondrial localization, association with VDAC, and mitochondrial metabolism.

RESULTS

HKDC1 has reduced HK activity, but co-localizes with mitochondria as other HKs.

We began by examining HKDC1's kinetic properties by purifying recombinant human HKDC1 and performing HK activity assays alongside GCK and HK1. Although we are able to approximate the Michaelis Menten Constant, Km, for both GCK and HK1, we could not determine the Km of HKDC1 due to its low level of activity (Fig. 1A). We additionally tested different experimental conditions that may affect its activity. First, we tested different nucleotides such as ATP, GTP, CTP, and TTP and found differences in activity, but nothing that surpassed the highest activity reading measured with ATP. Next, we measured activity after adding increasing amounts of ATP, but the maximum activity was still very low. Lastly, we measured activity titrating in increasing amounts of Mg^{2+}, but observed similarly low affinity HK activity for HKDC1 (Fig. 1B-D). Furthermore, given that HK1's catalytic activity is confined to the C-terminus and allosteric regulation occurs at the N-terminus (96), we explored if the inter-domain interaction of HKDC1 was interfering with its overall activity. However, after purifying the N- and C- terminal domains and running the HK activity assays separately, we observed similar low affinity HK activity as seen with the intact full-length protein (Fig. 1E).

A

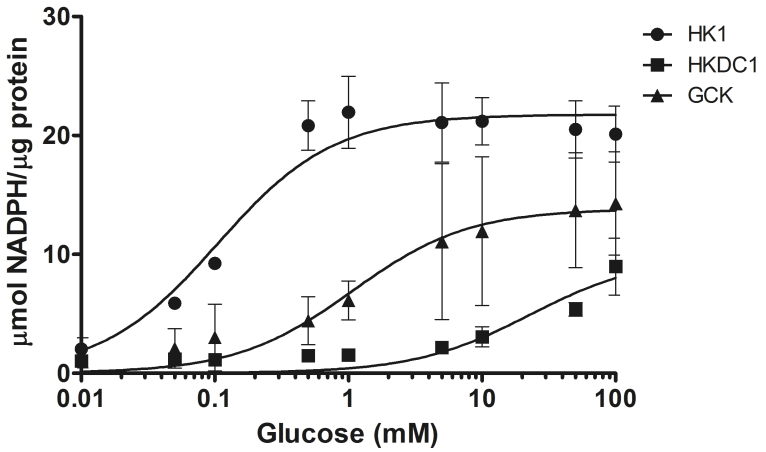

Figure 1. HKDC1 is a low activity hexokinase that is modulated by co-factors. (A) Specific activity of purified HKDC1, as compared to Hexokinase 1 (HK1) and Glucokinase (GCK), relative to NADPH standard measured from 0.01mM to 100mM glucose concentrations (circles = HK1, squares = HKDC1, triangles = GCK (n=3, where each n represents an individually prepared protein purification).

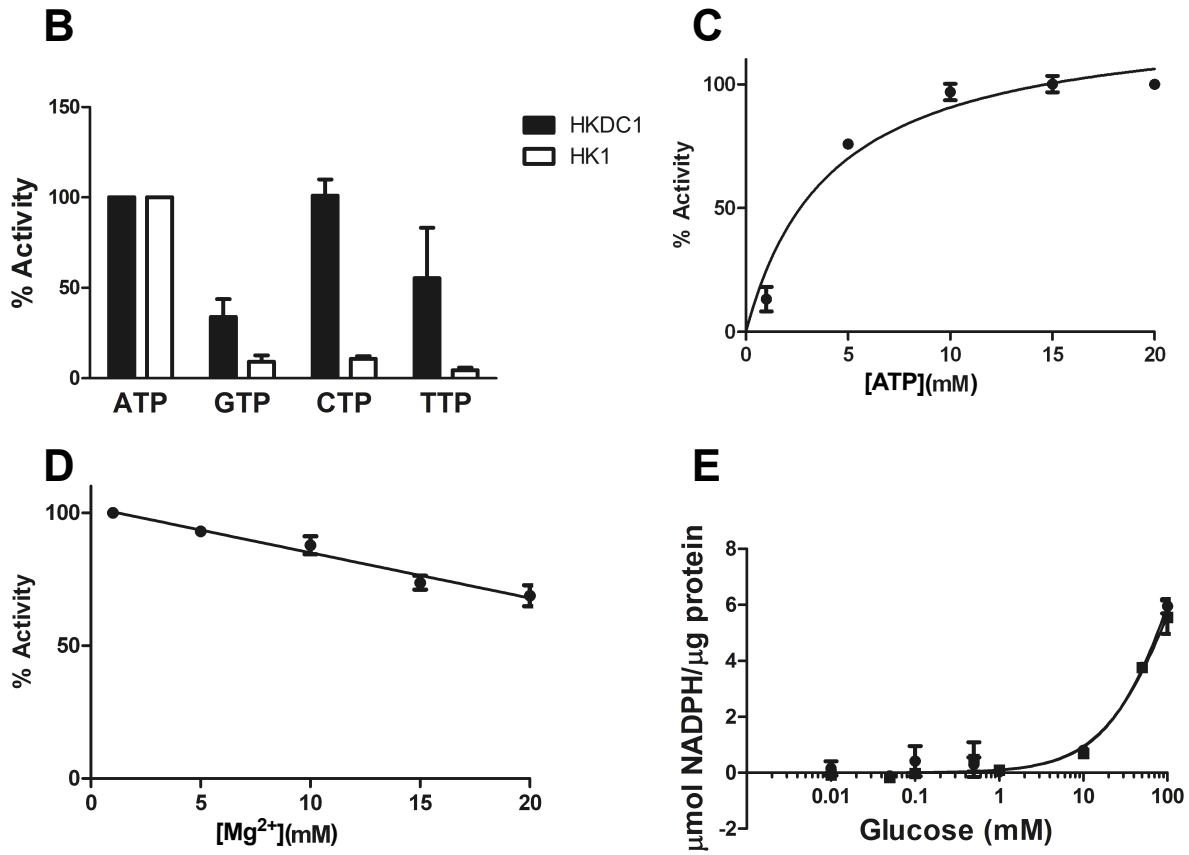

Figure 1. HKDC1 is a low activity hexokinase that is modulated by co-factors. (B) Percent activity of HKDC1 and HK1 supplemented with alternative nucleotides. Nucleotide and glucose concentrations were 5mM and 100mM, respectively (n=3 biological replicates). **(C)** ATP concentrations varied from 1-20mM (n=3 biological replicates). **(D)** Mg2+ concentrations ranged from 1-20mM (n=3 biological replicates). **(E)** Individual hexokinase activity of purified N- (circles) and C-terminal (squares) domains separately with varying glucose concentrations (0.01-100mM) (n=3 biological replicates). All values are mean ± S.E.M.

We next wanted to examine HKDC1's contribution to overall cellular HK activity, as it is possible HKDC1 requires posttranslational modifications or protein binding partners. We generated a stable HKDC1 over-expression cell line in MI5-4 CHO cells [an established line with minimal HK activity (97)] in order for exclusive determination of HKDC1 activity with minimal contribution from other HKs in examining HK activity. HKDC1 produced a significant but only modest amount of total HK activity compared to the empty vector (EV) stably over-expressed line at all concentrations of glucose but less than that of HK2 and GCK over-expression cell lines (Fig. 2A and B).

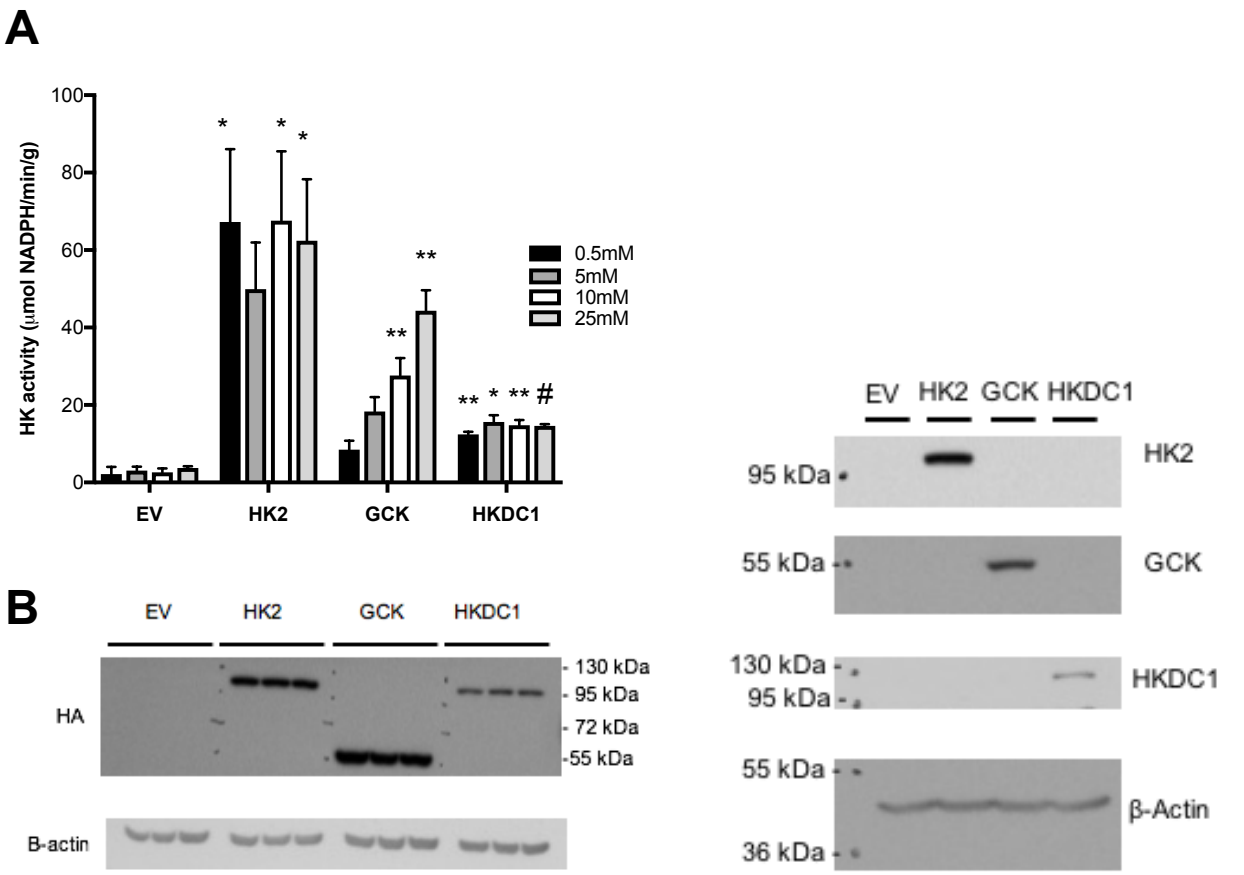

Figure 2. HKDC1 contributes a modest amount of hexokinase activity in cells. (A) HK activity measured in MI5-4 CHO cells overexpressing empty vector (EV), Hexokinase 2 (HK2), GCK, or HKDC1 at 0.5, 5, 10, and 25mM glucose concentration [n=3 biological replicates except for 5mM glucose (n=2)]. **(B) (A)** Immunoblot of CHO cells overexpressing Empty Vector (EV), Hexokinase 2 (HK2), Glucokinase (GCK), and HKDC1 where HK2, GCK, and HKDC1 were probed with HA (left) and HK2, GCK, and HKDC1 (right). Beta-actin served as loading controls for both (n=3 biological replicates). All values are mean ± S.E.M. *P<0.05, **P<0.001, #P<0.0001 (*Student's t-test*).

As previously reported, HKDC1 shares 71% sequence identity with HK1 (1). Given this high sequence homology, it was surprising to find that HKDC1 did not have similarly high activity. Therefore, to elucidate any salient structural differences that may account for the low activity observed, we obtained a predicted structural model of HKDC1 (98% of the residues were modeled with 100% confidence) using the *Phyre2 web portal* (98) and superimposed this model onto human HK1 using PyMol2.0 (Fig. 3A). Interestingly, the HKDC1 model aligned an appreciable amount with HK1 with similar positioning of the amino acids necessary for allosteric inter-domain communication and for carrying out catalysis (96). However, we noted a few deviations between some of the key amino acid residues involved in the allosteric (Fig. 3B and C) and catalytic (Fig. 3D) sites. For two of the main salt bridges involved in inter-domain communication in HKI, the distance between the residues for both HK1 and HKDC1 are the same, however, there is a shift of 4.4 angstroms (Fig. 3B). In the second site, the distance between the interaction of the residues is less for HKDC1 than that of HK1 and there is an additional 4.7 angstrom shift (Fig. 3C). Similar patterns were seen in the catalytic active site, where the distance between the key amino acids involved were about 2.1 angstroms closer for HKDC1 and a notable 8.5 angstrom shift from HK1 at its widest point (Fig. 3D). These structural differences between HKDC1 and HK1 in key residues involved in the catalytic and allosteric sites may impact the enzymatic activity of HKDC1.

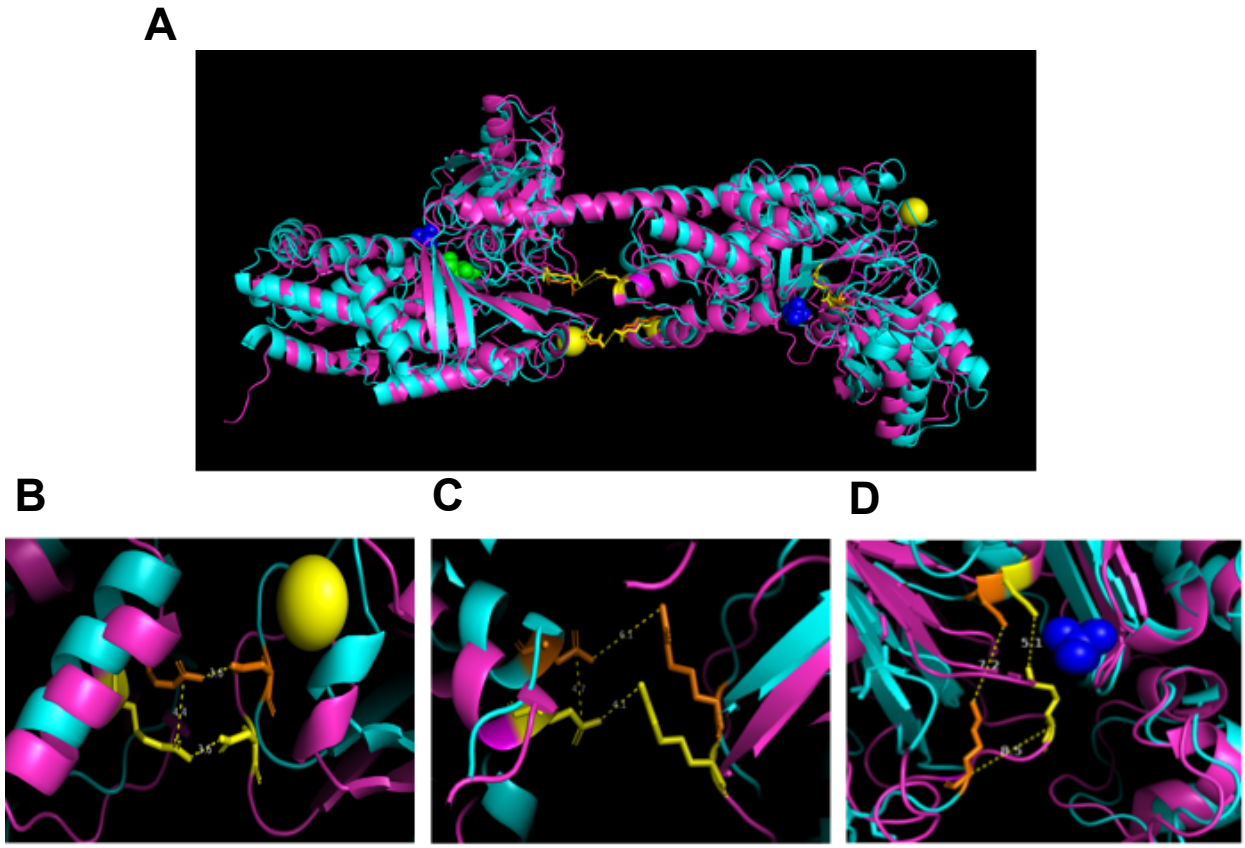

Figure 3. HKDC1 has deviations in catalytic and allosteric site residues. (A) Homology model of human HKDC1 (magenta) using the Phyre2 web portal for protein modeling, prediction and analysis superimposed on human HK1 (PDB:1hkc; cyan) complexed with K^+ (yellow), PO_4^{3-} (blue) and glucose (green) using PyMol2.0. **(B)** Inter-domain salt bridge site 1: distance between carboxy-groups of residues D251 (yellow left) and R800 (yellow right) for HKDC1 and D251 (orange left) and R801 (orange right) for HK1 are both 3.6 Å apart with a 4.4 Å shift between HKDC1 and HK1. **(C)** Site 2: distance between carboxy-groups of residues R69 (yellow left) and E813 (yellow right) for HKDC1 is 4.1 Å and R69 (orange left) and D814 (orange right) is 6.1 Å with a 4.7 Å shift between HKDC1 and HK1. **(D)** Catalytic active site distance between

D656 (yellow top) and Y620 (yellow bottom) residues for HKDC1 is 5.1 Å and D657 (orange top) and Y621 (orange bottom) for HK1 is 7.2 Å and between HKDC1 and HK1 is 8.5 Å.

In addition to their activity differences, HK isozymes are reported to have particular protein-binding partners and subcellular localization preferences that define their role in glucose metabolism (8); therefore, we first determined potential binding partners of HKDC1 by overexpressing FLAG-tagged human HKDC1 in HEK293 cells. Interestingly, mass spectrometry analysis from the Co-IP showed that HKDC1 might be associated with the outer mitochondrial membrane proteins Voltage Dependent Anion Channel 1 and 2 (VDACI and II), canonical mitochondrial binding partners of HKI and HKII (Fig. 4A). As the other HKs (HKI and II only) contain a N-terminal mitochondrial localization sequence region, we observed that human and mouse HKDC1 also share sequence similarity in this region of the protein (Fig. 4B).

A

Protein Abbreviation	Localization	Coverage	#Peptides	#PSM	#Amino Acids	MW
HKDC1	Cyto/Nuclear/Mito	39.59	32	107	917	102.5
RPS3	Cyto/Nuclear	15.64	3	6	243	26.7
DDx3Y	Cyto/Nuclear	6.39	3	6	657	72.9
FBL	Nuclear	18.78	3	6	229	25.3
DDX17	Cyto/Nuclear	6.13	3	6	652	72.5
THRAP3	Nuclear	3.46	3	5	955	108.6
HIST1H3A	Nuclear	30.15	2	3	136	15.4
RPS6	Cyto/Nuclear	9.64	2	3	249	28.7
WDR56	Cytoplasm	1.68	1	3	1250	144.9
DOCK4	Cyto/Golgi/Membrane	0.46	1	2	1966	225.1
RPL19	Cytoplasm	13.28	1	2	128	15.0
RPS2	Cyto/Nuclear	29.55	1	2	44	5.1
RPLP0	Cyto/Nuclear	8.11	1	2	111	12.2
FAM98A	Nuclear	4.81	1	2	312	34.4
CDK1	Cyto/Nuclear/Mito	6.73	1	1	297	34.1
DEFB119	Extracellular	10.71	1	1	84	9.8
RPL7	Cyto/Nuclear	5.29	1	1	208	24.4
LMNA	Cyto/Nuclear	2.65	1	1	491	55.7
ATP5B	Mitochondria	5.93	1	1	270	28.4
SRSF10	Cyto/Nuclear	6.40	1	1	172	20.9
RPS11	Cyto/Nuclear	22.78	1	1	79	9.5
HNRNPM	Nuclear	7.07	1	1	99	10.0
FLNA	Cytoplasm	2.15	1	1	604	66.6
RPS8	Cytoplasm	32.21	5	10	208	24.2
NONO	Nuclear	9.77	3	6	471	54.2
RPL24	Cytoplasm	10.74	1	5	121	14.4
HIST2H3A	Nuclear	30.15	2	4	136	15.4
TMEM263	Membrane	31.03	2	4	116	11.7
RPS27	Cyto/Nuclear	19.70	1	3	66	7.4
CHTOP	Nuclear	5.24	1	2	248	26.4
RPL4	Cyto/Nuclear	4.50	2	2	333	37.6
VDAC2	Mitochondria Outer Membrane	7.84	1	2	255	27.5
H3F3B	Nuclear	31.06	2	2	132	14.9
PABPC1	Cyto/Nuclear	22.67	1	2	75	8.4
HNRNPUL1	Nuclear	2.34	1	2	641	71.7
ATP5A1	Mitochondria Inner Membrane	19.48	1	2	77	8.3
SSBP1	Mitochondria	12.40	1	2	121	14.1
RPL13	Multiple locations	6.35	1	2	126	14.7
G3BP1	Cyto/Nuclear/Membrane	5.99	1	2	284	31.4
PKM	Cyto/Nuclear	6.41	1	2	281	30.7
EIF4A1	Cytoplasm	18.82	1	2	85	9.3
UBAP2L	Cytoplasm	3.92	1	2	383	40.2
G3BP2	Cytoplasm	2.70	1	1	482	54.1
PRDX1	Cytoplasm	5.03	1	1	199	22.1
RPS25	Cyto/Nuclear	8.00	1	1	125	13.7
FAU	Cytoplasm	16.95	1	1	59	6.6
VDAC1	Mitochondria Outer Membrane	8.13	1	1	283	30.8
RPL37A	Cyto/Nuclear	26.47	1	1	68	7.6
HSPD1	Mitochondrial Matrix	15.82	1	1	158	17.1
RPL11	Nuclear	10.69	1	1	131	14.9
UBB	Cyto/Nuclear	37.21	1	1	43	4.9
RPL26L1	Other	23.68	1	1	38	4.5
PHB	Mitochondria Outer Membrane	9.68	1	1	124	13.7

B

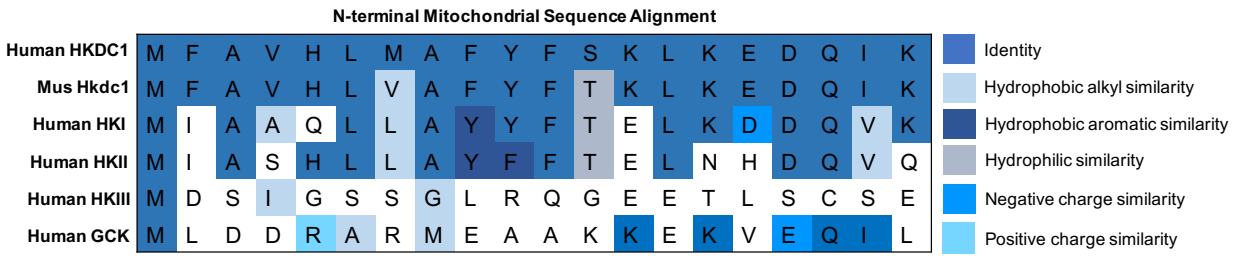

Figure 4. HKDC1 localizes to the mitochondria via its N-terminal localization sequence. (A) List of co-immunoprecipitated proteins by MS/MS-orbitrap analysis depicted by protein symbol, localization, coverage, number of peptides, number of peptide spectrum matches, number of amino acids, and molecular weight. Proteins of interest are highlighted in blue: HKDC1, VDAC1, and VDAC2. **(B)** N-terminal amino acid alignment and homology of human HKDC1 with mouse (mus) Hkdc1, human HKI, human HKII, human HKIII and human GCK where dark blue represents sequence identity with human HKDC1 and other colors represent similar homology based on the amino acid side groups.

Moreover, the HK isozymes are reported to interact with VDAC through this region (20–23). Because of this, we sought to determine whether HKDC1 localizes to the mitochondria via its N-terminal sequence in hepatocytes. We, therefore, transfected primary mouse hepatocytes with plasmid that contains GFP-tagged Full Length HKDC1 and GFP-tagged N-terminal truncated HKDC1 (first 20 residues that serve to bind to mitochondria are truncated), and determined its intracellular localization of HKDC1 under high and low glucose (25mM or 5mM, respectively) conditions. Full length HKDC1 significantly co-localized with the mitochondria, while the N-terminal truncated HKDC1 was observed in the cytosolic compartments under both high (Fig. 4C) and low glucose conditions (Fig. 4D). Furthermore, we discovered HKDC1 co-localized with VDAC in primary hepatocytes by immunofluorescence (Fig. 4E and Fig. S1A-B). Taken together, HKDC1 is a low activity HK that may, in part, be due to the differences noted in its structure when compared to HK1. Moreover, it appears to co-localize with the mitochondria through its N-terminal mitochondrial localization sequence, similar to HKI and II. Given its low HK activity and its interaction with the mitochondria, the next question that arises is whether hepatic HKDC1 expression alters metabolism in the liver.

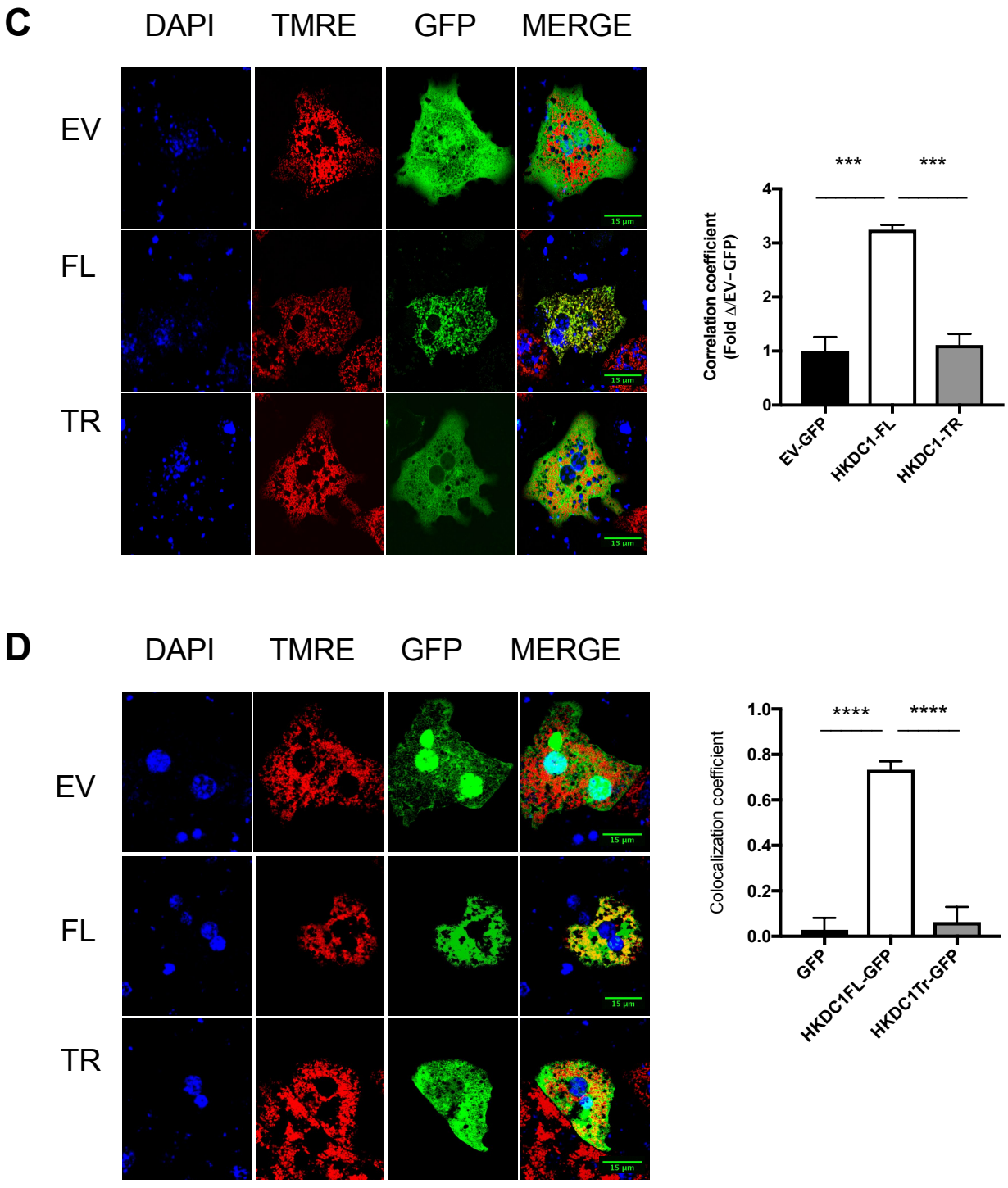

Figure 4. HKDC1 localizes to the mitochondria via its N-terminal localization sequence. (C) Representative 40X confocal images of transfected primary mouse hepatocytes with GFP-tagged

empty vector (EV), GFP-tagged HKDC1 full length (FL), and GFP-tagged HKDC1 truncated (TR, where HKDC1 is missing the first 20 amino acids) cultured in 25mM glucose (19-27 GFP+ hepatocytes co-localization coefficients were averaged). Hepatocytes were stained for DAPI and tetramethylrhodamine, ethyl ester (TMRE) and quantification of co-localization between GFP and TMRE was depicted via calculation of the co-localization coefficient (n=3 biological replicates). **(D)** Representative 40X confocal images of transfected primary mouse hepatocytes with GFP-tagged empty vector (GFP-EV), HKDC1 full length (GFP-HKDC1 FL), and HKDC1 truncated (GFP-HKDC1 TR, where HKDC1 is missing the first 20 amino acids) cultured at 5.5mM glucose. Hepatocytes were stained for DAPI and TMRE and quantification of co-localization between GFP and TMRE was depicted via calculation of the co-localization coefficient (10 individual hepatocytes with fluorescence was analyzed for co-localization coefficients per condition for each n, where n = 2 independent mouse hepatocyte isolations were prepared).

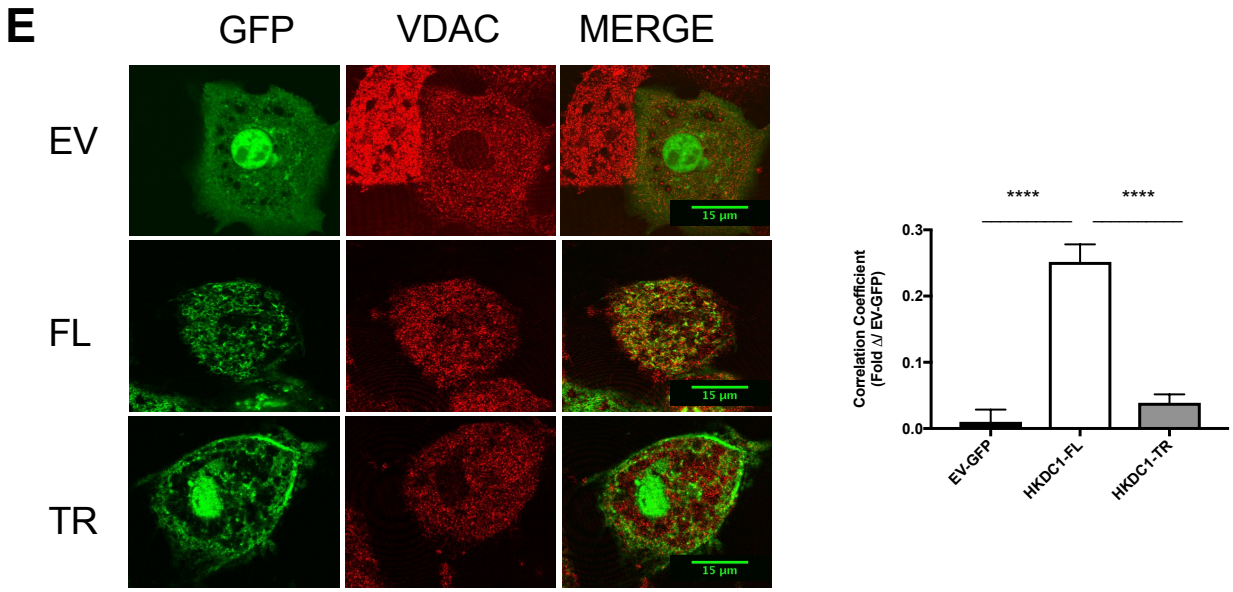

Figure 4. HKDC1 localizes to the mitochondria via its N-terminal localization sequence. (E) Representative 40X confocal images of transfected primary mouse hepatocytes with EV, FL, and TR cultured in 25mM glucose and stained with VDAC antibody (15-21 GFP+ hepatocytes co-localization coefficients were averaged). Quantification of GFP and VDAC was depicted via calculation of the co-localization coefficient (n=3 biological replicates). All values are mean ± S.E.M. ***P<0.001, ****P<0.0001 (*One-way ANOVA*).

Human HKDC1 reduces glycolytic capacity and mitochondrial activity in mouse hepatocytes.

To test how overexpression of HKDC1 affects hepatic metabolism, we isolated primary mouse hepatocytes and measured changes in extracellular acidification rate (ECAR) and oxygen consumption rate (OCR) after treating with Ad-HKDC1 or Ad-GFP. While we observed no overt differences in basal glycolysis, we found significantly reduced oligomycin-induced glycolysis (Fig. 5A), suggesting a defect in glycolytic metabolism. Next, we assessed differences in respiration and found a significant reduction in OCR after the addition of the un-coupler, FCCP (maximal mitochondrial respiration) for the cells treated with Ad-HKDC1, a sign of mitochondrial dysfunction, relative to Ad-GFP (Fig. 5B). Thus, the expression of this non-canonical hexokinase impairs both cellular glycolytic capacity and maximal respiration in primary hepatocytes.

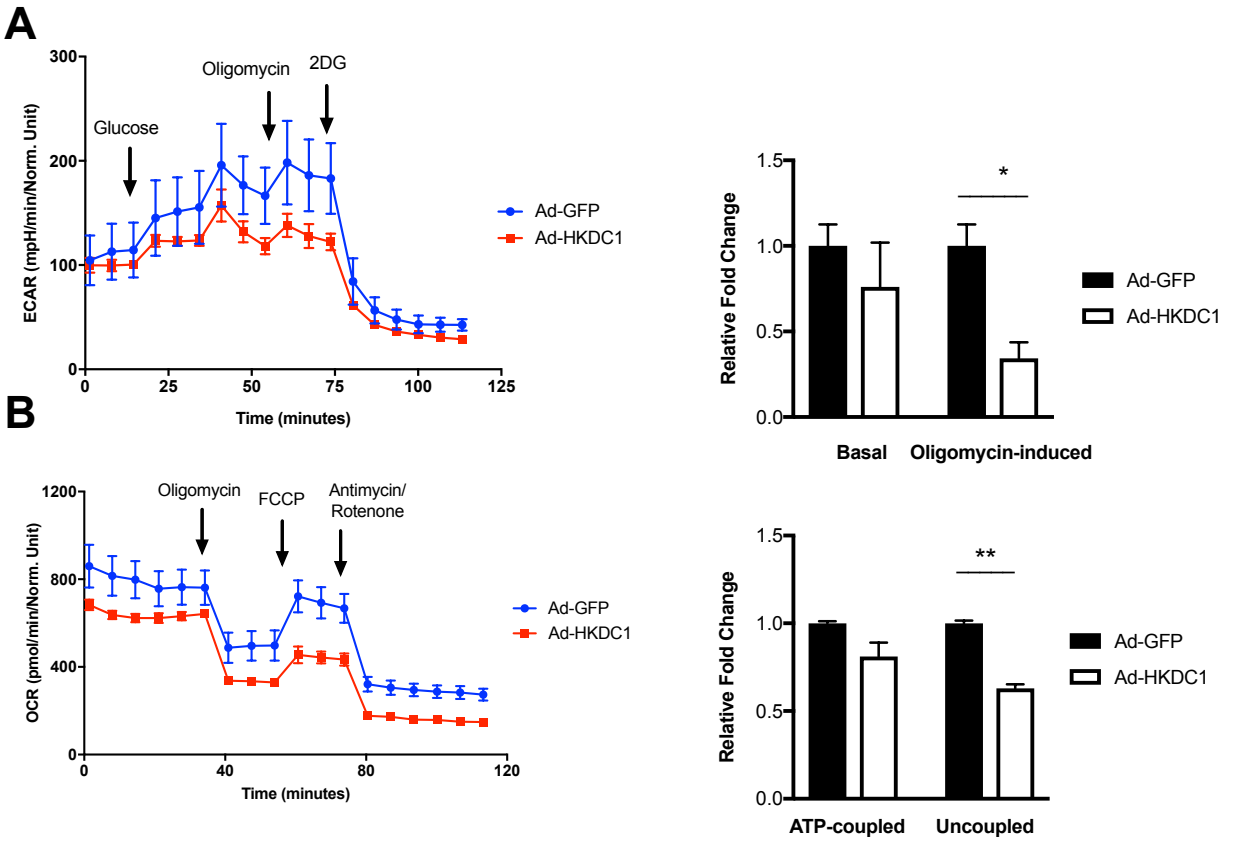

Figure 5. Overexpression of HKDC1 reduces glycolytic capacity and maximal respiration. Seahorse extracellular flux analyzer (SEFA) measurement of **(A)** ECAR or **(B)** OCR in primary mouse hepatocytes treated with adenovirus containing Human HKDC1 (Ad-HKDC1) or GFP (Ad-GFP). Bar graphs representing basal ECAR or oligomycin-induced ECAR **(A)** or ATP-coupled OCR and uncoupled OCR **(B)** (shown on the right). For **(A)** and **(B),** 4-6 individually treated wells were averaged per n, and n represents hepatocytes isolated from 1 mouse (n=2). All values are mean ± S.E.M. *P<0.05, **P<0.005 *(Student's t-test)*.

To investigate the reduced OCR phenotype further, we utilized ^{14}C-labeled glucose to directly measure glucose oxidation after overexpression of HKDC1 in primary hepatocytes and observed a significant decrease, consistent with our OCR finding (Fig. 6A). This finding is in contrast with what is found after adenoviral-mediated overexpression of GCK in rat hepatocytes, which results in significantly upregulated glucose oxidation (101). Also, overexpression of GCK in liver of mice leads to hepatic fat accumulation (69,71,102,103) and it is strongly associated with progression of NAFLD in mice and humans (75). To examine whether human HKDC1 contributes to the deposition of hepatic fat, we first measured the incorporation of ^{14}C-labeled glucose into the lipid phase and found it was significantly increased after overexpression of HKDC1 (Fig. 6B). However, studies have found that the amount of glucose incorporation into the glycerol backbone of triglycerides is approximately only 0.5% of metabolized glucose (83). Therefore, we examined if the Kennedy pathway (the pathway that converts glycerol-3-phosphate that is generated by the preparatory phase of glycolysis into the synthesis of triglycerides) was significantly affected after overexpression of HKDC1 but we found there were no changes in gene expression of the key enzymes (Fig. S2). To more directly assess the rate of lipogenesis, we utilized radiolabeled acetate. We again found that the labeled triglycerides were not altered in hepatocytes that overexpressed HKDC1 (Fig. 6C). Lastly, we analyzed fatty acid oxidation by ^{14}C-labeling of palmitic acid and observed a mild but not a significant reduction (Fig. 6D).

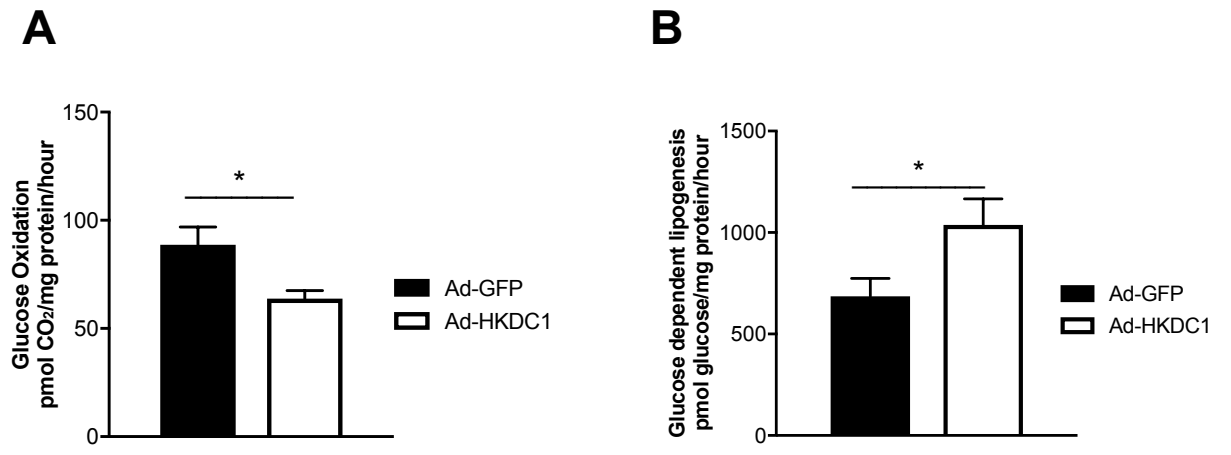

Figure 6. Overexpression of HKDC1 reveals signs of mitochondrial dysfunction. Isolated primary mouse hepatocytes were treated with indicated viruses where measurements of **(A)** Glucose oxidation was measured using ^{14}C-labeled glucose **(**n=4 adenoviral-treated wells) **(B)** Glucose-dependent lipogenesis was measured using ^{14}C-labeled glucose (n=4, each n represents separately plated and treated hepatocytes isolated from one mouse).

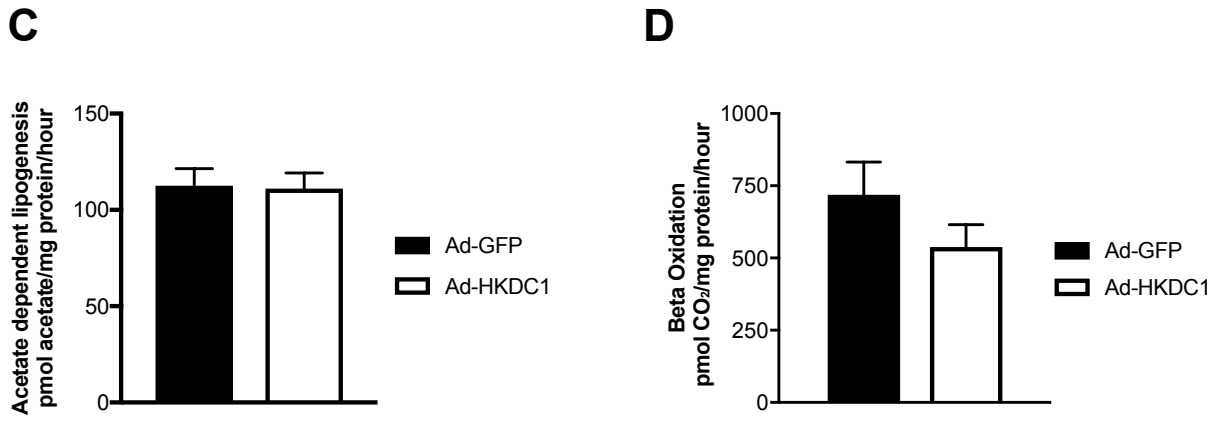

Figure 6. Overexpression of HKDC1 reveals signs of mitochondrial dysfunction. (C) Acetate-dependent lipogenesis was determined using ^{14}C-labeled acetate and **(D)** beta oxidation was determined using ^{14}C-labeled palmitate (n=4, each n represents separately plated and treated hepatocytes isolated from one mouse). All values are mean ± S.E.M. *P<0.05 *(Student's t-test)*.

Given that we found no direct changes in hepatic triglyceride accumulation but found reduced OCR and ECAR with overexpression of HKDC1, we next analyzed changes in mitochondrial function by measuring TMRE intensity as a marker for mitochondrial membrane potential (104). We tested the effects of overexpressing full length and truncated HKDC1 to assess if HKDC1 binding to the mitochondria is inducing changes in mitochondrial potential. We found that full length HKDC1 caused the intensity to significantly decrease (Fig. 7A and Fig. 7B).

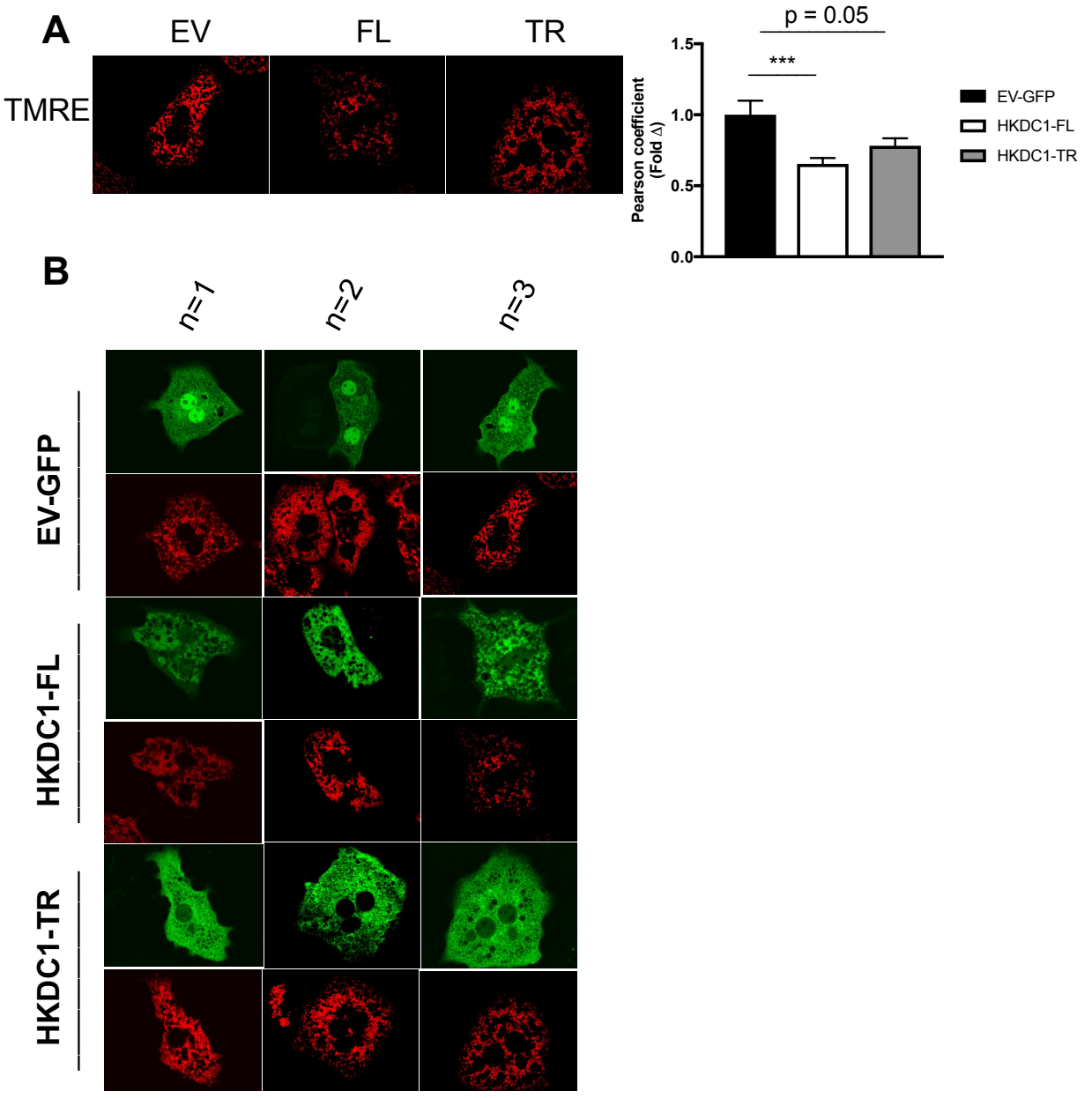

Figure 7. Mitochondrial membrane potential is diminished in hepatocytes overexpressing full length HKDC1. (A) Representative 40X confocal images after overexpression of GFP-tagged EV, FL, and TR in hepatocytes where mitochondria were stained with TMRE and the mitochondrial membrane potential was measured via fluorescence intensity (n=3, where each n

represents hepatocytes isolated from 1 mouse and intensity was averaged from a total of 16-32 individual hepatocytes). **(B)** Representative images of each biological replicate illustrating a GFP+ hepatocyte and its respective TMRE intensity for GFP-tagged EV, GFP-tagged HKDC1-FL and GFP-tagged HKDC1-TR (n=3). All values are mean ± S.E.M. ***P<0.0001 (*One-way ANOVA*).

Given that HKDC1 overexpression caused changes in mitochondrial potential, we investigated if there were any changes in mitochondrial morphology events such as mitochondria fusion and fission since fission is thought to correlate with reduced mitochondrial potential and dysfunction. Interestingly, we also found that overexpression of HKDC1 may play a role in mitochondrial dynamics as we noted the mitochondrial fusion protein, Mitofusion 2, and a mitochondrial fission protein, Dynamin-related-protein 1, to be significantly upregulated in mouse livers (Fig. 8A and 8B). These data suggest that the hepatic overexpression of HKDC1 shows signs of mitochondrial dysfunction, and does not directly drive lipogenesis under these above conditions.

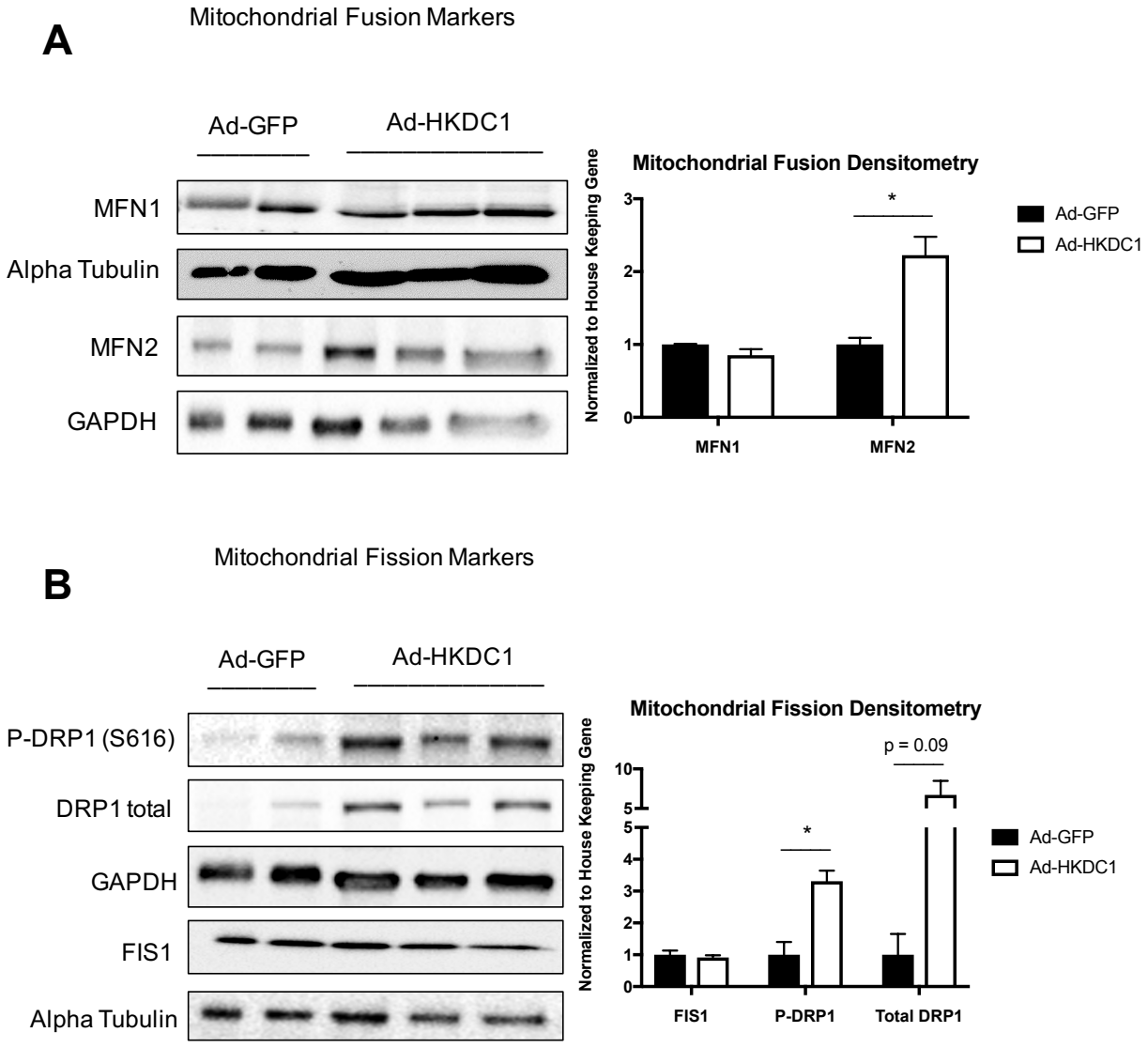

Figure 8. Overexpression of HKDC1 alters mitochondrial dynamics. (A) Western blots of mitochondrial fusion proteins mitofusin 1 (MFN1) and mitofusin2 (MFN2) after *in vivo* overexpression of Ad-GFP or Ad-HKDC1. Densitometry analysis of MFN1 was normalized to GAPDH and MFN2 was normalized to alpha-tubulin (n=2-3 biological replicates). **(B)** Western blots of mitochondrial fission proteins fission1 (FIS1), Dynamin-1-like protein (DRP1) and phosphorylated-DRP1 [P-DRP1(S616)] after *in vivo* overexpression of Ad-GFP or Ad-HKDC1. Densitometry analysis of FIS1 normalized to

alpha-tubulin and P-DRP1 and DRP1 total normalized to GAPDH (n=2-3 biological replicates). All values are mean ± S.E.M. *P<0.05.

Acute *in vivo* overexpression improves glucose tolerance but does not alter hepatic energy storage

To investigate the *in vivo* effects of overexpressing human HKDC1 in mouse livers, we injected 10^9 adenoviral particles of adenovirus containing human HKDC1 or GFP in wildtype mice after which they were sacrificed 7-10 days later. As illustrated, human HKDC1 was expressed significantly and exclusively in the liver, validating our approach of liver overexpression (Fig. 9A). In addition, the mouse *Hkdc1* expression was not altered in the mice overexpressing human HKDC1 (Fig. 9B).

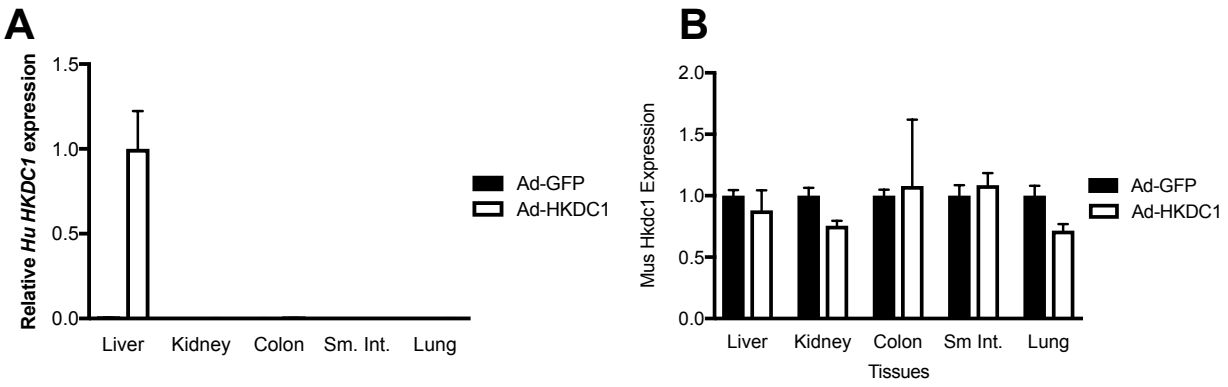

Figure 9. Verification of a hepatic-specific overexpression of HKDC1 mouse model. **(A)** Relative human *HKDC1* mRNA expression in various tissues seven days post injection of adenovirus containing human HKDC1 (Ad-HKDC1) or GFP (Ad-GFP, n=2-3 biological replicates). **(B)** Relative mouse *Hkdc1* mRNA expression in various tissues post injection.

We next performed an intraperitoneal glucose tolerance test (IPGTT) to observe the effects of hepatic overexpression. We observed a mild but significantly improved glucose tolerance at the time points 15 and 60 min, with a mild but non significant decrease in the area under the curve. During the IPGTT, no changes in insulin levels at time points 0 and 15 min were observed (Fig. 10A). These results are in line with what we found previously in our aged Hkdc1$^{+/-}$ mice, where they had significantly impaired glucose tolerance (2). In addition, we performed an insulin tolerance test and found a mild increase in insulin sensitivity in the mice overexpressing HKDC1, but it was not significant (Fig. 10B).

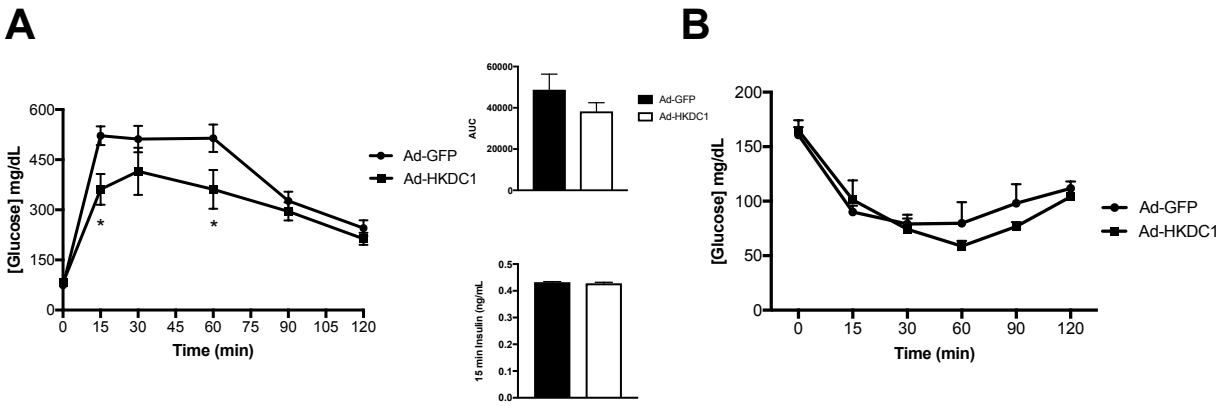

Figure 10. Characterization of hepatic-specific overexpression of HKDC1 mouse model. **(A)** Plasma glucose concentrations during an intraperitoneal glucose tolerance test (IPGTT) from mice 10 days post injection with corresponding area under the curve (AUC; n=5-6) and insulin values at 15 min (n=2-3 biological replicates). **(B)** Plasma glucose concentrations during an insulin tolerance test (ITT; n=3).

Furthermore, we looked at all the baseline parameters including body weight, liver weight, fasting plasma glucose, insulin, triglycerides (TGs), and non-esterified fatty acids (NEFAs) and found no significant changes (Fig. 10C). Similarly, we found no changes in hepatic gene expression from various metabolic pathways including glycolysis (Gapdh, Ldh, Pklr), citric acid cycle (Cs), gluconeogenesis (G6pc, Pck1), ppar regulation (Ppar α,β,γ), fatty acid synthesis (Scd1, Fas), fatty acid oxidation and export (Cpt1a, Cd36, Fabp1, Mtp; Fig. 10D), and the Kennedy Pathway genes (Plpp, Agpt1, Agpt2, Lpin1, Lpin2, Dgat1, Gpat; Fig. S2), nor changes in energy storage including triglycerides (illustrated with Oil red O stain and image quantification on the right) and glycogen (illustrated with PAS/DPAS stain and image quantification on the right; Fig. 10E). Lastly, to confirm this finding, we extracted triglycerides (Fig. 10F) and glycogen (Fig. 10G) and found no changes in their content. These data indicate that acute overexpression of HKDC1 on normal chow fed diet does not substantially alter glucose homeostasis or energy storage in the liver.

C

	Ad-GFP	Ad-HKDC1
Fasting Body Weight (g)	22.83 ± 0.64	22.63 ± 0.53
Liver: Body Weight ratio (g/BW)	0.061 ± 0.008	0.052 ± 0.0013
Fasting Glucose (mg/dL)	82.75 ± 7.92	75.56 ± 2.76
Fasting Insulin (ng/mL)	0.41 ± 0.018	0.40 ± 0.011
Fasting Plasma TGs (mg/dL)	76.16 ± 6.49	80.49 ± 8.56
Relative Fasting Plasma NEFA levels	1.04 ± 0.12	0.94 ± 0.072

D

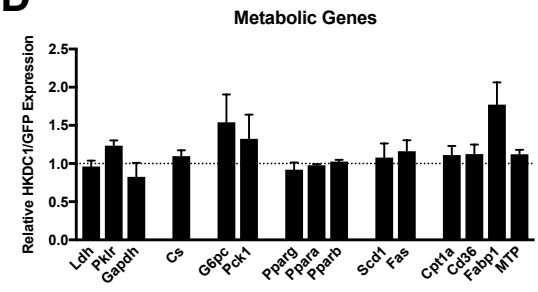

Figure 10. Characterization of hepatic-specific overexpression of HKDC1 mouse model. (C) Table with baseline characterization values including fasting body weight, liver to body weight ratio, fasting plasma glucose, fasting plasma insulin, fasting plasma triglycerides (TGs), and relative fasting plasma non-esterified fatty acid (NEFA) levels (n=3-9 biological replicates). **(D)** Selected gene expression measured from different metabolic pathways in the livers of mice 10 days post injection: lactate dehydrogenase (Ldh), pyruvate kinase (Pklr), glyceraldehyde-3-phosphate dehydrogenase (Gapdh), citrate synthase (Cs), glucose-6-phosphatase (G6pc), phosphoenolpyruvate carboxykinase 1, peroxisome proliferator-activated receptor γ,α,β, (PPAR γ,α,β), stearoyl-coA desaturase-1 (Scd1), fatty acid synthase (Fas), carnitine palmitoyltransferase 1 (Cpt1a), fatty acid translocase (Cd36), fatty acid binding protein 1 (Fabp1), microsomal triglyceride transfer protein (Mtp, n=3-6 biological replicates).

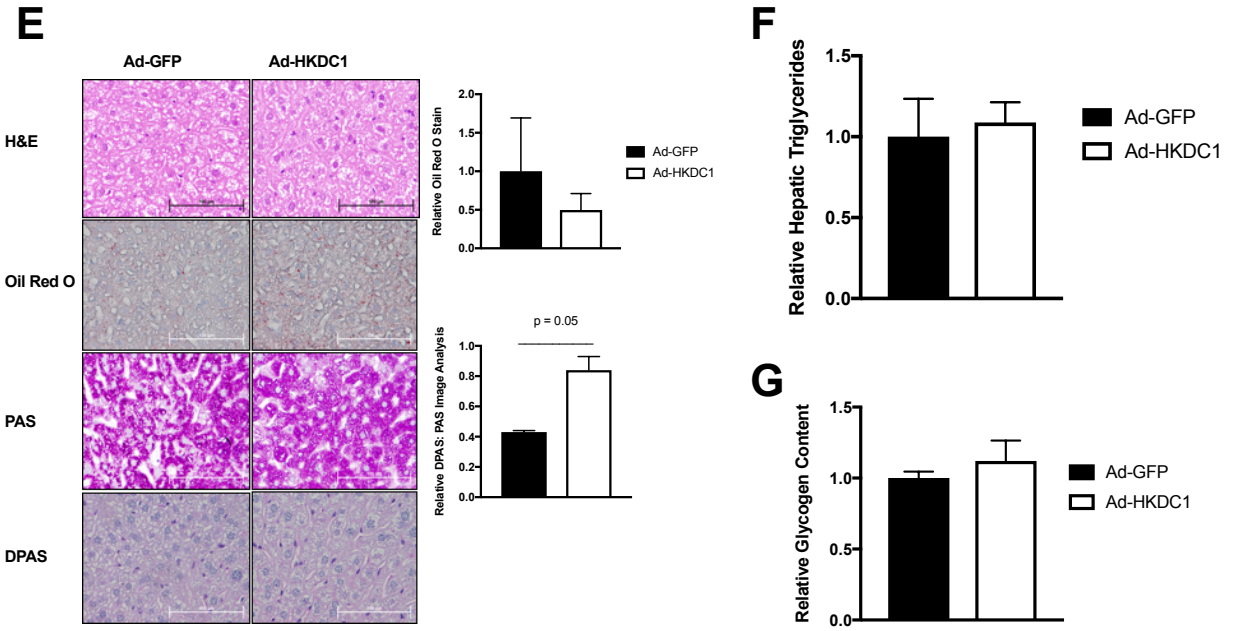

Figure 10. Characterization of hepatic-specific overexpression of HKDC1 mouse model. (E) Representative H&E, Oil red O, PAS, and DPAS staining of liver sections of mice injected with indicated viruses. Images were taken at 40X and scale represents 100μm. Image Stain intensity quantification (right) of Oil red O stain for intracellular triglyceride levels and image stain intensity quantification of the ratio of anti-stain of DPAS to PAS, as an indicator of glycogen content (n=3 biological replicates where each n represents 4-5 images from one mouse liver section). **(F)** Hepatic triglyceride content and **(G)** hepatic glycogen content of mouse livers in the re-fed state, where mice were fasted for 16 hours overnight and then re-fed for 4 hours (n=4-6 biological replicates). All data are represented as mean ± SEM. *P<0.05 (*Student's t-test*).

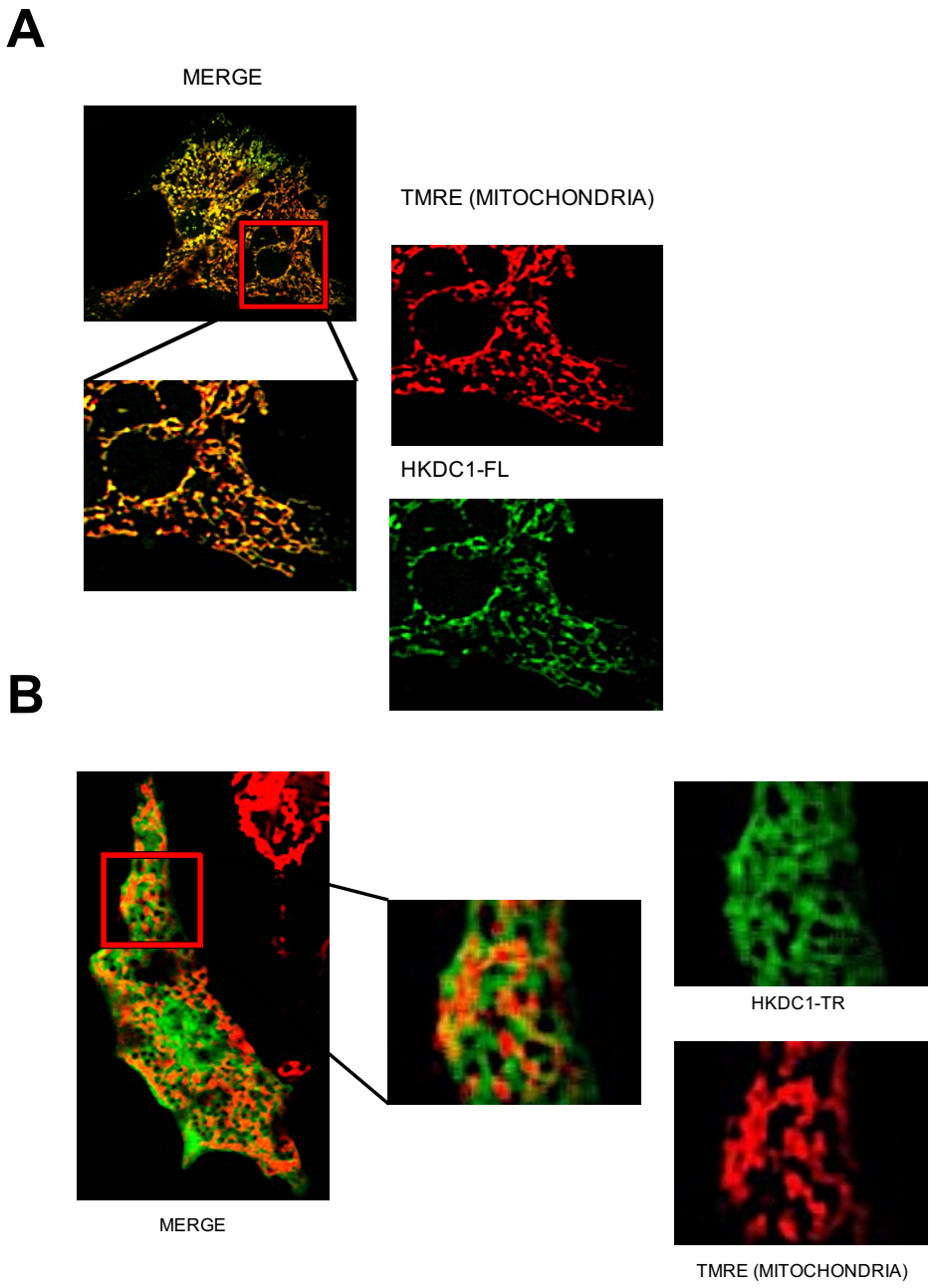

Supplemental Figure 1. HKDC1 localizes to the mitochondria via its N-terminal localization sequence. (A) Zoomed in representative image of co-localization of GFP-tagged HKDC1-FL and the mitochondrial stain TMRE. **(B)** Zoomed in representative image of co-localization of GFP-tagged HKDC1-TR and the mitochondrial stain TMRE.

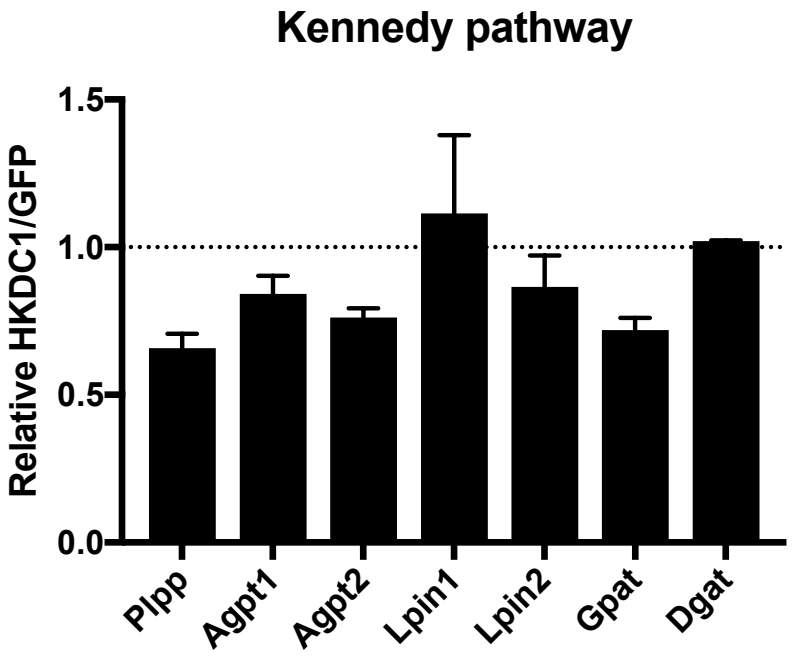

Supplemental Figure 2. Overexpression of HKDC1 does not affect genes in the Kennedy Pathway. Relative expression of the Kennedy pathway measured from the livers of mice overexpressed *in vivo* with adenovirus containing HKDC1 relative to adenovirus containing GFP. Genes include Phospholipid Phosphatase 1 (Plpp), Angiopoietin 1 (Agpt1), Angiopoietin 2 (Agpt2), Lipin-1 (Lpin1), Lipin-2 (Lpin2), Glycerol-3-Phosphate Acyltransferase1 (Gpat1) and Diacylglycerol O-Acyltransferase 1 (Dgat1) (n=3-5 biological replicates).

Supplemental Table 1. Primer Sequences Used for qPCR.

Gene	Forward Primer	Reverse Primer
Mus Hkdc1	5’ CAAAATGTTGAGATGGAGAGCC 3’	5’ GCAGTCGGCTACGTAGTCAAAAAG 3’
Mus 18S	5’ CTCAACACGGGAAACCTCAC 3’	5’ AGACAAATCGCTCCACCAAC 3’
Human HKDC1	5’ GGTCAGGATGCTGCCCACCT 3’	5’ CCCAAGATCCAGGGCGAGAA 3’
Human Beta Actin	5’ GTGGCCATCTCTTGCTGCAAG 3’	5’ GGGAAATCGTGCGTGACATTAAG 3’.
Cloning Primers for GFP-HKDC1-TR	5’ TACCGGACTCAGATCTCGAGATGGTGGACAGGTTCCTGTATCACATGCGG 3’	5’ CACCATGGTGGCGATGGATCCGTTCTCCTTCTGTGCCTGCTGTAACC 3’
Cloning Primers for GFP-HKDC1-FL	5’ TACCGGACTCAGATCTCGAGATGTTTGCGGTCCACTTGATGGCA 3’	5’ CACCATGGTGGCGATGGATCCGTTCTCCTTCTGTGCCTGCTGTAACC 3’
Amplification of pEGFP-N3-FL-HKDC1	5’ GACTCTAGAGGATCCAATGTTTGCGGTCCACTTGAT 3’	5’ CACAGAAGGAGAACTACCCATACGATGTTCCTGACTATGCGTAGCGCGGTTCGAAGGTA 3’
Lactate dehydrogenase (Ldh)	5’ TGCCTACGAGGTGATCAAGCT 3’	5’GCACCCGCCTAAGGTTCTTC 3’
Carnitine palmitoyltransferase 1a (Cpt1a)	5’ ACCAACGGGCTCATCTTCTAA 3’	5’ CAAAATGACCTAGCCTTCTATCGA 3’
Peroxisome proliferator-activated receptor alpha (Pparα)	5’ CAGGAGAGCAGGGATTTGCA 3’	5’ CCTACGCTCAGCCCTCTTCAT 3’
Fatty acid binding protein 1 (Fabp1)	5’ TCAAGCTGGAAGGTGACAATAA 3’	5’ GTCTCCATTGAGTTCAGTCACG 3’

Cluster of differentiation 36 (Cd36)	5’ TGGCCTTACTTGGGATTGG 3’	5’ CCAGTGTATATGTAGGCTCATCCA 3’
Pyruvate Kinase (Pklr)	5’ AGGAGTCTTCCCCTTGCTCT AC 3’	5’GGAGAGGCGTTTCAGGATATG 3’
Microsomal triglyceride transfer protein (Mtp)	5’ TGGTGAAAGGGCTTATTCT GTT 3’	5’ TTGCAGCTGAATATCCTGAGAA 3’
Citrate synthase (Cs)	5’ GGAAGGCTAAGAACCCTTG G 3’	5’ TCATCTCCGTCATGCCATAGT 3’
Glucose-6-phosphatase (G6pc)	5’ TCGAGGAAAGAAAAAGCC AAC 3’	5’ CAATGCCTGACAAGACTCCA 3’
Phosphoenol pyruvate carboxykinase 1 (Pck1)	5’ TGGGGTGTTTGTAGGAGCA G 3’	5’ CCAGGTATTTGCCGAAGTTG 3’
Peroxisome proliferator-activated receptor g (Pparg)	5’ GTGCCAGTTTCGATCCGTA GA 3’	5’GGCCAGCATCGTGTAGATGA 3’
Stearoyl-coA desaturase-1 (Scd1)	5’ GTCAGGAGGGCAGGTTTC 3’	5’ GAGCGTGGACTTCGGTTC 3’
Fatty acid synthase (Fas)	5’ GCTGCGGAAACTTCAGGAA AT 3’	5’ AGAGACGTGTCACTCCTGGACTT 3’
Phospholipid Phosphatase 1 (Plpp)	5’ AATCAACTGCAGTGATGGC T 3’	5’ AAGACAACCTGCCCTCCTTG 3’
Angiopoietin 1 (Agpt1)	5’ CACCCAGGATGTGAGAGTC TG 3’	5’ CGTTTGAAGGGCAGCATGGA 3’
Angiopoietin 2 (Agpt2)	5’ CTTCATCAACCGCCAGCAA G 3’	5’ ACACTTTGAGATTCTCCTTGACCA 3’
Lipin-1 (Lpin1)	5’ CCTTCTATGCTGCTTTTGGG AACC 3’	5’ GTGATCGACCACTTCGCAGAGC 3’
Lipin-2 (Lpin2)	5’ AGTTGACCCCATCACCGTA	5’ CCCAAAGCATCAGACTTGGT 3’

	G 3’	
Glycerol-3-Phosphate Acyltransferase1 (Gpat1)	5’ CAACACCATCCCCGACATC 3’	5’ GTGACCTTCGATTATGCGATCA 3’
Diacylglycerol O-Acyltransferase 1 (Dgat1)	5’ TGGTGTGTGGTGATGCTGATC 3’	5’ GCCAGGCGCTTCTCAA 3’
Glyceraldehyde-3-phosphate dehydrogenase (Gapdh)	5’ TCACCACCATGGAGAAGGC 3’	5’ GCTAAGCAGTTGGTGGTGCA 3’

MATERIALS AND METHODS

Animals

All mice were 8-12-week-old male mice with a C57Bl/6 background (unless otherwise noted) and were obtained from Jackson Laboratory and housed under a 12-hour light, 12-hour dark cycle with *ad libitum* access to normal chow (Envigo) unless otherwise noted. All mouse studies were approved by IACUC and performed in accordance with the Guide for the Care and Use of Laboratory Animals at both Northwestern University and University of Illinois at Chicago.

Adenovirus Construction and Production

Adenovirus construction was produced as previously described (7,105). Briefly, the plasmid RC221178 (OriGene) containing the 2,750 bp HKDC1 open reading frame was cloned into the adenoviral shuttle vector pShuttle-CMV (Agilent) from the BamHI/NotI site. From there, the HKDC1 adenoviral shuttles were linearized and transformed into BJ5138-AD1 cells (Agilent). The recombinant clones were then isolated and digested using PacI. Next, the digested recombinant plasmid DNA and FuGene were transfected into HEK293 cells (Clontech) to generate the recombinant adenovirus. Viral lysate was then collected in 2mL freeze/thaw buffer (10mM Tris/HCl, pH 8.0, 1mM $MgCl_2$) and after two freeze thaws, the virus was purified via ultracentrifugation on a CsCl gradient. Afterwards, the virus was de-salted with a 7k MWCO column (Thermo Scientific) and equilibrated with 10% glycerol-supplemented freeze/thaw buffer. Titer was determined by measured by OD_{260} and by plaque assay.

Overexpression of Human HKDC1 in mice

In vivo transduction of adenovirus

Mice were injected 10^9 viral particles (106) of adenovirus containing either human HKDC1 (Ad-HKDC1) or GFP (Ad-GFP) via the penile vein at 10-12 weeks of age. Mouse tissues were harvested 7-10 days post injection for end-point analyses.

Metabolites

Mice were fasted for 16 hours overnight and the following metabolites were measured: glucose, insulin, NEFA levels, and triglycerides. For glucose, blood was obtained from tail veins and measured with a One-Touch Ultra Glucometer. Blood was also obtained from tail vein using heparinized capillary tubes and centrifuged at 8000 rpm for 15 min for serum collection. Insulin levels were then determined by an ELISA (ALPCO). NEFA levels were measured following the manufacturers' instructions (Wako Diagnostics, Richmond, VA). Triglycerides were determined using Infinity Triglyceride Solution (ThermoFisher Scientific).

Hepatic Triglycerides and Glycogen

Animals were fasted for 16 hours overnight and were either sacrificed or then re-fed for 4 hours before being sacrificed. Harvested livers were immediately flash frozen in liquid nitrogen and then stored at -80° until analyses were performed. For triglycerides, livers were homogenized on ice using a glass douncer and PBS. Homogenates were cleared by centrifugation at 13,000 rpm, and the supernatant was collected. Hepatic triglycerides were determined using the Infinity Triglyceride Solution (ThermoFisher Scientific). For glycogen, flash-frozen liver samples were either determined using the Glycogen Assay Kit (Sigma, MAK016-1KT) or analyzed by ^{13}C-nuclear magnetic resonance for glycogen levels at the Yale Mouse Metabolic Phenotyping

Center (Yale University, New Haven, CT).

Histology

Sections of liver were either embedded in OCT or paraffin. Briefly, for OCT, a section of the liver was stored in 4% paraformaldehyde (PFA) for 1 hour at room temperature (RT) and subsequently washed in PBS. After the washes, the liver sections were subjected to a sucrose gradient and then stored in 10% sucrose at 4° C O/N. The next day, liver sections were embedded in OCT and stored in -80° C. For paraffin embedding, liver sections were fixed in 4% PFA for 24 hours at RT. The next day, sections were washed in 50% ethanol and then stored in 70% ethanol until embedding in paraffin. Embedded sections were sent to the Mouse Histology and Phenotyping Laboratory (supported by NCI P30-CA060553 awarded to the Robert H Lurie Comprehensive Cancer Center) for embedding in paraffin and further sectioning of both OCT and paraffin embedded liver sections and stained with H&E, Oil Red O, PAS, or DPAS. Images were taken with Olympus BX51 Fluorescence Microscope from Resources Research Center at the University of Illinois at Chicago.

For image analysis, Fiji (Image J) software was used for analysis of Oil Red O, PAS, and DPAS stains. For Oil Red O, tiff files were converted into 32 bit images and the threshold was set to select the Oil Red O intensity of each image. Once threshold was performed, pixel intensity was measured along with image area. The image intensity divided by the area gave a quantification of Oil Red O staining intensity per image. An ImageJ macro was created to systematically quantify multiple images. For PAS, the stain was quantified using the same method as for Oil Red O. For DPAS, tiff files were converted into 32 bit images and inverted color threshold was used to quantify the white pixel intensity and area of each image file. The white area represented the

amount of PAS stain that was removed, which was a quantification of glycogen that was removed by diastase. DPAS measurement was divided by the PAS stain to obtain the amount of glycogen per group.

Glucose and Insulin tolerance test

Intraperitoneal glucose tolerance tests (IPGTTs) were performed on mice fasted 16 hours overnight with glucose given by intraperitoneal injection at a dose of 2g glucose/kg of body weight. Glucose levels were measured by the tail vein, as mentioned above, and taken at multiple time points (from 0 - 120 min) during the IPGTT. Area under the curve (AUC) values were calculated by standard approaches using the trapezoidal rule and represented as mean ± SEM. Additionally, blood was collected at 0 and 15 minutes in heparinized capillary tubes and centrifuged at 8000 rpm for 15 minutes to collect the serum. Insulin levels in these samples were determined as mentioned above. Insulin tolerance tests (ITT) were performed on mice fasted for 6 hours and then IP injected with 0.75 U/kg body weight of Humalog insulin (Eli Lily & Co). Blood glucose levels were determined similarly as the GTT.

Lentivirus Production in MI5-4 CHO cells

Dr. Nissim Hay (University of Illinois Chicago) kindly provided MI5-4 CHO cells. These CHO cells were cultured in α-MEM (Cellgro) and supplemented with 10% FBS and 1% penicillin/streptomycin. Lentivirus production was performed according to Addgene's protocol https://www.addgene.org/protocols/lentivirus-production/. Briefly, pLenti6-D-TOPO vector, containing rat-HK2, human GCK, or human HKDC1 were also provided by Dr. Nissim Hay and

were co-transfected with both psPAX2 and pMD2.G into 293 T-cells. Transduction was performed overnight in the presence of polybrene without antibiotics. Blasticidin (10ug/ml) was then used for selection of successfully transduced cells for one week.

RNA isolation and qPCR

RNA was extracted from 10mg of livers using TRIzol Reagent (Life Technologies) and chloroform for phase separation. RNA was then purified using the Rneasy minikit (Qiagen) and treated with RNase-Free DNase (Qiagen). 1μg of purified RNA was then reverse transcribed using qScript Reverse Transcriptase (Quanta Biosciences) and quantified via qPCR using PerfeCTa SYBR Green SuperMix (Quanta Biosciences) where final primer concentrations were 0.625μM for each reaction and data were analyzed via the CFX Connect Real-Time PCR Detection System (BioRad). See list of primers (Supplemental Table 1).

Hexokinase Activity Assay

Hexokinase Microplate Assays for purified hexokinases

To assay hexokinase activity, 2μg of purified full length HK proteins, or C- and N- terminal domains of HKDC1 separately, were diluted in 20 μl of HK dilution buffer (20mM KH_2PO_4, 100mM KCl, 1mM $MgCl_2$, 1mM EDTA, 1mM DTT, 60g/l glycerol, 1g/l bovine serum albumin). Samples were loaded onto a microplate and mixed with 100 μl of reaction buffer (50mM HEPES pH 7.4, 100mM KCl, 8mM $MgCl_2$, 5mM ATP, 0.5mM $NADP^+$, 1 unit/ml G6PDH (from *Leuconostoc mesenteroides*), 1mM DTT, 1g/l bovine serum albumin, and 0.01 to 100mM D-(+)-glucose). Alternative nucleotides GTP, CTP, and TTP were substituted for ATP at a concentration of 5mM. ATP and Mg^{2+} concentrations were tested between 0 and 20mM.

Reactions were incubated at 37°C for 1 hour and stopped with 174 µl of buffer C (0.46mM SDS and 300mM NaH_2PO_4, pH 8.0). Fluorescence of NADPH was measured at Excitation/Emission (Ex/Em) of 340/450nm. Specific activity was determined using an NADPH standard.

Hexokinase Assay Using MI5-4-CHO cells With Stable Overexpression of HK2, GCK and HKDC1

Hexokinase activity was determined as previously described (107). Briefly, $8x10^6$ cells were plated on 6-cm dishes and allowed to attach overnight. The next day, cells were washed once with PBS and harvested by scraping and pelleted at 4,000 rpm for 5 minutes. Cell were lysed by sonication, 5 pulses of 1 second, in 100µl homogenization buffer: 0.2% Triton X-100, 0.5mM EGTA, 10mM D-(+)-glucose, 11.1mM monothioglycerol, 45mM Tris-HCl (pH 8.2), and 50mM KH_2PO_4. After sonication, lysates were centrifuged at 8,000 RPM for 5 minutes. HK activity was determined by whole-cell lysate's ability to phosphorylate glucose over 2 minutes in an assay mixture with final concentrations of: 50mM triethanolamine chloride, 7.5mM MgCl2, 0.5mM EGTA, 11mM monothioglycerol, 0.5mM to 25mM glucose, 6.6mM ATP, 0.5mg/ml NADP, and 0.5U/mL G6PDH, pH 8.5. Glucose-6-phosphate formation was measured indirectly by NADPH production from G6P dehydrogenase by measuring absorbance at 340nm on a spectrophotometer and was normalized to protein concentration as determined using Bio-Rad protein Assay Dye Reagent Concentrate.

Protein Purification

Protein was purified as previously described (7). Briefly, Rosetta 2 (DE3) (EMD Millipore) cells were transformed with pReceiver-B01 plasmid (Addgene) containing *HKDC1*, *HK1*, or *GCK*.

100ml of TPM media (Sigma) containing 50mg/ml ampicillin and 34mg/ml chloramphenicol were inoculated with a single colony and grown overnight at 37°C. The pre-growth culture was added to 500mL of the same media and grown to an OD of ~0.6. Protein expression was induced at room temperature by adding IPTG to a final concentration of 1mM and grown for an additional 4 hours. Cultures were centrifuged at 10,000 x g for 30 min and resuspended in lysis buffer (50mM NaH_2PO_4, 300mM NaCl, 0.25% Tween-20, 5% sucrose, 5% glycerol, 2mM imidazole) supplemented with protease inhibitors (1mM PMSF, 2mg/ml aprotinin, 0.5mg/ml leupeptin, 0.7mg/ml pepstatin A). Cells were sonicated on ice for 5 minutes followed by DNase I treatment (4 U/ml) for 15 min. Lysates were clarified by centrifugation at 10,000 x g for 30 min and the supernatant was passed over a HisTALON column (Clontech). The column was washed with 25 mL of wash buffer (Lysis buffer pH 7.0, 25mM imidazole). Protein was eluted from the column in 1 mL fractions using wash buffer with 500mM imidazole. DTT was added to a final concentration of 1mM.

Western blot

Hexokinase Activity Blots

After performing HK-activity assays, whole-cell lysates were saved for western blotting. Equal amounts of protein were loaded on an 8% SDS-PAGE gel and resolved by electrophoresis. Protein was transferred to a PVDF (Bio-Rad) membrane. Membranes were blocked in 5% milk/tris-buffered saline with tween (TBS-T) and both primary and secondary antibody incubations were performed in 2.5% milk/TBS-T. All primary antibodies were incubated overnight at 4°C, except HA which was incubated for 45 minutes. Secondary incubations were done for 90 minutes at room temperature. Antibodies and dilutions were as follows: HK2 (Cell

Signaling C64G5) 1:3000, GCK (Santa Cruz 7908) 1:1000, HKDC1 (Sigma, HPA011956) 1:500, HA (Convance, MMS101R) 1:5000, Beta-Actin (Sigma, A5441) 1:10,000.

Mitochondrial dynamics blots

Proteins were separated using 10% SDS-polyacrylamide gels and transferred to nitrocellulose membrane and blocked for 1 hr at RT in Phosphate buffered saline with 0.1% Tween (PBS-T) containing 5% nonfat dry milk. Membranes were then probed with the appropriate primary antibody: 1:1000 MFN1 (Abcam, ab57602), 1:1000 MFN2 (Sigma, M6319), 1:1000 (S616) P-DRP1 (Cell Signaling Technology 2118S), 1:1000 DRP1 (Abcam, ab184247), 1:1000 FIS1 (Proteintech, 10956-1-AP), 1:5000 Alpha Tubulin (Proteintech, 66031-1-1g), and 1:5000 GAPDH (Cell Signaling Technology, 2118S). Protein bands were visualized using the ChemiDoc MP Imaging System (Bio-Rad).

Hepatocyte Isolations and Adenoviral Infection

Mouse hepatocytes were isolated based off a two-step collagenase perfusion protocol as previously described (108). Briefly, mice were anesthetized with 5U of a mixture of ketamine (90mg/kg) and xylazine (5-10mg/kg). An abdominal incision was made to expose the liver and portal vein. An IV catheter was inserted into the portal vein and perfused with HBSS buffer without phenol red (Corning) and then perfused with collagenase from *Clostridium histolyticum* (Sigma) diluted in DMEM (Gibco). Livers were then removed and torn gently apart for the release of hepatocytes. Cells were then washed with DMEM and plated. After 4 hours of allowing hepatocytes to attach, adenoviruses were added for 4 hours or overnight at a

multiplicity of infection (MOI) of 5-10 in serum-free DMEM.

Construction of Plasmids

GFP-tagged plasmids

To generate the full length and truncated GFP-HKDC1 plasmids, In-Fusion cloning PCR primers were designed to the first (FL-HKDC1-GFP) or second exon (Tr-HKDC1-GFP) of the 2,754 bp fragment from pReceiver-B01 containing HKDC1. To perform the InFusion reaction, the PCR primers also contained overhang regions for XhoI and BamI-HF restriction enzyme sites and a 15bp homology portion to the pEGFP-N3 (Addgene) vector to facilitate recombination.

HA-tagged plasmids

Rat HK2 or human GCK cDNA was subcloned into pcDNA3-HA vector. The HA-tagged cDNAs were then further subcloned into pLenti6-D-TOPO vector (Invitrogen). HKDC1 was subcloned by Gibson assembly where briefly, HKDC1 was amplified from pEGFP-N3-FL-HKDC1 (as described above).

FLAG-tagged HKDC1 plasmid

Human HKDC1 cDNA was cloned into pCMV6-XL4 containing a Myc-DDK tag (HKDC1-FLAG, Origene).

Confocal Imaging

35mm glass bottom confocal dishes (VWR) were coated with 60nM fibronectin (Sigma) diluted in 0.1% gelatin overnight. Before plating cells, confocal dishes were washed twice with PBS.

Hepatocytes were plated on collagen coated 6-well plates with coverslips (for immunofluorescence) or without (for TMRE co-localization) for 2 hours and then transfected using Targefect-Hepatocyte (Targetingsystems) following the manufacturer's instructions. Briefly, 5 μL of either GFP-N3 control, HKDC1 full-length-GFP, or HKDC1 truncated-GFP plasmid DNA was added to 600μL OptiMEM and vortexed for 30 seconds, then 8 μL of Targefect reagent was added to the DNA-OptiMEM mix and vortexed for 30 seconds followed by addition of 8 μL of Virofect enhancer reagent. After the transfection mix was incubated in a 37°C water bath, 600 μL of the transfection mix was added to each confocal dish and incubated for 2 hours. After a 2 hour incubation, 1.4 mL of either 25mM or 5.5mM DMEM (supplemented with 2mM glutamine and 2mM sodium pyruvate) was added to the confocal dishes. 24 hours after transfection, media was changed to fresh DMEM with either 25mM or 5.5mM glucose.

TMRE Co-localization

Hepatocytes were washed with PBS and changed to either 25mM or 5.5mM glucose confocal buffer (1.8mM $CaCl_2$, 2.5mM KCl, 140mM NaCl, 2mM Sodium Pyruvate, 2mM Glutamine, 20mM HEPES pH 7.5, 1mM $MgCl_2$). Hepatocytes were then stained with 5nM TMRE (for mitochondrial stain) and 2 drops/mL of NucRed Live 647 ReadyProbes (ThermoFisher Scientific) for 20 min. Hepatocytes were then washed with PBS and fresh 25mM or 5.5mM glucose confocal buffer was added.

Immunofluorescence: Co-localization with VDAC

48 hours post transfection, cells were fixed in 4% paraformaldehyde in PBS for 10 min at RT. Cells were then washed in PBS and stored at 4 degrees overnight. The next day, cells were

permeabilized in 0.1% Triton-X-100 in PBS for 10 min at RT. Cells were then blocked in 5% Goat serum in 0.1% Triton-X-100 in PBS for 1 hour after which they were incubated in 1:150 VDAC antibody (Thermofisher Scientific, PA1-954A) at 4 degrees overnight. The next day, cells were washed 3X in Phosphate Buffered Solution supplemented with 0.1% tween (PBST) for 10 min at RT after which they were incubated in 1:200 secondary antibody Alexafluor 594 affinipure goat anti-rabbit (H+L) (Jackson Laboratory, 111-585-144) for 2 hours at room temperature protected from light. Cells were then rinsed with PBST and then incubated with 20 nM Hoechst 33342 Solution (ThermoFisher Scientific, 62249) for 10 min at room temperature. Coverslips were then mounted on slides and left to dry overnight.

Hepatocytes were imaged using LSM510 META laser scanning confocal microscope (Zeiss AxioObserver.Z1). Multichannel laser setting was used to image GFP (Ex/Em, 488/510nm), TMRE (Ex/Em: 549/575nm), NucRed (Ex 638, Em 686 nm) and Alexafluor 594 (Ex/Em: 591/614 nm).

Mitochondrial Membrane Potential Measurement

Confocal images of hepatocytes overexpressed with GFP-tagged empty vector, HKDC1 full length, and HKDC1 truncated in 25mM glucose media were stained with 5nM TMRE in Hank's Balanced Salt Solution (HBSS) in a non-CO_2 37 degree incubator for 15 min and its fluorescence intensity was measured using Image J. Pixel intensity was normalized to area for each individual cell expressing GFP.

Oxygen Consumption Rate and Extracellular Acidification Rate (OCR and ECAR)

Hepatocytes were plated onto XF96 plates for 4 hours before media change into DMEM 10% FBS overnight. The media was then replaced with serum-free DMEM with respective adenoviruses to an MOI of 5. Media was changed 6 hours later to the baseline Seahorse media. OCR and ECAR were measured using XFe96 extracellular flux analyzer (Seahorse Bioscience). Basal mitochondrial respiration was measured by taking the initial OCR readings and subtracting the OCR values after treatment with 10 μM antimycin A and 10 μM rotenone (Sigma). Maximal respiration was measured by subtracting the non-mitochondrial respiration by the maximum rate measurement after 1μM FCCP injection. Glycolysis was determined by subtracting the last rate measurement before glucose injection by the maximum rate measurement before oligomycin injection. Glycolytic capacity was measured by subtracting the last rate measurement before glucose injection by the maximum rate measurement after oligomycin injection. 50mM 2 deoxy-glucose (2DG, Sigma) was used to return ECAR to baseline. Experiments were performed in DMEM with no glucose or bicarbonate containing 2mM glutamine (Sigma).

Identification of HKDC1 Binding Partners Through Mass Spectrometry

Co-Immunoprecipitation

HEK293-T cells were transfected with HKDC1-FLAG plasmid using Lipofectamine reagent (ThermoScientific Fisher) and whole cell lysates were collected after 48 hours. Lysates were then immunoprecipitated using Anti-FLAG M2 affinity gel (EZview Red Anti-FLAG M2 Affinity gel, Sigma Aldrich). Eluted samples were given to the Northwestern Proteomics Core where they performed in solution enzymatic digest followed by reversed-phase liquid chromatography using the MS/MS-orbitrap apparatus, LTQ Orbitrap Velos, at a 100 min gradient. Protein peaks were analyzed and yielded percent coverage, number of peptides, number

of peptide spectrum matches, number of amino acids, and the molecular weight of identified proteins.

Measurement of Beta-Oxidation, Glucose Oxidation, and De Novo Lipogenesis Using Radioactivity

^{14}C-labeling experiments were carried out as previously described with some modifications (109). Hepatocytes were plated on collagen-coated 6-well tissue culture plates. The hepatocytes were either allowed to attach for 4 hours, adenovirus containing human *HKDC1* or *GFP* were then supplemented for an additional 4 hours, after which the media was changed to 25mM glucose DMEM supplemented with 10% FBS for 16 hours (overnight).

Beta oxidation

Cells were glucose starved for 2 hours and 0.5-1 μCi of radiolabeled 1-^{14}C palmitic acid (Perkin Elmer) was added to the growth media at the end of the 2 hours. A Whatman chromatography paper cut to the size of a 6-well plate was soaked in 3M NaOH and placed on the lid of the plate, such that each well was properly covered to ensure trapping of any released CO_2. The cells were incubated at 37°C for 2 hours. Following the incubation, 500 μl of 70% perchloric acid was added to each well and the released CO_2 was trapped in the Whatman paper for 1 hr. The filter paper was left for drying overnight and the ^{14}C levels were estimated using a β-counter (Perkin-Elmer). Cells were then scrapped and pelleted down after a brief centrifugation at 5000 x g for 5 min at 4°C. The pellet was then washed twice with 1 × PBS and lysed using 0.5N NaOH, vortexed and centrifuged to isolate the cell lysate at 18,000 x g for 10 min at 4 °C. Experiments were carried out in quadruplicate and normalized to total cellular protein.

Glucose Oxidation

Cells were glucose starved for 2 hours and 0.5-1 μCi of radiolabeled U-^{14}C Glucose (Perkin Elmer) was added to the growth media at the end of 2 hours and carried out as described above.

De novo Lipogenesis

Incorporation of radiolabeled acetate or glucose in cells via the lipogenesis pathway was carried out using ^{14}C-labelled acetate or glucose. Cells were glucose starved for 2 hours and 1 μCi of 1,2-^{14}C acetic acid (Perkin Elmer) or 0.5-1 μCi of radiolabeled U-^{14}C Glucose (Perkin Elmer) was added to the growth media at the end of 2 hours. At the end of 2 hours, cells were washed with warm 1 X PBS 3 times and total intracellular lipids was extracted with hexane and 2-propanol (3:2 (vol/vol)) mixture. Incorporation of carbons from 1,2-^{14}C acetic acid or U-^{14}C glucose into the lipid phase was assayed by scintillation counting and carried out as described above.

HKDC1 Structure

HKDC1 structural homology model was created using the Phyre2 web portal for protein modeling, prediction and analysis and superimposed on Human Hexokinase 1 (PDB 1HKC) complexed with glucose and phosphate using PyMOL2.0 (pymol.org).

Statistical analysis

Data are presented as mean ± SEM. All data were compared by a two-tailed unpaired Student's *t* test for statistical significance or One-way ANOVA multiple comparisons (GraphPad Prism), as specified in the figure legends.

Chapter 3

Role of HKDC1 in NAFLD

ABSTRACT

Under normal physiological conditions, glucokinase is the dominant hepatic hexokinase (HK) isozyme. In pathologic liver states, such as NAFLD, the levels of hepatic GCK changes along with the metabolism. Whether the other HK isozymes contribute to the transformation of the metabolism or involvement in the progressiveness of the disease remains unclear. Our initial *in vivo* characterization of HKDC1, using heterozygous *Hkdc1* knockout mice, shows impaired glucose tolerance in aged and pregnant mice, reduced hepatic triglycerides, and reduced peripheral tissue glucose uptake. Altogether, this suggests a possible role of HKDC1 in glucose sensing tissues such as the liver. Using a publically available gene database by *Keller et al.,* we performed *in silico* analysis on extensively profiled mouse gene expression from multiple tissues (including liver) and found hepatic *Hkdc1* expression was increased in B6 mice (diabetes resistant mice) with the ob/ob mutation only after 4 weeks of age and in BTBR mice (diabetes susceptible mice) after 10 weeks of age. We next examined if *HKDC1* was expressed in the liver under NAFLD conditions, by first analyzing various human liver biopsies with different degrees of steatosis and fibrosis via mRNA analysis and immunohistochemistry methods. We observed *HKDC1* mRNA expression to be elevated in livers with higher fat percentage and with higher level of fibrosis. Similarly, we observed staining of HKDC1 in hepatocytes with steatosis and more intense staining in samples that had marked steatohepatitis compared to normal hepatocytes. From here, we hypothesized that diets that induce fatty liver and steatohepatitis would elevate hepatic HKDC1 expression. We found that after we put 8-week old C57BL/6 mice on high fat, high fat and high glucose, and high fat and high glucose diets for 20 weeks, there was increased *Hkdc1* expression, where there were correspondingly more hepatic triglycerides

accumulated. Additionally, we observed higher expression of hepatic *Hkdc1* expression in mice on diets that induce conditions of NASH such as inflammation. We observed that after feeding mice methionine- and choline- deficient diet (MCD) for 3 weeks and feeding mice a high fat, methionine-restricted and choline-deficient diet (CDA-HFD) for 3 and 6 weeks, there were higher hepatic *Hkdc1* expression levels when compared to the mice on nutrient-matched control diets. Together, these results suggest a significant positive association between hepatic expression of HKDC1 and NAFLD progression in mice and humans.

INTRODUCTION

Non-alcoholic fatty liver disease (NAFLD) is the predominant cause of liver diseases globally. The characteristic feature of fatty liver is the predominance of steatosis and its progression to non-alcoholic steatohepatitis (NASH) is caused by many factors, such as mitochondrial dysfunction, oxidative stress, ER stress, and activation of the inflammatory pathway (79–92).

The literature has established glucokinase (GCK) as the main hepatic hexokinase that regulates catabolism and anabolism. Glucokinase, operates as a glucose sensor to regulate normal glucose metabolism (1,8,46). In pathologic liver conditions such as NAFLD, the expression and activity of GCK has been extensively studied, while the presence and contribution of other hepatic HK isozymes have not yet been examined. Reports have shown that hepatic-specific knockout of GCK worsens glucose mobilization as evidenced by the reduction of glycogen stores, impairment of glucose tolerance, and reduction of gene expression in pathways pertinent for the synthesis of triglycerides such as *de novo* lipogenesis (DNL) (67) . Another group studied liver-specific heterozygous knockdown of GCK and reported significantly higher glucose levels and impaired glucose tolerance (68). Overexpression models of hepatic GCK models revealed significantly increased levels of circulating triglycerides, higher rates of hepatic lipogenesis, and signs of insulin resistance (69). In addition to these studies, it has been reported that hepatic GCK expression stimulates hepatic fat accumulation and positively correlates with fatty liver disease in both mice and humans, respectively (70,71).

The only other HK isozyme that has been largely examined in the liver is hexokinase 2 (HK2) in the context of hepatocellular carcinoma (HCC). Reports have revealed an HK isozyme switch from GCK to HK2 when hepatocytes undergo a malignant transformation in order to sustain the increased glycolysis rates described as the Warburg effect (70,76). However, a very recent report detected HKDC1 expression to be significantly upregulated in liver carcinoma tissues and suggested involvement in the cell proliferation and migration pathways (78). To date, however, there have been no studies that have explored the possibility of other HK isozyme involvement in NAFLD.

Our group recently proposed Hexokinase Domain Containing-1 (HKDC1) to be a novel 5th HK, where its expression was observed in the liver in humans and mice (2,6). Through a genome wide association study (GWAS), we identified variants near the *HKDC1* gene to significantly associate with 2-hour plasma glucose levels in women 28 weeks of gestation (6). A subsequent report from our group determined that regulatory regions that were affiliated with gestational hyperglycemia reduced levels of HKDC1 (7). These findings suggested a metabolic role for HKDC1 and led us to investigate its function *in vivo*. We began initial characterization in HKDC1 heterozygous global knockout mice (genetic global ablation of HKDC1 in mice is embryonic lethal) and observed impairment in glucose clearance in aged and pregnant mice and reduced peripheral tissue glucose disposal and hepatic triglycerides levels (2). In sum, these findings lead us to hypothesize a potential role of HKDC1 in the liver which we have investigated here.

RESULTS

HKDC1 expression is positively associated with the progression of NAFLD in mice and humans

As HKDC1 heterozygous mice have lower hepatic triglycerides, we next investigated the conditions necessary to induce HKDC1 expression, specifically looking at conditions related to fat in the liver. We began by using a publicly available gene database that extensively profiled mouse liver gene expression as a function of age, strain, and obesity [4 vs 10 weeks, C57Bl/6 (B6) vs BTBR, and lean vs mice with ob/ob mutation, respectively] (110). We found increased hepatic *Hkdc1* expression in B6 mice (diabetes resistant mice) after only 4 weeks and in BTBR mice (diabetes susceptible mice) after 10 weeks of age (Fig. 11A), which suggested that in mice predisposed to fatty liver, the expression of *Hkdc1* may be increased.

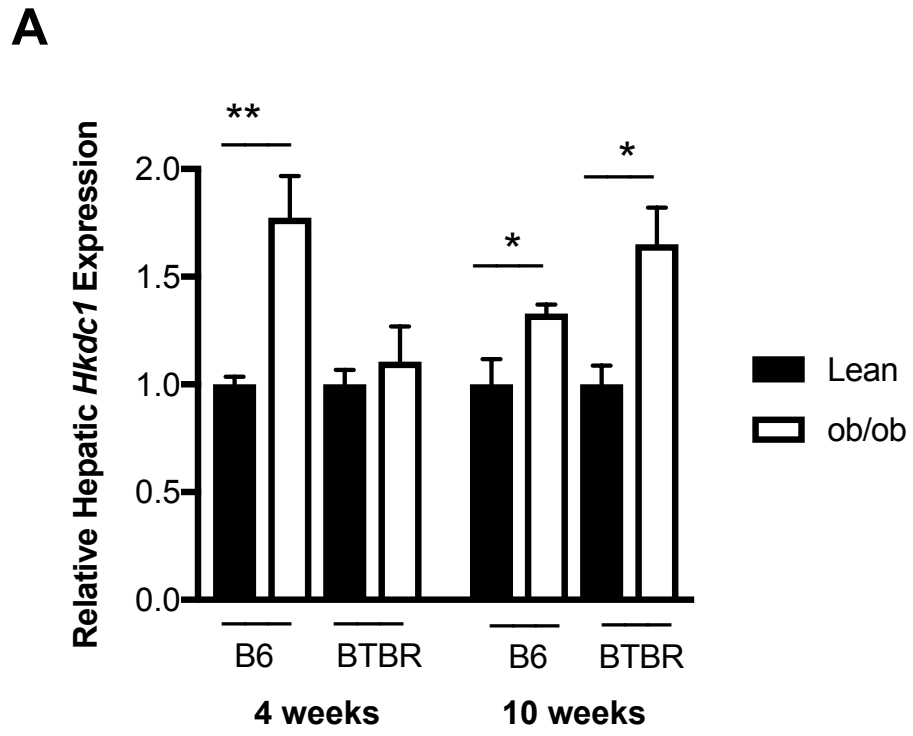

Figure 11. HKDC1 expression associates with NAFLD conditions. (A) *Hkdc1* expression assessed in lean and *ob/ob* mice at 4 and 10 weeks in C57Bl/6 (B6) and BTBR mouse strains (n=5 biological replicates).

To determine if there was a positive relationship between hepatic HKDC1 expression and hepatic fat content in humans with various stages of non-alcoholic fatty liver disease (NAFLD), we measured the relative expression of *HKDC1* from human liver biopsies that contained varying percentages of fat by qPCR. There was a significant increase in the expression of hepatic *HKDC1* between patients with 10-15% of fat and those with >15% fat content (Fig. 11B). In addition, we found the expression of hepatic *HKDC1* to be significantly increased with the progression of liver disease state, where each progressive stage has increased amounts of fibrosis (Fig.11C). However, it was difficult to differentiate to what degree *HKDC1* expression correlated with steatosis versus inflammation and fibrosis. To gain more insight, we performed immunohistochemistry (IHC) to detect HKDC1 protein levels in patients with livers that are normal, fatty (steatosis), or contain high levels of inflammation and fibrosis [non-alcoholic steatohepatitis (NASH)]. We observed darker staining in livers with steatosis but the darkest staining to be in patients with steatohepatitis (Fig. 11D).

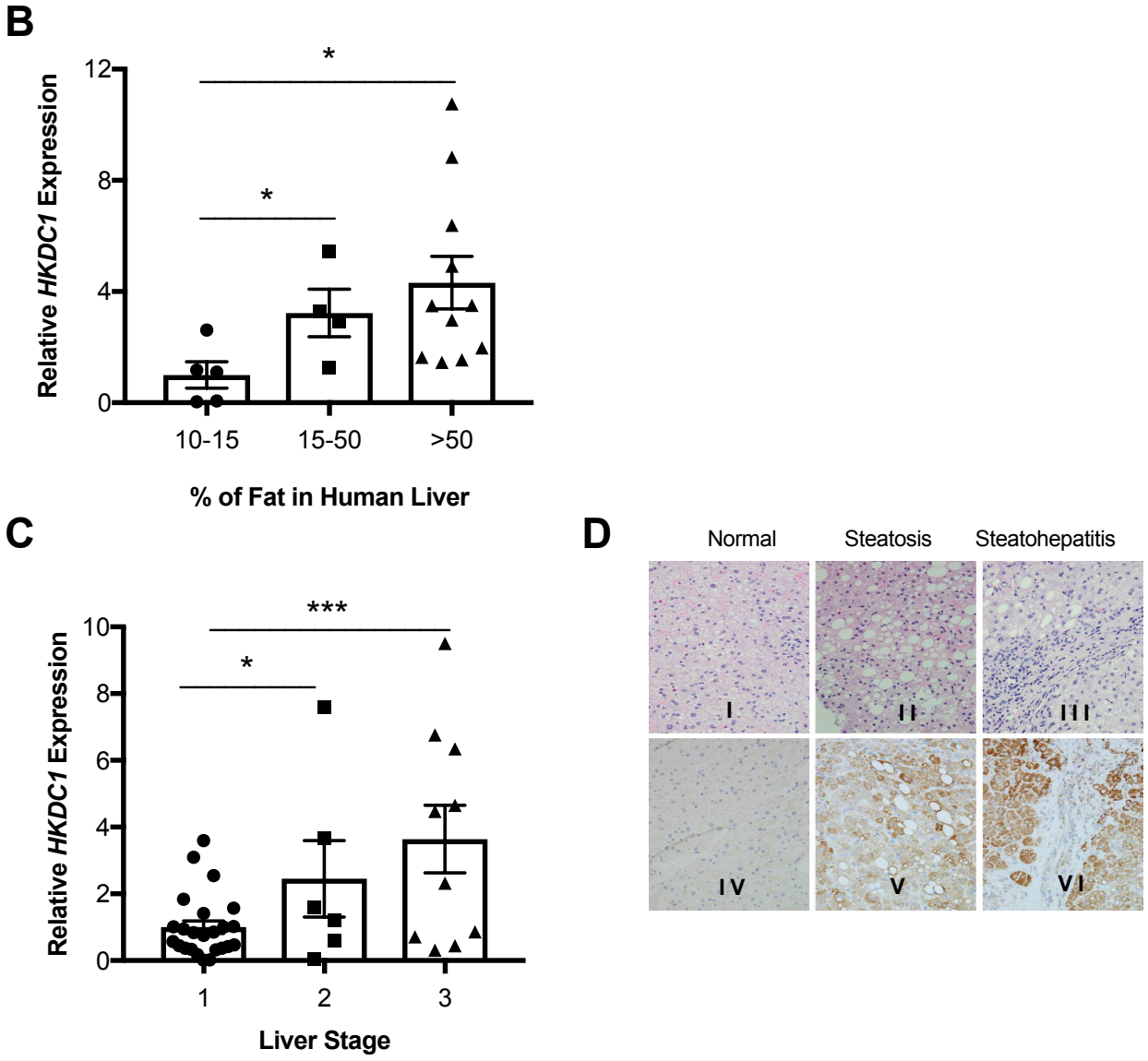

Figure 11. HKDC1 expression associates with NAFLD conditions. *HKDC1* expression measured in liver biopsies of human subjects comparing **(B)** relative percentage of liver fat with stage 1 fibrosis (n=4-11 biological replicates) and **(C)** liver stage progression 1-3 with varying levels of steatosis (n=6-24 biological replicates). **(D)** Representative human hepatocyte sections that are normal (I and IV), with steatosis (II and V), and with steatohepatitis and fibrosis (III and VI) were stained with H&E (top panel) and anti-HKDC1 antibody (lower panel) (n=3 for each

condition, pictures taken at 40X). All data are represented as mean ± SEM. *P<0.05, **P<0.001, (*One-way ANOVA*).

HKDC1 Expression is Elevated in Mice on High Fat/High Sugar Diets

To determine if these results could be recapitulated in mice, we induced obesity and hepatic steatosis in mice with high fat, high carbohydrates (glucose or fructose, 25.5% Kcal) diets for two to six months. Interestingly, *Hkdc1* expression was not increased between normal low fat fed mice versus high fat diet (Fig. 12A). However, *Hkdc1* expression was most significantly elevated in mice on high fat/high fructose (HF+HFr) diet, where there was subsequently more liver triglyceride content than those fed only a high-fat diet (HF; 60 Kcal from fat) or high fat/high glucose diet (HF+HG; Fig. 12B, Fig. 12C). In addition, the increase of *Hkdc1* expression in the livers of mice fed HF+HFr was progressively associated with the accumulation of hepatic fat over time (Fig. 12D, Fig. 12E). Thus, HKDC1 expression is also elevated in fatty liver.

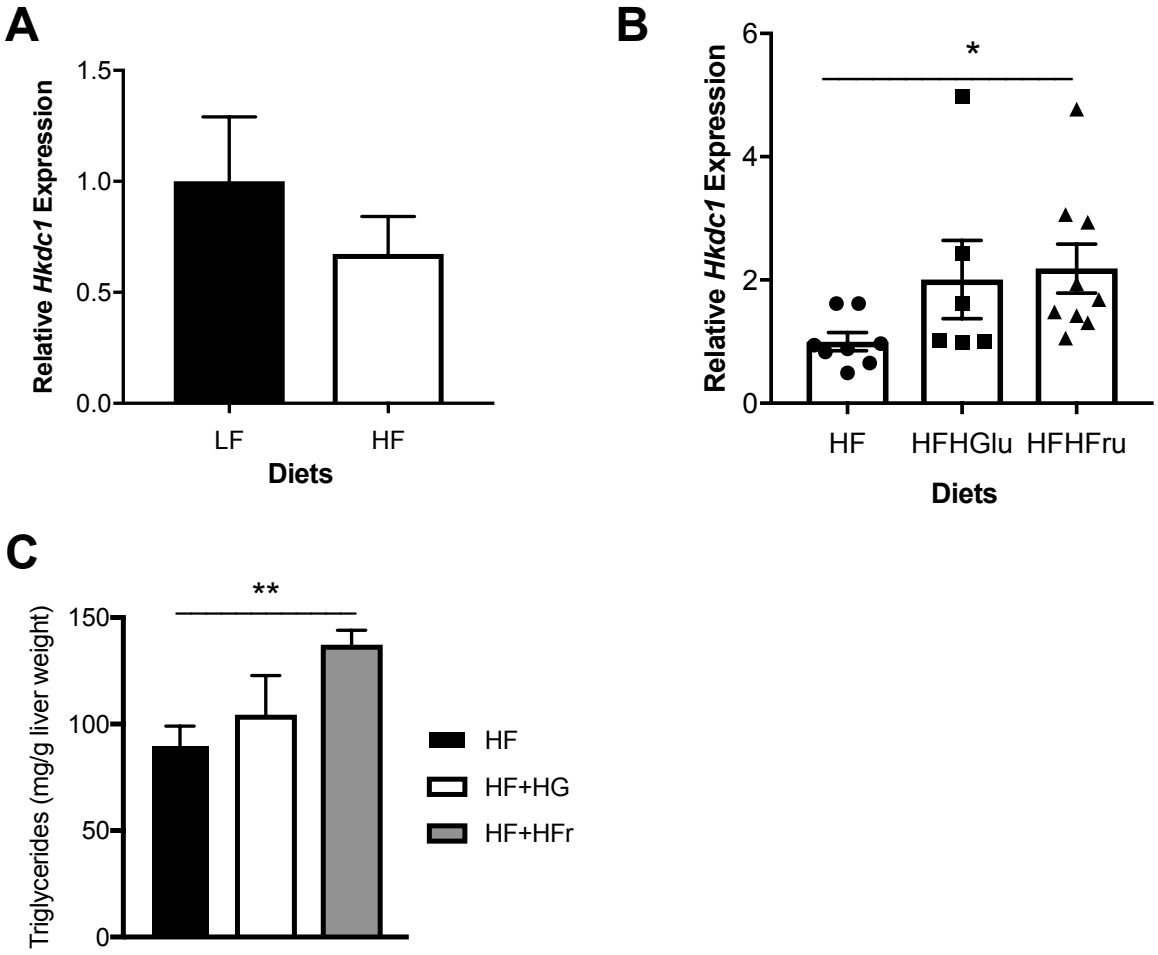

Figure 12. Hepatic *Hkdc1* expression does not increase in HF diet but does correlate with triglyceride content in high fat and sugar diets. (A) Relative hepatic *Hkdc1* expression in mice fed low fat (LF) and high fat (HF) diet after 14 weeks on diet (n=5 biological replicates). **(B)** Hepatic Hkdc1 expression measured in B6 mice after 20 weeks on high fat (HF), high fat and high glucose (HF+HG), or high fat and high fructose (HF+HFr) diets beginning at 8 weeks of age (n=6-10 biological replicates). (**C)** Triglyceride content in mice fed HF diet, high fat, high glucose (HF + HG), and high fat, high fructose (HF + HFr) diet after 20 weeks beginning at 8 weeks of age (n=6-10 biological replicates).

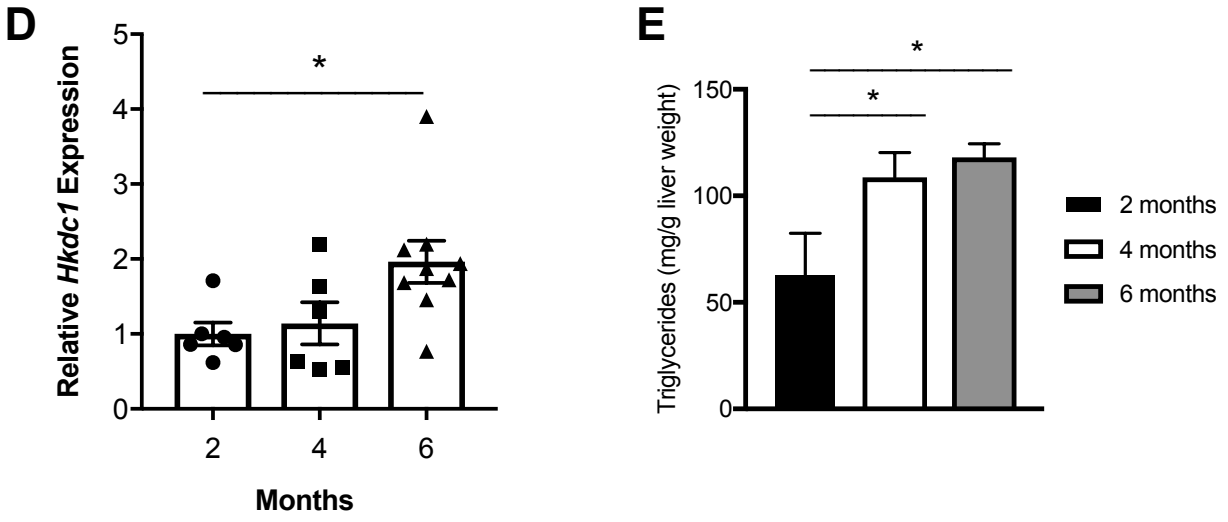

Figure 12. Hepatic *Hkdc1* expression does not increase in HF diet but does correlate with triglyceride content in high fat and sugar diets. (D) Hepatic *Hkdc1* expression measured in mice on HF+HFr diet after 2, 4, and 6 months of feeding beginning at 8 weeks of age (n=6-10 biological replicates). **(E)** Triglyceride content in mice fed HF + HFr diet beginning at 8 weeks of age after 2, 4, and 6 months (n=6-10 biological replicates). All data are represented as mean ± SEM. All data are represented as mean ± SEM. *P<0.05, **P<0.005 (*One way ANOVA).*

HKDC1 Expression is Induced in Diets Modeling NASH

To further gain insight if this expression change is related to the stages of fatty liver disease such as inflammation and fibrosis, we evaluated mice fed on a few additional diets. First, we measured *Hkdc1* expression in B6 mice after 8 weeks on low fat, low cholesterol, and low fructose (LFCF) diet and compared with high fat, high cholesterol, high fructose (HFCF) diet (Fig. 13A). Mice on this diet (HFCF) are reported have marked steatosis after 8 weeks with modest indications of liver injury and fibrosis (111). We then measured Hkdc1 expression in mice fed a methionine- and choline- supplemented diet (MSD) or methionine- and choline-deficient diet (MCD; a diet known to dramatically increase levels of serum alanine aminotransferase (ALT) and inflammation (112–114) after just 2 weeks but is coupled with significant weight loss). We additionally found significantly increased *Hkdc1* expression in this model (Fig. 13B). And lastly, we assessed *Hkdc1* expression in another model of NASH reported to develop enlarged fatty livers and fibrosis without a significant loss of body weight and more reflective of the physiology that occurs in humans, the high fat, methionine-restricted (0.1%) and choline-deficient diet (CDA-HFD) and compared with the control diet, high fat, methionine-restricted and choline-supplemented diet (MSD-HFD) after 3 and 6 weeks (115). As was seen with the MCD feeding, we also observed *Hkdc1* expression to be significantly increased after just 3 weeks and even more elevated after 6 weeks on the CDA-HFD when compared to MSD-HFD (Fig. 13C). Altogether, we conclude that HKDC1 expression may be more associated with NAFLD/NASH where inflammation and fibrosis is apparent, as suggested here in mice and humans.

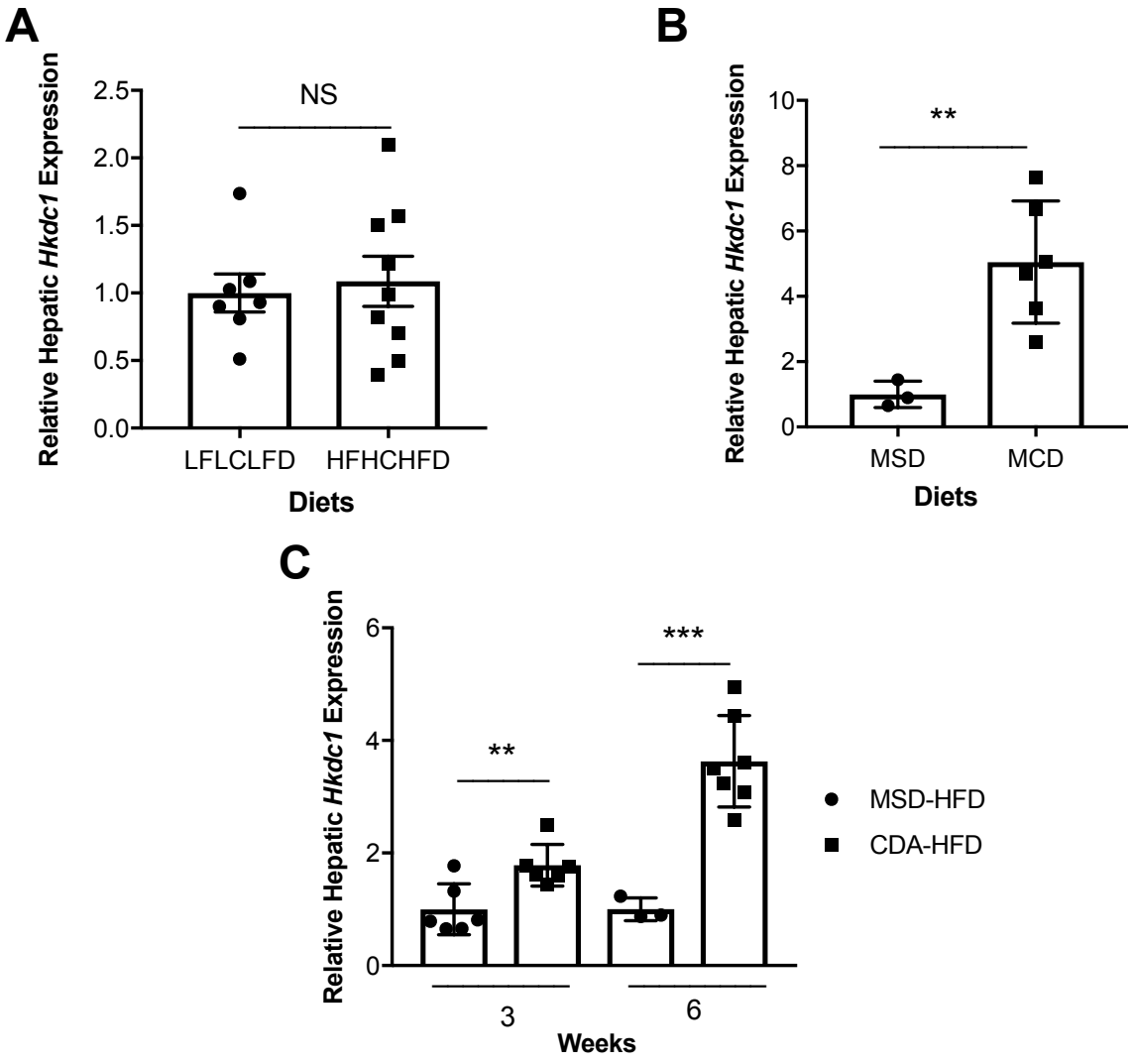

Figure 13. *HKDC1* expression associates with diet-induced inflammation and fibrosis. (A) *Hkdc1* expression measured in B6 mice after 8 weeks on either low fat, low cholesterol, and low fructose (LFCF) diet or high fat, high cholesterol, high fructose (HFCF) diet (n=7-9 biological replicates). **(B)** *Hkdc1* expression was measured in B6 mice after 3 weeks on methionine- and choline- supplemented diet (MSD) or methionine- and choline- deficient diet (MCD) (n=3-6 biological replicates). **(C)** Hkdc1 expression was measured in B6 mice after 3 or 6 weeks on

either high fat, methionine-restricted and choline-supplemented diet (MSD-HFD) or high fat, methionine-restricted and choline-deficient diet (CDA-HFD) (n=3-7 biological replicates). All data are represented as mean ± SEM. **P<0.001, ***P<0.0001 (*One-way ANOVA*).

Supplemental Table 2: Characteristics of Human Liver Samples Used for Immunohistochemistry Only.

	NASH (N=26)	Normal (N=21)
Race		
White	20 (59%)	14 (41%)
Black	4 (40%)	6 (60%)
Ethnicity		
Hispanic	6 (75%)	2 (25%)
Non-hispanic	20 (51%)	19 (49%)
Gender		
Male	6 (55%)	5 (45%)
Female	20 (56%)	16 (44%)
Cirrhosis		
Yes	6 (100%)	0
No	19 (48%)	21 (53%)
Diabetes		
Yes	10 (83%)	2 (17%)
No	16 (46%)	19 (54%)
Hyperlipidemia		
Yes	11 (58%)	8 (42%)
No	15 (54%)	13 (46%)
BMI	38.75 (32.89 – 44.38)	36.02 (26.91 – 42.94)
Age at time of biopsy	51.50 (35.75 – 56.75)	51.00 (33.50 – 56.00)
Grade of steatosis	2.00 (1.00 – 3.00)	0.00 (0.00 – 0.00)
Percent steatosis	60.00 (27.50 – 80.00)	0.00 (0.00 – 1.00)
Grade of ballooning	(0 – 1.00)	--
Numbers and percentages are reported for categorical variables. Median and interquartile range are reported for continuous variables.		

MATERIALS AND METHODS

Human Studies

Liver Biopsy Samples

Liver biopsy samples were obtained from Stephen Harrison, Division of Gastroenterology and Hepatology, Brooke Army Medical Center, San Antonio, Texas. In Fig. 5b and 5c, liver samples for the percentage of steatosis had stage 1 fibrosis only and included 16 male subjects and 4 female subjects (steatosis across group ranged 10-66%). Samples for the stages of fibrosis included 29 male subjects (72.5% of sample size) and 11 female subjects (27.5% of sample size) with varying amounts of steatosis. The samples were RNA extracted and purified, and qPCR was performed as described below.

Immunohistochemistry (IHC)

The liver specimens were obtained from Xianzhong Ding, at Loyola University Chicago, Department of Pathology, Maywood, IL, and were surgical pathology or autopsy cases from Department of Pathology, from 2014 to 2016 with IRB approval (#207299) and prepared as published (116). All cases examined here had no clinical history of alcohol and hepatotoxic medication intake. Serum ceruloplasmin, alpha1-antitrypsin, and ferritin levels were within normal ranges. All cases had negative serological tests for antinuclear antibody, anti-smooth muscle actin antibody, anti-mitochondrial antibody, hepatitis B and hepatitis C. The specimens included normal liver, non-alcoholic fatty liver disease, non-alcoholic steatohepatitis with and without cirrhosis. Assessment of the degree of steatosis was based on a semi-quantitative scale by evaluating the percentage involvement of parenchyma, which is expressed as grades (grade 1:

5% to 33%; grade 2: 33% to 66%; and grade 3: > 66%). Ballooned hepatocytes (an essential histologic feature of steatohepatitis) are characterized by enlarged hepatocytes with rarefied reticulated cytoplasm and with or without fat droplets and Mallory-Denk bodies. Hepatocyte ballooning was scored based on frequency of ballooning cells (grade 0 if rare and grade 1 if it is easily identified microscopically). The H&E stains and immunohistochemistry was reviewed and scored by a histologist (co-author, Ding Ding), and representative images are shown based on his review (see Supplemental Table 2).

Mouse diets

High fat (HF), high fat high glucose (HF+HG), high fat high sucrose (HF+HFru) diets

A subset of 8 week-old mice were fed for 20 weeks on the various diets as indicated in the Results section. Additionally, mice on HF+HFr were analyzed for Hkdc1 expression and triglycerides after 2, 4, or 6 months on the diet starting at 2 months of age. High fat diet contents were 60% Kcal from fat (Research Diets). High Fat High Fructose (HF+HFr, Sucrose) diet contents were 58% Kcal fat, 25.5% carbohydrate, 16.4% protein (OpenSource Diets; D12331). High Fat High Glucose (HF+HG) (corn starch) diet contents were 58% Kcal fat, 25.5% carbohydrate, 16.4% protein. HF+HFr and HF+HG diets were additionally supplemented with fructose/sucrose or glucose in the water.

Additional diets

10-week-old chow-fed male C57Bl6/J mice were obtained from Jackson Laboratories and bred-in house. Mice were injected with a single dose of AAV8-TBGp-Null (1.5*10e11 genome copies) in the lateral tail vein and used as wildtype mice. Two weeks later, mice were switched

to different diets. The methinonine- and choline-deficient diet (MCD, Cat # A02082002BR, Research Diets) and methinonine- and choline-supplemented diet (MSD, Cat # A02082003BY, Research Diets) were fed to the mice for 3 weeks after which the mice were sacrificed. Both diets are nutrient- and energy content-matched. MSD and MCD diets have 20% Kcal from fat (corn oil). The high fat, methinonine-restricted and choline-deficient diet (CDA-HFD, Cat # A06071302, Research Diets) and the high fat, methinonine-restricted and choline-supplemented diet (MSDHFD, Cat # A06071306, Research Diets) were fed to the mice for either 3 or 6 weeks after which the mice were sacrificed. Both diets are nutrient- and energy content-matched. Source of fat is mostly lard. The high fat (40% Kcal from fat), high cholesterol (2%) and high fructose (20% Kcal) diet (HFCF) diet, Cat # D16010101, Research Diets) and the low fat, low cholesterol and low fructose diet (LFCF) diet, Cat # D09100304, Research Diets) were fed to the mice for 8 weeks after which the mice were sacrificed. Both diets are nutrient-matched.

RNA isolation and qPCR

RNA was extracted from 10mg of livers using TRIzol Reagent (Life Technologies) and chloroform for phase separation. RNA was then purified using the Rneasy minikit (Qiagen) and treated with RNase-Free DNase (Qiagen). 1µg of purified RNA was then reverse transcribed using qScript Reverse Transcriptase (Quanta Biosciences) and quantified via qPCR using PerfeCTa SYBR Green SuperMix (Quanta Biosciences) where final primer concentrations were 0.625µM for each reaction and data were analyzed via the CFX Connect Real-Time PCR Detection System (BioRad).

Chapter 4

Discussion and Future Directions

DISCUSSION

To date, HKDC1 has been examined mainly in the context of gestational diabetes, as the gene was found to be significantly associated with glycemic traits during pregnancy (6). In subsequent studies, our group has established this enzyme to contribute to overall cellular hexokinase activity when overexpressed in cancer cells and to be a novel 5th hexokinase (7). Here, we report a more comprehensive characterization of HKDC1's hexokinase abilities and its influence on hepatocyte metabolism and present observational data which suggests a role in NAFLD. We have shown HKDC1 to function as a low activity HK that localizes to the mitochondria, at least in hepatocytes, suggesting a role in mitochondrial function. In support of this, we show that overexpression of HKDC1 in hepatocytes significantly reduces glycolytic capacity, maximal respiration, glucose oxidation and diminishes mitochondrial membrane potential. Furthermore, acute *in vivo* overexpression of human HKDC1 mildly improves glucose tolerance. And finally, we report a positive association of HKDC1 expression with NAFLD/NASH, in particular, when inflammation and fibrosis are apparent.

Given the high sequence and structural similarity with the low Km HK, HK1, we initially predicted HKDC1 to have high glucose phosphorylating activity. In our initial findings, we reported that HKDC1 contributes to overall cellular HK activity as determined by overexpression and knockdown studies in cancer cell lines (97), however, it is known that cancer cells upregulate low Km hexokinases (i.e., HK1 & HK2) expression and this may have suggested greater HK activity contribution from HKDC1. In our report here, we saw minimal HK activity from HKDC1 when purified and also a mild increase in HK activity in HKDC1-overexpressing MI54-CHO cells. Moreover, our *in silico* structural analysis comparing HKDC1 and HK1 show shifts in key amino acids involved in the allosteric and catalytic active site which may help

explain the low activity we see for HKDC1. Future enzymatic structure and function studies will need to be performed to address these amino acid shifts along with other condition variables.

Although HKDC1 appears to have low HK activity, subcellular localization of HKs is another component believed to be important for regulating the metabolic fate of glucose (8). High activity HK isozymes, HKI and HKII, are reported to regulate metabolism, in part, by their localization to the mitochondria through their interaction with VDAC (14,117,118). VDAC has been reported to play a critical role in mitochondrial function (95,119) and interaction with VDAC may have significant consequences in hepatic metabolism. For instance, even though HKI and HKII are known to not be expressed at high levels in normal liver physiology, HKII is known to change hepatocyte metabolism through its interaction with VDAC in liver cancer. There are high levels of HKII in liver cancer and binding to VDAC are thought to allow minimized product inhibition of HKII and ultimately acts as a driver of the Warburg effect [providing ATP by increased glycolysis, while diminishing ATP produced by oxidative phosphorylation (120)]. Little information is known about the expression, localization, and contribution of these HK isozymes in the context of NAFLD. Our finding that a low activity HK localizes to the mitochondria (particularly co-localizing with VDAC), and shows signs of mitochondrial dysfunction was surprising and will need to be further explored in its role in hepatic disease. Future studies will evaluate 1) under what conditions HKDC1 localizes to the mitochondria and 2) if HKDC1 is directly interacting with VDAC in a similar fashion as HKI and II and 3) how this binding alters downstream anabolic and catabolic pathways.

The changes noted *ex vivo* led us to investigate the effects of overexpressing HKDC1 in mouse livers *in vivo*. We observed that with *in vivo* overexpression of HKDC1 in the liver there were corresponding increases in the mitochondrial fusion protein mitofusion-2 (MFN2), the mitochondrial fission protein Dynamin related protein 1 (DRP1), and the DRP1 Ser616

phosphorylation site, which corresponds with increased mitochondrial fission. Because both MFN2 and DRP1 represent opposite mitochondrial dynamics events, more investigation is needed in order to assess precisely how HKDC1 is regulating these events. However, the increase in the DRP1 protein and its phosphorylation are more pronounced over MFN2 and the literature suggests that mitochondrial dysfunction (as observed with reduced cellular respiration and ATP) result predominately from upregulation of DRP1 (121,122). Furthermore, it has been noted that excessive fragmentation can generate mitochondria with reduced mtDNA, leading to impaired cellular respiration (123). Altogether, we note that with overexpression of HKDC1 in hepatocytes, there are signs of mitochondrial dysfunction as we have found a reduction in maximal respiration, glucose oxidation, and reduced mitochondrial potential that may, in part, be due to the increased fission protein, DRP1.

Next, given that our heterozygous deletion of *Hkdc1* mice had reduced tissue-specific glucose disposal and hepatic triglycerides (2), and that we find signs of mitochondrial dysfunction in overexpressed hepatocytes *ex vivo*, we hypothesized that acute overexpression of hepatic HKDC1 *in vivo* would alter glucose homeostasis and possibly hepatic energy storage. Although not studied in the context of liver disease, there is evidence suggesting that acute *in vivo* adenoviral overexpression of HK2 is enough to cause hepatic steatosis after just 7 days (106). We performed a similar method of overexpression, but observed no changes in energy storage nor signs of increased DNL, with only mild changes in glucose homeostasis. These data also contrast with studies reporting that GCK overexpression causes an increase in lipogenic genes in the DNL pathway (102). Additionally, GCK is strongly associated with hepatic steatosis seen in NAFLD in mice and humans, which is significant given that DNL is essential for the development of steatosis as one third of accumulated triglycerides in patients with fatty liver

comes from DNL (27,75). Though acute overexpression of HKDC1 may not be sufficient to induce any consequential changes in fat accumulation *in vivo*, future work will assess how chronic overexpression of hepatic HKDC1 alters hepatic energy metabolism. Moreover, we note that when glucose was provided as a tracer for lipogenesis, HKDC1 overexpression in hepatocytes reveals increased lipogenesis. However, since most of the label is not incorporated in triglycerides as glycerol (83), an enrichment of labeled-glycerol in the triglyceride pool is not the best method for determining changes in lipogenesis. This observation is further supported as evidenced by a lack of change in the Kennedy pathway genes. However, even when provided with labeled acetate, there were no changes in lipogenesis. Future radiolabeled studies are needed to follow how glucose metabolism is directed in the presence and absence of HKDC1.

Although we did not find overexpression of HKDC1 to drive DNL like reported for GCK, we did find evidence of heightened HKDC1 expression in conditions defined in NAFLD. Moreover, it is clear that HKDC1 expression and protein levels are elevated in livers with steatosis but much more so in human patients whose livers have progressed to the steatohepatitis stage. We were additionally able to recapitulate these findings in mouse models of NASH. Interestingly, the diets that induced Hkdc1 expression were the models in which the diets were not simply ones that caused hepatic steatosis (like the HFCF diet after 8 weeks of feeding), but rather diets that induce inflammation and fibrosis (MCD and CDA-HFD diets), which is indicative of a more advanced stage of NAFLD. Some potential explanations have been proposed to describe the changes that occur from simple steatosis to more progressive stages such as NASH. For example, one hypothesis proposes the “two-hit” model where the first “hit” is fat infiltration into the liver (steatosis) and the second “hit” is from free radicals resulting from oxidative stress, thereby

causing inflammation (124). The particular mechanisms describing this transition is still under investigation (83,125–127) but suggests a link with mitochondrial dysfunction. Given that we observe signs of mitochondrial dysfunction in hepatocytes with HKDC1 overexpression, as well as, *in vivo* changes to mitochondrial fusion and fission proteins, with no direct contribution to triglyceride synthesis, it may be that HKDC1 plays an important role in the progression of hepatosteatosis into more advanced stages of NAFLD through these processes. Supporting our data, two studies that reported whole RNA gene changes in NAFLD illustrate that *HKDC1* is indeed more expressed in advanced stages of non-alcoholic steatohepatitis when compared to liver with simple steatosis (128,129). However, a limitation of our work is that our viral overexpression model only results in overexpression for a few weeks, and therefore, we could not directly use it to test the role of HKDC1 in the development of NAFLD through different diets (as NAFLD development takes many weeks). Additionally, sex differences need to be explored due to our previous findings in female mice (2) and that HKDC1 was identified from genetic studies in pregnancy (6) .

FUTURE DIRECTIONS

The studies from this project have greatly enhanced our knowledge of the novel hexokinase, HKDC1, and have opened many doors of exploration for its role in the liver and beyond. As stated previously in the discussion, we found HKDC1 to localize to the mitochondria, with particular association with VDAC. However, we do not know whether this association with VDAC is through direct binding, such is what is seen for HK1 and HK2, or indirect binding possibly through a bigger binding complex. Future studies would benefit from assessing if this is

a direct interaction via a co-immunoprecipitation assay and verification of binding by western blot and if this interaction is mediated by the same N-terminal sequence amino acid residues of HK1 and HK2 found to interact with VDAC. Other studies that would confirm if interaction with VDAC requires the N-terminal sequence is to supplement hepatocytes with N-terminal peptides mimicking the N-terminal sequence of HKDC1 and observe whether HKDC1 is dislodged from the mitochondria.

Furthermore, it will be imperative to determine how HKDC1 function and localization to the mitochondria effects downstream catabolism and anabolism. Thus, in order to depict the precise metabolic pathways that are influenced by HKDC1, we propose to perform $U^{13}C$-labeled glucose and $1,2^{13}C$-labeled glucose flux experiments in cells lines (some of which include MI54 CHO, HEPG2, and primary hepatocytes cell lines) overexpressing full length and N-terminal sequence truncated versions, as well as, silencing of HKDC1.

Additionally, as we have demonstrated through our confocal analysis, overexpression of HKDC1 in primary hepatocytes alters protein levels that are involved in the mitochondrial dynamics pathways - mitochondrial fusion and fission. Specifically, overexpression of HKDC1 increased the protein levels of the mitochondrial fusion marker, MFN2, and the mitochondrial fission marker DRP-1. Future studies are needed to assess through what methods HKDC1 is affecting the mitochondrial dynamics processes to help clarify how the alterations in machinery may be leading to diminished mitochondria function as observed in these studies.

Along these lines, we propose to perform inhibitor studies in hepatic cell lines to examine under what cellular conditions HKDC1 expression is induced. Because the progression of NAFLD is thought to be caused by several different factors including mitochondrial dysfunction, ER stress, oxidative stress, and activation of inflammatory pathways, inhibitors in these various pathways will provide a more holistic understanding of HKDC1's contribution to the development of NAFLD.

In conjunction with the above *in vitro* studies, we hope to supplement our work with an *in vivo* assessment of hepatic HKDC1. We will use an adenoviral-associated virus serotype 8 (AAV8)-mediated liver-specific knockout of *Hkdc1* mouse model put on various NASH diets and measure the corresponding effects on glucose homeostasis, hepatic fat metabolism, and inflammation. This will help clarify whether HKDC1 is playing a protective effect against the overproduction of hepatic triglyceride accumulation seen in simple steatosis or whether it is driving the progression to NASH. Overall, this work has taken the first steps in understanding the potential role of the HK isozyme, HKDC1, in the liver, where more studies are needed to clarify its role in NAFLD, and other physiological and pathological states.

REFERENCES

1. **Irwin DM, Tan H.** Molecular evolution of the vertebrate hexokinase gene family: Identification of a conserved fifth vertebrate hexokinase gene. *Comp. Biochem. Physiol. Part D Genomics Proteomics* 2008;3(1):96–107.

2. **Ludvik AE, Pusec CM, Priyadarshini M, Angueira AR, Guo C, Lo A, Hershenhouse KS, Yang G-Y, Ding X, Reddy TE, Lowe WL, Layden BT.** HKDC1 Is a Novel Hexokinase Involved in Whole-Body Glucose Use. *Endocrinology* 2016;157(9):3452–3461.

3. **Buchanan TA.** Glucose metabolism during pregnancy: normal physiology and implications for diabetes mellitus. *Isr. J. Med. Sci.* 1991;27(8–9):432–441.

4. **Metzger BE.** Long-term outcomes in mothers diagnosed with gestational diabetes mellitus and their offspring. *Clin. Obstet. Gynecol.* 2007;50(4):972–979.

5. **Silverman BL, Metzger BE, Cho NH, Loeb CA.** Impaired glucose tolerance in adolescent offspring of diabetic mothers. Relationship to fetal hyperinsulinism. *Diabetes Care* 1995;18(5):611–617.

6. **Hayes MG, Urbanek M, Hivert M-F, Armstrong LL, Morrison J, Guo C, Lowe LP, Scheftner DA, Pluzhnikov A, Levine DM, McHugh CP, Ackerman CM, Bouchard L, Brisson D, Layden BT, Mirel D, Doheny KF, Leya MV, Lown-Hecht RN, Dyer AR, Metzger BE, Reddy TE, Cox NJ, Lowe WL, HAPO Study Cooperative Research Group.** Identification of HKDC1 and BACE2 as genes influencing glycemic traits during pregnancy through genome-wide association studies. *Diabetes* 2013;62(9):3282–3291.

7. **Guo C, Ludvik AE, Arlotto ME, Hayes MG, Armstrong LL, Scholtens DM, Brown CD, Newgard CB, Becker TC, Layden BT, Lowe WL, Reddy TE.** Coordinated regulatory variation associated with gestational hyperglycaemia regulates expression of the novel hexokinase *HKDC1*. *Nat. Commun.* 2015;6:6069.

8. **Wilson JE.** Isozymes of mammalian hexokinase: structure, subcellular localization and metabolic function. *J. Exp. Biol.* 2003;206(Pt 12):2049–2057.

9. **Mueckler M.** Facilitative glucose transporters. *Eur. J. Biochem.* 1994;219(3):713–725.

10. **Ureta T.** The comparative isozymology of vertebrate hexokinases. *Comp. Biochem. Physiol. Part B Comp. Biochem.* 1982;71(4):549–555.

11. **Tsai HJ, Wilson JE.** Functional Organization of Mammalian Hexokinases: Both N- and C-Terminal Halves of the Rat Type II Isozyme Possess Catalytic Sites. *Arch. Biochem. Biophys.* 1996;329(1):17–23.

12. **Ardehali H, Printz RL, Whitesell RR, May JM, Granner DK.** Functional interaction between the N- and C-terminal halves of human hexokinase II. *J. Biol. Chem.* 1999;274(23):15986–15989.

13. **Arora KK, Filburn CR, Pedersen PL.** Structure/function relationships in hexokinase. Site-directed mutational analyses and characterization of overexpressed fragments implicate different functions for the N- and C-terminal halves of the enzyme. *J. Biol. Chem.* 1993;268(24):18259–18266.

14. **Wilson JE.** Hexokinases. *Rev. Physiol. Biochem. Pharmacol.* 1995;126:65–198.

15. **White TK, Wilson JE.** Isolation and characterization of the discrete N- and C-terminal halves of rat brain hexokinase: retention of full catalytic activity in the isolated C-terminal half. *Arch. Biochem. Biophys.* 1989;274(2):375–393.

16. **Baijal M, Wilson JE.** Functional consequences of mutation of highly conserved serine residues, found at equivalent positions in the N- and C-terminal domains of mammalian hexokinases. *Arch. Biochem. Biophys.* 1992;298(1):271–278.

17. **Rijksen G, Staal GE, Streefkerk M, de Vries AC, Batenburg JJ, Heesbeen EC, van Golde LM.** Activity and isoenzyme patterns of glycolytic enzymes during perinatal development of rat lung. *Biochim. Biophys. Acta* 1985;838(1):114–121.

18. **Quintens R, Hendrickx N, Lemaire K, Schuit F.** Why expression of some genes is disallowed in beta-cells. *Biochem. Soc. Trans.* 2008;36(Pt 3):300–305.

19. **Heikkinen S, Suppola S, Malkki M, Deeb SS, Jänne J, Laakso M.** Mouse hexokinase II gene: structure, cDNA, promoter analysis, and expression pattern. *Mamm. Genome Off. J. Int. Mamm. Genome Soc.* 2000;11(2):91–96.

20. **Osawa H, Printz RL, Whitesell RR, Granner DK.** Regulation of hexokinase II gene transcription and glucose phosphorylation by catecholamines, cyclic AMP, and insulin. *Diabetes* 1995;44(12):1426–1432.

21. **Riddle SR, Ahmad A, Ahmad S, Deeb SS, Malkki M, Schneider BK, Allen CB, White CW.** Hypoxia induces hexokinase II gene expression in human lung cell line A549. *Am. J. Physiol. Lung Cell. Mol. Physiol.* 2000;278(2):L407-416.

22. **Roberts DJ, Miyamoto S.** Hexokinase II integrates energy metabolism and cellular protection: Akting on mitochondria and TORCing to autophagy. *Cell Death Differ.* 2015;22(2):248–257.

23. **Mathupala SP, Rempel A, Pedersen PL.** Aberrant glycolytic metabolism of cancer cells: a remarkable coordination of genetic, transcriptional, post-translational, and mutational events that lead to a critical role for type II hexokinase. *J. Bioenerg. Biomembr.* 1997;29(4):339–343.

24. **Tsai HJ, Wilson JE.** Functional organization of mammalian hexokinases: characterization of the rat type III isozyme and its chimeric forms, constructed with the N- and C-terminal halves of the type I and type II isozymes. *Arch. Biochem. Biophys.* 1997;338(2):183–192.

25. **Fukumoto H, Seino S, Imura H, Seino Y, Eddy RL, Fukushima Y, Byers MG, Shows TB, Bell GI.** Sequence, tissue distribution, and chromosomal localization of mRNA encoding a human glucose transporter-like protein. *Proc. Natl. Acad. Sci. U. S. A.* 1988;85(15):5434–5438.

26. **Kamata K, Mitsuya M, Nishimura T, Eiki J-I, Nagata Y.** Structural basis for allosteric regulation of the monomeric allosteric enzyme human glucokinase. *Struct. Lond. Engl. 1993* 2004;12(3):429–438.

27. **Iynedjian PB, Marie S, Gjinovci A, Genin B, Deng SP, Buhler L, Morel P, Mentha G.** Glucokinase and cytosolic phosphoenolpyruvate carboxykinase (GTP) in the human liver. Regulation of gene expression in cultured hepatocytes. *J. Clin. Invest.* 1995;95(5):1966–1973.

28. **Beer NL, Tribble ND, McCulloch LJ, Roos C, Johnson PRV, Orho-Melander M, Gloyn AL.** The P446L variant in GCKR associated with fasting plasma glucose and triglyceride levels exerts its effect through increased glucokinase activity in liver. *Hum. Mol. Genet.* 2009;18(21):4081–4088.

29. **Lemaigre FP, Rousseau GG.** Transcriptional control of genes that regulate glycolysis and gluconeogenesis in adult liver. *Biochem. J.* 1994;303(Pt 1):1–14.

30. **Adeva-Andany MM, Pérez-Felpete N, Fernández-Fernández C, Donapetry-García C, Pazos-García C.** Liver glucose metabolism in humans. *Biosci. Rep.* 2016;36(6). doi:10.1042/BSR20160385.

31. **Johnson MK.** The intracellular distribution of glycolytic and other enzymes in rat-brain homogenates and mitochondrial preparations. *Biochem. J.* 1960;77(3):610–618.

32. **Rose IA, Warms JVB.** Mitochondrial Hexokinase RELEASE, REBINDING, AND LOCATION. *J. Biol. Chem.* 1967;242(7):1635–1645.

33. **Kropp ES, Wilson JE.** Hexokinase binding sites on mitochondrial membranes. *Biochem. Biophys. Res. Commun.* 1970;38(1):74–79.

34. **Pastorino JG, Shulga N, Hoek JB.** Mitochondrial binding of hexokinase II inhibits Bax-induced cytochrome c release and apoptosis. *J. Biol. Chem.* 2002;277(9):7610–7618.

35. **Rempel A, Bannasch P, Mayer D.** Microheterogeneity of cytosolic and membrane-bound hexokinase II in Morris hepatoma 3924A. *Biochem. J.* 1994;303(Pt 1):269–274.

36. **John S, Weiss JN, Ribalet B.** Subcellular Localization of Hexokinases I and II Directs the Metabolic Fate of Glucose. *PLOS ONE* 2011;6(3):e17674.

37. **Nakashima RA, Mangan PS, Colombini M, Pedersen PL.** Hexokinase receptor complex in hepatoma mitochondria: evidence from N,N'-dicyclohexylcarbodiimide-labeling studies for the involvement of the pore-forming protein VDAC. *Biochemistry (Mosc.)* 1986;25(5):1015–1021.

38. **Polakis PG, Wilson JE.** An intact hydrophobic N-terminal sequence is critical for binding of rat brain hexokinase to mitochondria. *Arch. Biochem. Biophys.* 1985;236(1):328–337.

39. **Xie GC, Wilson JE.** Rat brain hexokinase: the hydrophobic N-terminus of the mitochondrially bound enzyme is inserted in the lipid bilayer. *Arch. Biochem. Biophys.* 1988;267(2):803–810.

40. **Felgner PL, Messer JL, Wilson JE.** Purification of a hexokinase-binding protein from the outer mitochondrial membrane. *J. Biol. Chem.* 1979;254(12):4946–4949.

41. **Sui D, Wilson JE.** Structural determinants for the intracellular localization of the isozymes of mammalian hexokinase: intracellular localization of fusion constructs incorporating structural elements from the hexokinase isozymes and the green fluorescent protein. *Arch. Biochem. Biophys.* 1997;345(1):111–125.

42. **Lindén M, Gellerfors P, Nelson BD.** Pore protein and the hexokinase-binding protein from the outer membrane of rat liver mitochondria are identical. *FEBS Lett.* 1982;141(2):189–192.

43. **Fiek C, Benz R, Roos N, Brdiczka D.** Evidence for identity between the hexokinase-binding protein and the mitochondrial porin in the outer membrane of rat liver mitochondria. *Biochim. Biophys. Acta* 1982;688(2):429–440.

44. **Danial NN, Gramm CF, Scorrano L, Zhang C-Y, Krauss S, Ranger AM, Datta SR, Greenberg ME, Licklider LJ, Lowell BB, Gygi SP, Korsmeyer SJ.** BAD and glucokinase reside in a mitochondrial complex that integrates glycolysis and apoptosis. *Nature* 2003;424(6951):952–956.

45. **Cullen KS, Al-Oanzi ZH, O'Harte FPM, Agius L, Arden C.** Glucagon induces translocation of glucokinase from the cytoplasm to the nucleus of hepatocytes by transfer between 6-phosphofructo 2-kinase/fructose 2,6-bisphosphatase-2 and the glucokinase regulatory protein. *Biochim. Biophys. Acta* 2014;1843(6):1123–1134.

46. **Agius L.** The physiological role of glucokinase binding and translocation in hepatocytes. *Adv. Enzyme Regul.* 1998;38:303–331.

47. **Colombini M.** VDAC: the channel at the interface between mitochondria and the cytosol. *Mol. Cell. Biochem.* 2004;256–257(1–2):107–115.

48. **Shoshan-Barmatz V, De Pinto V, Zweckstetter M, Raviv Z, Keinan N, Arbel N.** VDAC, a multi-functional mitochondrial protein regulating cell life and death. *Mol. Aspects Med.* 2010;31(3):227–285.

49. **Arzoine L, Zilberberg N, Ben-Romano R, Shoshan-Barmatz V.** Voltage-dependent anion channel 1-based peptides interact with hexokinase to prevent its anti-apoptotic activity. *J. Biol. Chem.* 2009;284(6):3946–3955.

50. **Azoulay-Zohar H, Israelson A, Abu-Hamad S, Shoshan-Barmatz V.** In self-defence: hexokinase promotes voltage-dependent anion channel closure and prevents mitochondria-mediated apoptotic cell death. *Biochem. J.* 2004;377(Pt 2):347–355.

51. **BeltrandelRio H, Wilson JE.** Interaction of mitochondrially bound rat brain hexokinase with intramitochondrial compartments of ATP generated by oxidative phosphorylation and creatine kinase. *Arch. Biochem. Biophys.* 1992;299(1):116–124.

52. **Robey RB, Hay N.** Mitochondrial hexokinases: guardians of the mitochondria. *Cell Cycle Georget. Tex* 2005;4(5):654–658.

53. **Pastorino JG, Hoek JB.** Regulation of Hexokinase Binding to VDAC. *J. Bioenerg. Biomembr.* 2008;40(3):171–182.

54. **Gimenez-Cassina A, Lim F, Cerrato T, Palomo GM, Diaz-Nido J.** Mitochondrial hexokinase II promotes neuronal survival and acts downstream of glycogen synthase kinase-3. *J. Biol. Chem.* 2009;284(5):3001–3011.

55. **Carelli V, Chan DC.** Mitochondrial DNA: impacting central and peripheral nervous systems. *Neuron* 2014;84(6):1126–1142.

56. **Lightowlers RN, Taylor RW, Turnbull DM.** Mutations causing mitochondrial disease: What is new and what challenges remain? *Science* 2015;349(6255):1494–1499.

57. **Labbé K, Murley A, Nunnari J.** Determinants and functions of mitochondrial behavior. *Annu. Rev. Cell Dev. Biol.* 2014;30:357–391.

58. **Mishra P, Chan DC.** Metabolic regulation of mitochondrial dynamics. *J. Cell Biol.* 2016;212(4):379–387.

59. **Hermann GJ, Thatcher JW, Mills JP, Hales KG, Fuller MT, Nunnari J, Shaw JM.** Mitochondrial Fusion in Yeast Requires the Transmembrane GTPase Fzo1p. *J. Cell Biol.* 1998;143(2):359–373.

60. **Chen H, Chomyn A, Chan DC.** Disruption of fusion results in mitochondrial heterogeneity and dysfunction. *J. Biol. Chem.* 2005;280(28):26185–26192.

61. **Chen H, McCaffery JM, Chan DC.** Mitochondrial fusion protects against neurodegeneration in the cerebellum. *Cell* 2007;130(3):548–562.

62. **Chen H, Vermulst M, Wang YE, Chomyn A, Prolla TA, McCaffery JM, Chan DC.** Mitochondrial fusion is required for mtDNA stability in skeletal muscle and tolerance of mtDNA mutations. *Cell* 2010;141(2):280–289.

63. **Lima AR, Santos L, Correia M, Soares P, Sobrinho-Simões M, Melo M, Máximo V.** Dynamin-Related Protein 1 at the Crossroads of Cancer. *Genes* 2018;9(2). doi:10.3390/genes9020115.

64. **Heikkinen S, Pietilä M, Halmekytö M, Suppola S, Pirinen E, Deeb SS, Jänne J, Laakso M.** Hexokinase II-deficient mice. Prenatal death of homozygotes without disturbances in glucose tolerance in heterozygotes. *J. Biol. Chem.* 1999;274(32):22517–22523.

65. **Bali D, Svetlanov A, Lee HW, Fusco-DeMane D, Leiser M, Li B, Barzilai N, Surana M, Hou H, Fleischer N.** Animal model for maturity-onset diabetes of the young generated by disruption of the mouse glucokinase gene. *J. Biol. Chem.* 1995;270(37):21464–21467.

66. **Grupe A, Hultgren B, Ryan A, Ma YH, Bauer M, Stewart TA.** Transgenic knockouts reveal a critical requirement for pancreatic beta cell glucokinase in maintaining glucose homeostasis. *Cell* 1995;83(1):69–78.

67. **Hayashi H, Sato Y, Li Z, Yamamura K, Yoshizawa T, Yamagata K.** Roles of hepatic glucokinase in intertissue metabolic communication: Examination of novel liver-specific glucokinase knockout mice. *Biochem. Biophys. Res. Commun.* 2015;460(3):727–732.

68. **Zhang Y, Tan X, Xiao M, Li H, Mao Y, Yang X, Tan H.** Establishment of liver specific glucokinase gene knockout mice: a new animal model for screening anti-diabetic drugs. *Acta Pharmacol. Sin.* 2004;25(12):1659–1665.

69. **O'Doherty RM, Lehman DL, Télémaque-Potts S, Newgard CB.** Metabolic impact of glucokinase overexpression in liver: lowering of blood glucose in fed rats is accompanied by hyperlipidemia. *Diabetes* 1999;48(10):2022–2027.

70. **Pedersen PL, Mathupala S, Rempel A, Geschwind JF, Ko YH.** Mitochondrial bound type II hexokinase: a key player in the growth and survival of many cancers and an ideal prospect for therapeutic intervention. *Biochim. Biophys. Acta* 2002;1555(1–3):14–20.

71. **Ferre T, Riu E, Franckhauser S, Agudo J, Bosch F.** Long-term overexpression of glucokinase in the liver of transgenic mice leads to insulin resistance. *Diabetologia* 2003;46(12):1662–1668.

72. **Matschinsky FM, Magnuson MA, Zelent D, Jetton TL, Doliba N, Han Y, Taub R, Grimsby J.** The network of glucokinase-expressing cells in glucose homeostasis and the potential of glucokinase activators for diabetes therapy. *Diabetes* 2006;55(1):1–12.

73. **Caro JF, Triester S, Patel VK, Tapscott EB, Frazier NL, Dohm GL.** Liver glucokinase: decreased activity in patients with type II diabetes. *Horm. Metab. Res. Horm. Stoffwechselforschung Horm. Metab.* 1995;27(1):19–22.

74. **Haeusler RA, Camastra S, Astiarraga B, Nannipieri M, Anselmino M, Ferrannini E.** Decreased expression of hepatic glucokinase in type 2 diabetes. *Mol. Metab.* 2014;4(3):222–226.

75. **Peter A, Stefan N, Cegan A, Walenta M, Wagner S, Königsrainer A, Königsrainer I, Machicao F, Schick F, Häring H-U, Schleicher E.** Hepatic glucokinase expression is associated with lipogenesis and fatty liver in humans. *J. Clin. Endocrinol. Metab.* 2011;96(7):E1126-1130.

76. **DeWaal D, Nogueira V, Terry AR, Patra KC, Jeon S-M, Guzman G, Au J, Long CP, Antoniewicz MR, Hay N.** Hexokinase-2 depletion inhibits glycolysis and induces oxidative phosphorylation in hepatocellular carcinoma and sensitizes to metformin. *Nat. Commun.* 2018;9(1):446.

77. **Bustamante E, Pedersen PL.** High aerobic glycolysis of rat hepatoma cells in culture: role of mitochondrial hexokinase. *Proc. Natl. Acad. Sci. U. S. A.* 1977;74(9):3735–3739.

78. **Zhang Z, Huang S, Wang H, Wu J, Chen D, Peng B, Zhou Q.** High expression of hexokinase domain containing 1 is associated with poor prognosis and aggressive phenotype in hepatocarcinoma. *Biochem. Biophys. Res. Commun.* 2016;474(4):673–679.

79. **Loomba R, Sanyal AJ.** The global NAFLD epidemic. *Nat. Rev. Gastroenterol. Hepatol.* 2013;10(11):686–690.

80. **Chalasani N, Younossi Z, Lavine JE, Diehl AM, Brunt EM, Cusi K, Charlton M, Sanyal AJ.** The diagnosis and management of non-alcoholic fatty liver disease: practice Guideline by the American Association for the Study of Liver Diseases, American College of Gastroenterology, and the American Gastroenterological Association. *Hepatol. Baltim. Md* 2012;55(6):2005–2023.

81. **Wong VW-S, Wong GL-H, Choi PC-L, Chan AW-H, Li MK-P, Chan H-Y, Chim AM-L, Yu J, Sung JJ-Y, Chan HL-Y.** Disease progression of non-alcoholic fatty liver disease: a prospective study with paired liver biopsies at 3 years. *Gut* 2010;59(7):969–974.

82. **Benedict M, Zhang X.** Non-alcoholic fatty liver disease: An expanded review. *World J. Hepatol.* 2017;9(16):715–732.

83. **Paglialunga S, Dehn CA.** Clinical assessment of hepatic de novo lipogenesis in non-alcoholic fatty liver disease. *Lipids Health Dis.* 2016;15. doi:10.1186/s12944-016-0321-5.

84. **Peverill W, Powell LW, Skoien R.** Evolving concepts in the pathogenesis of NASH: beyond steatosis and inflammation. *Int. J. Mol. Sci.* 2014;15(5):8591–8638.

85. **Tilg H, Moschen AR.** Evolution of inflammation in nonalcoholic fatty liver disease: the multiple parallel hits hypothesis. *Hepatol. Baltim. Md* 2010;52(5):1836–1846.

86. **Buzzetti E, Pinzani M, Tsochatzis EA.** The multiple-hit pathogenesis of non-alcoholic fatty liver disease (NAFLD). *Metabolism.* 2016;65(8):1038–1048.

87. **Guilherme A, Virbasius JV, Puri V, Czech MP.** Adipocyte dysfunctions linking obesity to insulin resistance and type 2 diabetes. *Nat. Rev. Mol. Cell Biol.* 2008;9(5):367–377.

88. **Bugianesi E, Gastaldelli A, Vanni E, Gambino R, Cassader M, Baldi S, Ponti V, Pagano G, Ferrannini E, Rizzetto M.** Insulin resistance in non-diabetic patients with non-alcoholic fatty liver disease: sites and mechanisms. *Diabetologia* 2005;48(4):634–642.

89. **Kang YE, Kim JM, Joung KH, Lee JH, You BR, Choi MJ, Ryu MJ, Ko YB, Lee MA, Lee J, Ku BJ, Shong M, Lee KH, Kim HJ.** The Roles of Adipokines, Proinflammatory Cytokines, and Adipose Tissue Macrophages in Obesity-Associated Insulin Resistance in Modest Obesity and Early Metabolic Dysfunction. *PLoS ONE* 2016;11(4). doi:10.1371/journal.pone.0154003.

90. **Zámbó V, Simon-Szabó L, Szelényi P, Kereszturi É, Bánhegyi G, Csala M.** Lipotoxicity in the liver. *World J. Hepatol.* 2013;5(10):550–557.

91. **Meex RCR, Watt MJ.** Hepatokines: linking nonalcoholic fatty liver disease and insulin resistance. *Nat. Rev. Endocrinol.* 2017;13(9):509–520.

92. **Zhang X-Q, Xu C-F, Yu C-H, Chen W-X, Li Y-M.** Role of endoplasmic reticulum stress in the pathogenesis of nonalcoholic fatty liver disease. *World J. Gastroenterol. WJG* 2014;20(7):1768–1776.

93. **Takaki A, Kawai D, Yamamoto K.** Multiple Hits, Including Oxidative Stress, as Pathogenesis and Treatment Target in Non-Alcoholic Steatohepatitis (NASH). *Int. J. Mol. Sci.* 2013;14(10):20704–20728.

94. **Evstafieva AG, Kovaleva IE, Shoshinova MS, Budanov AV, Chumakov PM.** Implication of KRT16, FAM129A and HKDC1 genes as ATF4 regulated components of the integrated stress response. *PLoS ONE* 2018;13(2). doi:10.1371/journal.pone.0191107.

95. **Shoshan-Barmatz V, De Pinto V, Zweckstetter M, Raviv Z, Keinan N, Arbel N.** VDAC, a multi-functional mitochondrial protein regulating cell life and death. *Mol. Aspects Med.* 2010;31(3):227–285.

96. **Aleshin AE, Zeng C, Bartunik HD, Fromm HJ, Honzatko RB.** Regulation of hexokinase I: crystal structure of recombinant human brain hexokinase complexed with glucose and phosphate. *J. Mol. Biol.* 1998;282(2):345–357.

97. **O'Rear JL, Scocca JR, Walker BK, Kaiden A, Krag SS.** Chinese hamster ovary cells with reduced hexokinase activity maintain normal GDP-mannose levels. *J. Cell. Biochem.* 1999;72(1):56–66.

98. **Kelley LA, Mezulis S, Yates CM, Wass MN, Sternberg MJE.** The Phyre2 web portal for protein modeling, prediction and analysis. *Nat. Protoc.* 2015;10(6):845–858.

99. **Bustamante E, Morris HP, Pedersen PL.** Energy metabolism of tumor cells. Requirement for a form of hexokinase with a propensity for mitochondrial binding. *J. Biol. Chem.* 1981;256(16):8699–8704.

100. **Gelb BD, Adams V, Jones SN, Griffin LD, MacGregor GR, McCabe ER.** Targeting of hexokinase 1 to liver and hepatoma mitochondria. *Proc. Natl. Acad. Sci. U. S. A.* 1992;89(1):202–206.

101. **Takeuchi H, Inoue Y, Ishihara H, Oka Y.** Overexpression of either liver type or pancreatic beta cell type glucokinase via recombinant adenovirus enhances glucose oxidation in isolated rat hepatocytes. *FEBS Lett.* 1996;393(1):60–64.

102. **Morral N, Edenberg HJ, Witting SR, Altomonte J, Chu T, Brown M.** Effects of glucose metabolism on the regulation of genes of fatty acid synthesis and triglyceride secretion in the liver. *J. Lipid Res.* 2007;48(7):1499–1510.

103. **Niswender KD, Shiota M, Postic C, Cherrington AD, Magnuson MA.** Effects of increased glucokinase gene copy number on glucose homeostasis and hepatic glucose metabolism. *J. Biol. Chem.* 1997;272(36):22570–22575.

104. **Crowley LC, Christensen ME, Waterhouse NJ.** Measuring Mitochondrial Transmembrane Potential by TMRE Staining. *Cold Spring Harb. Protoc.* 2016;2016(12):pdb.prot087361.

105. **Becker TC, BeltrandelRio H, Noel RJ, Johnson JH, Newgard CB.** Overexpression of hexokinase I in isolated islets of Langerhans via recombinant adenovirus. Enhancement of glucose metabolism and insulin secretion at basal but not stimulatory glucose levels. *J. Biol. Chem.* 1994;269(33):21234–21238.

106. **Panasyuk G, Espeillac C, Chauvin C, Pradelli LA, Horie Y, Suzuki A, Annicotte J-S, Fajas L, Foretz M, Verdeguer F, Pontoglio M, Ferré P, Scoazec J-Y, Birnbaum MJ, Ricci J-E, Pende M.** PPARγ contributes to PKM2 and HK2 expression in fatty liver. *Nat. Commun.* 2012;3:672.

107. **Majewski N, Nogueira V, Robey RB, Hay N.** Akt inhibits apoptosis downstream of BID cleavage via a glucose-dependent mechanism involving mitochondrial hexokinases. *Mol. Cell. Biol.* 2004;24(2):730–740.

108. **Severgnini M, Sherman J, Sehgal A, Jayaprakash NK, Aubin J, Wang G, Zhang L, Peng CG, Yucius K, Butler J, Fitzgerald K.** A rapid two-step method for isolation of functional primary mouse hepatocytes: cell characterization and asialoglycoprotein receptor based assay development. *Cytotechnology* 2012;64(2):187–195.

109. **Khan MW, Biswas D, Ghosh M, Mandloi S, Chakrabarti S, Chakrabarti P.** mTORC2 controls cancer cell survival by modulating gluconeogenesis. *Cell Death Discov.* 2015;1:15016.

110. **Keller MP, Choi Y, Wang P, Davis DB, Rabaglia ME, Oler AT, Stapleton DS, Argmann C, Schueler KL, Edwards S, Steinberg HA, Chaibub Neto E, Kleinhanz R, Turner S, Hellerstein MK, Schadt EE, Yandell BS, Kendziorski C, Attie AD.** A gene expression network model of type 2 diabetes links cell cycle regulation in islets with diabetes susceptibility. *Genome Res.* 2008;18(5):706–716.

111. **Ganz M, Bukong TN, Csak T, Saha B, Park J-K, Ambade A, Kodys K, Szabo G.** Progression of non-alcoholic steatosis to steatohepatitis and fibrosis parallels cumulative accumulation of danger signals that promote inflammation and liver tumors in a high fat–cholesterol–sugar diet model in mice. *J. Transl. Med.* 2015;13. doi:10.1186/s12967-015-0552-7.

112. **Caballero F, Fernández A, Matías N, Martínez L, Fucho R, Elena M, Caballeria J, Morales A, Fernández-Checa JC, García-Ruiz C.** Specific contribution of methionine and choline in nutritional nonalcoholic steatohepatitis: impact on mitochondrial S-adenosyl-L-methionine and glutathione. *J. Biol. Chem.* 2010;285(24):18528–18536.

113. **Dela Peña A, Leclercq I, Field J, George J, Jones B, Farrell G.** NF-kappaB activation, rather than TNF, mediates hepatic inflammation in a murine dietary model of steatohepatitis. *Gastroenterology* 2005;129(5):1663–1674.

114. **Itagaki H, Shimizu K, Morikawa S, Ogawa K, Ezaki T.** Morphological and functional characterization of non-alcoholic fatty liver disease induced by a methionine-choline-deficient diet in C57BL/6 mice. *Int. J. Clin. Exp. Pathol.* 2013;6(12):2683–2696.

115. **Matsumoto M, Hada N, Sakamaki Y, Uno A, Shiga T, Tanaka C, Ito T, Katsume A, Sudoh M.** An improved mouse model that rapidly develops fibrosis in non-alcoholic steatohepatitis. *Int. J. Exp. Pathol.* 2013;94(2):93–103.

116. **Khan MW, Ding X, Cotler SJ, Clarke M, Layden BT.** Studies on the Tissue Localization of HKDC1, a Putative Novel Fifth Hexokinase, in Humans. *J. Histochem. Cytochem. Off. J. Histochem. Soc.* 2018;66(5):385–392.

117. **Arora KK, Pedersen PL.** Functional significance of mitochondrial bound hexokinase in tumor cell metabolism. Evidence for preferential phosphorylation of glucose by intramitochondrially generated ATP. *J. Biol. Chem.* 1988;263(33):17422–17428.

118. **Nelson BD, Kabir F.** The role of the mitochondrial outer membrane in energy metabolism of tumor cells. *Biochimie* 1986;68(3):407–415.

119. **Lemasters JJ, Holmuhamedov E.** Voltage-dependent anion channel (VDAC) as mitochondrial governator—Thinking outside the box. *Biochim. Biophys. Acta BBA - Mol. Basis Dis.* 2006;1762(2):181–190.

120. **Lis P, Dyląg M, Niedźwiecka K, Ko YH, Pedersen PL, Goffeau A, Ułaszewski S.** The HK2 Dependent "Warburg Effect" and Mitochondrial Oxidative Phosphorylation in Cancer: Targets for Effective Therapy with 3-Bromopyruvate. *Mol. Basel Switz.* 2016;21(12). doi:10.3390/molecules21121730.

121. **Yu T, Robotham JL, Yoon Y.** Increased production of reactive oxygen species in hyperglycemic conditions requires dynamic change of mitochondrial morphology. *Proc. Natl. Acad. Sci. U. S. A.* 2006;103(8):2653–2658.

122. **Theurey P, Rieusset J.** Mitochondria-Associated Membranes Response to Nutrient Availability and Role in Metabolic Diseases. *Trends Endocrinol. Metab. TEM* 2017;28(1):32–45.

123. **Itoh K, Nakamura K, Iijima M, Sesaki H.** Mitochondrial dynamics in neurodegeneration. *Trends Cell Biol.* 2013;23(2):64–71.

124. **Day CP, James OF.** Steatohepatitis: a tale of two "hits"? *Gastroenterology* 1998;114(4):842–845.

125. **García-Ruiz C, Baulies A, Mari M, García-Rovés PM, Fernandez-Checa JC.** Mitochondrial dysfunction in non-alcoholic fatty liver disease and insulin resistance: cause or consequence? *Free Radic. Res.* 2013;47(11):854–868.

126. **Sunny NE, Bril F, Cusi K.** Mitochondrial Adaptation in Nonalcoholic Fatty Liver Disease: Novel Mechanisms and Treatment Strategies. *Trends Endocrinol. Metab. TEM* 2017;28(4):250–260.

127. **Wei Y, Rector RS, Thyfault JP, Ibdah JA.** Nonalcoholic fatty liver disease and mitochondrial dysfunction. *World J. Gastroenterol. WJG* 2008;14(2):193–199.

128. **Ryaboshapkina M, Hammar M.** Human hepatic gene expression signature of non-alcoholic fatty liver disease progression, a meta-analysis. *Sci. Rep.* 2017;7(1):12361.

129. **Arendt BM, Comelli EM, Ma DWL, Lou W, Teterina A, Kim T, Fung SK, Wong DKH, McGilvray I, Fischer SE, Allard JP.** Altered hepatic gene expression in nonalcoholic fatty liver disease is associated with lower hepatic n-3 and n-6 polyunsaturated fatty acids. *Hepatol. Baltim. Md* 2015;61(5):1565–1578.